IDENTIFICATION OF ELECTROCHEMICAL PROCESSES BY FREQUENCY RESPONSE ANALYSIS

TECHNICAL REPORT NUMBER 004/83

IDENTIFICATION OF ELECTROCHEMICAL PROCESSES BY FREQUENCY RESPONSE ANALYSIS

TECHNICAL REPORT NUMBER 004/83

Claude Gabrielli

Ing Ecole Superieure d'Electricite

Docteur es Sciences

Centre National de la Recherche Scientifique

GR4 Physique des Liquides et Electrochimie

Universite P et M Curie, 4 Place Jussieu, T22

75230 Paris Cedex 05, France

Issue 3 March 1998

This monograph is dedicated to the late Professor Israel Epelboin, who spent much of his life introducing and developing the impedance techniques used in electrochemistry and who provided the inspiration and guidance for much of the work described.

Claude Gabrielli

September 1980

The aim of this monograph, commissioned by Solartron, is to aid in the understanding of impedance measurement in the important field of electrochemistry. The author, Claude Gabrielli, is one of the foremost authorities in this field and has provided a broad view of the many aspects of electrochemical impedance measurement, including some of the latest applications in research and industry. The monograph does not aim to be a deep study, but a comprehensive set of references to classical treatises and scientific papers is included.

CONTENTS

INTRODUCTION

Charge transfer at an electrochemical interface occurs at the end of a succession of more or less coupled elementary phenomena:

- transport of reactive species in the bulk of the solution, often associated with chemical reactions in the bulk phase.
- adsorption of the reactive species on the electrode
- electrochemical and chemical interfacial reactions.

Adsorption and reactions take place on the electrode surface, but mass transport is an homogeneous phase phenomenon that has to be carefully controlled. The aim of the electrochemist is to be able to study each elementary phenomenon in isolation from the others. Hence, he has to use a technique able to extract the data which allow these phenomena to be separated.

Some techniques able to characterise the state of the surface or adsorbed species on the interface necessitate the use of vacuum techniques (LEED, Auger ...), therefore they cannot be employed for an "in situ" analysis of the electrochemical interface. Other techniques using electromagnetic waves (optics: ellipsometry or X-rays: EXAFS) are beginning to be used in the study of the electrochemical interface but can hardly be applied when an alteration (dissolution, deposit ...) of the surface has occured. Hence electrical methods are often the only possible recourse for "in situ" investigations.

As a matter of fact, the use of electrical quantities allows a kinetic study to be done, which permits dissection of the couplings between elementary phenomena by control of the reaction rates. This enables the mono-electronic steps in the reaction mechanisms to be distinguished and the often unstable reaction intermediates involved in these reactions to be counted. If these techniques do not allow a real identification of the bondings and the reaction intermediates from a chemical point of view, they give information on the kinetics of the reaction mechanism governing the behaviour of the electrochemical interface and some characterization of these intermediates.

In addition to steady-state techniques, which allow simple processes to be studied, non-steady state techniques are necessary for investigating more complex electrochemical systems. The use of these techniques rests on principles analogous to those which justify relaxation methods employed at equilibrium state in chemical kinetics. Disturbing the reaction from the steady-state by applying a perturbation to the electrochemical system allows the system to relax to a new steady-state. As the various elementary processes change at different rates, the response can be analysed to dissect the overall electrochemical process.

The choice of technique depends on whether one is trying to establish a reaction mechanism, i.e. testing a model, or determining kinetic parameters of a known, or at least commonly assumed, mechanism. Some transient techniques are extensively used because they are well suited for extracting kinetic parameters when the mass transport is tedious. In some very favourable cases several techniques may be of comparable utility. However, when complex heterogeneous reactions interact with mass transport, time analysis of the transients will lead to very poor results in trying to extract a reaction mechanism, and a frequency analysis is more efficient. Hence, the use of impedance measurements over a wide frequency range is increasing, as will be seen later.

Devising the measurement procedure, and elaborating models which have to be compared with the experimental data, require an accurate description of the kinetic and electric laws governing the interface.

This, therefore, is the topic of Chapter 1. Chapter 2 describes the measurement techniques. Chapter 3 gives applications of impedance measurements in various fields and Chapter 4 briefly describes other related ac techniques. This monograph does not aim to be an extensive study and readers are referred to the classical treatises (e.g. References 1 to 12 for Chapter 1) if more detailed information is required.

1. General Concepts of Electrochemical Impedance

1.1 System Analysis

1.1.1 Linear System Analysis

The response *y(t)* of a linear system to a perturbation *x(t)* is determined by a differential equation of *n*th order in *y(t)*:

$$b_o \frac{d^n y(t)}{dt^n} + b_1 \frac{d^{n-1} y(t)}{dt^{n-1}} + ... + b_n y(t) = a_o \frac{d^m x(t)}{dt^m} + a_1 \frac{d^{m-1} x(t)}{dt^{m-1}} + ... + a_m x(t) \quad (1)$$

or a set of *n* differential equations of the first order. However, more complex linear systems can also be governed by linear partial differential equations.

Hence if *x(t)* is a sine wave input

$$x(t) = A \sin \omega t \quad (2)$$

the response, *y(t)*, is also a sine wave

$$y(t) = B \sin (\omega t + \phi) \quad (3)$$

and a transfer function can be defined

$$H(\omega) = |H(\omega)| e^{j\phi} \quad (4)$$

where $|H(\omega)| = B / A$ (5)

and $|H|$ and ϕ are the modulus and the phase shift of the transfer function.

If *x(t)* is a current and *y(t)* a voltage, $H(\omega)$ is an impedance value; conversely, if *x(t)* is a voltage and *y*(*t*) a current, $H(\omega)$ is an admittance value.

If the inverse Fourier transform, *h*(*t*), is considered

$$h(t) = \Im^{-1} |H(w)| \quad (6)$$

then $$y(t) = \int_{-\infty}^{+\infty} h(q) x(q - t) dq \quad (7)$$

In the case where *x*(*t*) is a Dirac impulse (Fourier transform of white noise)

$$y(t) = \int_{-\infty}^{+\infty} h(q) d(q - t) dq \equiv h(t) \quad (8)$$

Hence *h*(*t*) is called the impulse response and it can be measured by using white noise (see § 2.4.2.7).

From a theoretical point of view any type of perturbating signal *x*(*t*) - white noise, step, impulse or sine wave - can be used to obtain the value of $H(\omega)$ and hence the impedance. This is because eqn (7), by Fourier's transform, is equivalent to

$$Y(\omega) = H(\omega).X(\omega) \quad (9)$$

in the frequency domain. From a practical view-point, however, the accuracy and convenience of the measurement determine which perturbating signal is the most suitable.

Given the instruments available to date, sine wave analysis is, as will be seen later, the most appropriate for electrochemical studies.

The impedance $Z(\omega)$ of the electrochemical interface is a complex number which can be represented either in polar co-ordinates or in Cartesian co-ordinates:

$$Z(w) = |Z|\, e^{j\,f} \tag{10}$$

$$Z(w) = ReZ + j\, ImZ \tag{11}$$

Where *ReZ* and *ImZ* are the real part and the imaginary part of the impedance. The relationships between these quantities are:

$$|Z|^2 = (ReZ)^2 + (ImZ)^2 \tag{12}$$

$$f = Arc\tan\frac{Im\,Z}{Re\,Z} \tag{13}$$

$$Re\,(Z) = |Z| \cos f \tag{14}$$

$$Im\,(Z) = |Z| \sin f \tag{15}$$

Two types of plot are used to describe these relationships and these are illustrated in an example of an equivalent circuit of an electrochemical cell (Fig 1.1).

In Fig 1.1a the equivalent circuit of an electrochernical interface is depicted; its irnpedance is:

$$Z(w) = \frac{E}{I} = R_1 + \frac{1}{\frac{1}{R_2} + jCw} \tag{16}$$

Other quantities can be plotted in the same way, e.g. the admittance $Y(W) = Z^{-1}(W)$. Quantities coming from dielectric relaxation analysis have been used, typically in solid electrolyte spectra [12].

Pseudo complex permittivity $\quad e*(w) = \frac{Y(w)}{jw}$ (17)

and Pseudo complex modulus $\quad M(w) = jwZ(w)$ (18)

1.1.2 Non-linear System Analysis

When an interface is perturbed from its equilibrium by means of an external energy source, a permanent flow of charge and matter appears in it. This is due to:

i) the existence of electrochemical reactions allowing the electric charge transfer between the electronic conductor (metal or semi-conductor) electrode and the ionic conductor (liquid or solid electrolyte) and

ii) the gradients of electric and chemical potentials which make possible the transport of the reacting species between the bulk of the electrolyte and the interfacial reaction zone.

The elementary laws which govern the kinetics of mass transport and those of the various electrochemical reactions, as well as the complex couplings between these elementary processes, assign to the electrochemical system of interest a non-linear behaviour which can often be very pronounced.

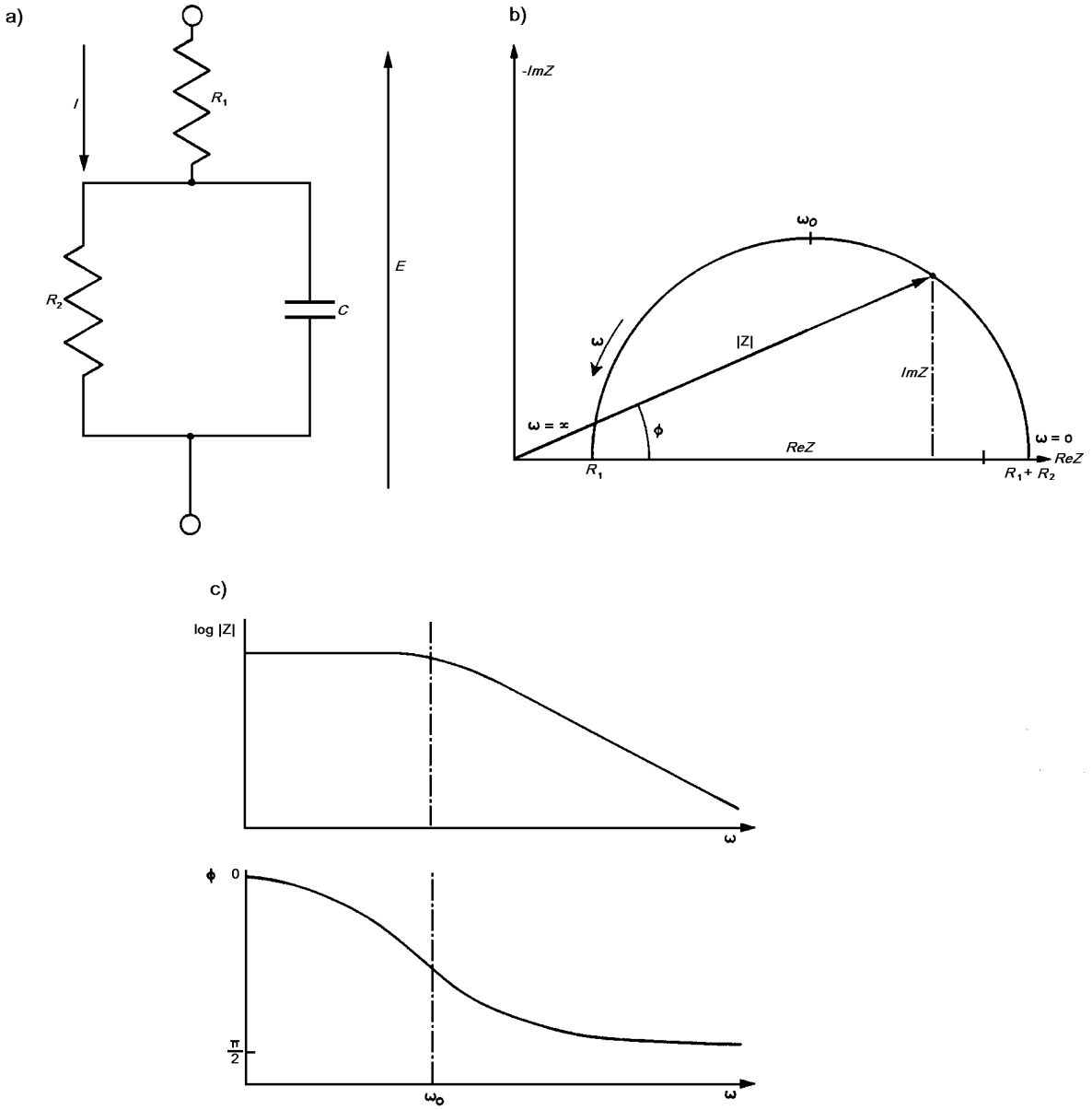

Fig 1.1 Equivalent circuit and impedance plots of an electrochemical cell

(a) equivalent circuit

(b) plotting in the complex plane (negative imaginary parts plotted above the real axis)

$$w_0 = \frac{1}{R_2 C}$$

(c) Bode plot of the impedance

For example, it is well-known that charge transfer generally obeys, at least approximately, an exponential activation law (Tafel's law) leading to a relationship between the Faradaic current I_F and the potential E [9] such that:

$$I_F = I_0 \exp \frac{anF}{RT} \tag{19}$$

where a is the transfer coefficient, n the number of electrons implied in the transfer, F the Faraday constant (=96500C), R the molar gas constant, T the absolute temperature and I_0 a constant.

Experimentally, there are many obvious examples of non-linear behaviour:

- N-shaped current-potential curve observed in the case of iron passivation in neutral medium (see § 3.2.1.1);
- S-shaped curve in the case of zinc electrocrystallization in Leclanche-cell medium (see § 3.4.2);
- Z-shaped curve in the case of iron passivation in molar sulphuric acid medium (pH = 0) (see § 3.2.1.2).

It can be shown that the behaviour of a non-linear system can be defined entirely in linear terms if the equivalent linear equations are known at every point of the steady-state characteristic [13, 14]. Hence, the local analysis of a non-linear system can be confined to the field of linear system theory. From an experimental point of view, it is satisfactory to measure the impedance of an electrochemical cell about a given polarisation point (E_0, I_0) by using a perturbation signal of very low amplitude.

As shown in Fig 1.2, a low amplitude sine wave $\Delta E \sin wt$ is superimposed on the dc polarisation voltage E_0. Hence, a low amplitude sine wave $\Delta I \sin(wt-f)$, is observed superimposed on the dc current. If the two sine waves are plotted on an X-Y recorder, a Lissajous figure (ellipse) similar to that shown in Fig 1.2 can be observed. Hence measurement of the electrochemical impedance all along the polarisation curve allows a complete characterisation of the interface and enables comparison with a model.

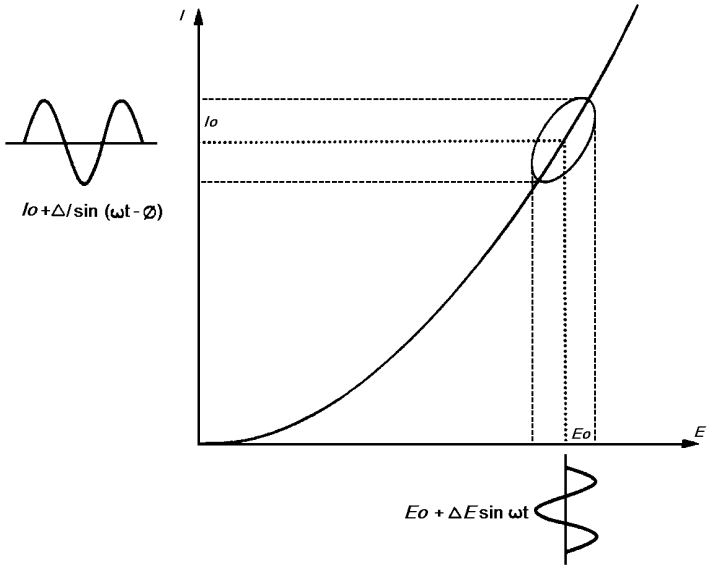

Fig 1.2 Small-signal analysis of an electrochemical non-linear system: A Lissajous ellipse is observed on an X-Y recorder when a sine wave voltage is superimposed on the dc polarisation voltage.

Taylor expansion of the current is:

$$DI = \left(\frac{dI}{dE}\right)_{E_0,I_0} DE + \frac{1}{2}\left(\frac{d^2I}{dE^2}\right)_{E_0,I_0} DE^2 + ... \qquad (20)$$

The magnitude of the perturbating signal should be such that the terms $\frac{1}{2}\left(\frac{d^2I}{dE^2}\right)_{E_0,I_0} DE^2 + ...$

are negligible compared with the first term, in order that the small-signal analysis can be considered to be in a linear regime. This process is known as quasi-linearisation and is used in many fields of non-linear system analysis.

1.2 General considerations on the state equations of the interface

The study of a physical phenomenon often leads to the elaboration of a model; in other words, the study is simply an identification problem [15]. One looks for a model that is a rational representation, often mathematical, of a phenomenon and which contains only the essential features of the real situation. Such a model has a two-fold purpose; first, it can account for all the facts discovered experimentally and second, it can predict the behaviour of a system under various conditions. The model often deals with the very structure of a system, but, in certain cases, it can also be useful to elaborate a model of the "input-output" type (equivalent circuit for example), which describes the behaviour of a system with respect to its environment.

The aim of the electrochemist is generally to identify the processes occurring at the interface, either by elaborating a model for the interface behaviour or by trying to find the value of some parameters of the system of interest when the reaction mechanism involved is already known. However, in some practical cases, empirical relationships are sufficient.

The elaboration of a model for the interface behaviour is derived from the general equations of physics that take account of the non-linear character of the processes involved. The comparison of the model with experimental data involves further calculations, of a complexity related to that of the model. The linearisation procedure, using small-signal analysis of the non-linear equations that describe the model, is particularly efficient [16, 17].

The space distribution of the state variables E(M,t) and c_i(M, t) - the potential and concentration of species i at point M and time t - is determined by a set of integral-differential equations (Maxwell equations and mass balance equations), subject to the appropriate boundary and initial conditions.

$$\nabla^2 E = -r_c + \nabla\vec{P} \qquad (21)$$

$$\frac{\partial c_i}{\partial t} = -\nabla\vec{J} + x_i \qquad \text{where } 1 \le i \le m \qquad (22)$$

The first of these (m + 1) coupled equations generalises the Poisson equation, where p_c is the electric charge density per unit volume and P the dielectric polarisation. The second set of equations generalises the hydrodynamic equations and applies to the *m* types of chemical entities involved in the system; c_i is either a surface or a bulk concentration, J_i is the flux, and ξi is a term representing the sources (production and consumption) of the entities i generally arising from chemical and electrochemical reactions. This last term can be made explicit from the mass balance of the reaction scheme to be tested and from the laws of homogeneous or heterogeneous kinetics [18].

Starting from this general framework the elaboration of a model for the interface will be performed by making a certain number of hypotheses which generally allows one to simplify the initial equations (21) and (22). These simplifying hypotheses fall into several categories, each of which is now briefly described.

1.2.1 The Poisson Equation

The charge density, r_c, in eqn (21) can be considered as non-zero in particular situations. Firstly, around a reference ion in the solution, in the Debye-Huckel theory [10]. Secondly, in the double layer where a static theory of the space charge distribution has been given by Gouy and Chapman [10]. A dynamic theory including the presence and effects of space charge has been proposed later [19-21].

However, it is often assumed in practice that the Laplace equation is a good approximation of the Poisson equation:

$$\nabla^2 E = 0 \tag{23}$$

This is valid at every point of the solution, since the electrolytic solution, as a whole, is electro-neutral ($r_c = 0$). Although the influence of radial gradients has been studied by J. Newman [22] who calculated the current distribution at the electrode surface, only the perpendicular potential gradient is generally considered. This leads to the concept that the ohmic drop due to the electrolyte resistance R_e is added to the potential difference across the interface.

$$E_{ref} = R_e I + E \tag{24}$$

where E_{ref} is the difference of potential between the electrode and the bulk of the solution, measured using a reference electrode.

1.2.2 Equations Describing the Concentration Change

The hypothesis often made is that of a dilute solution for which the flux of a species *i* can be separated into a flux due to diffusion and a flux due to migration in an electric field [23]. Assuming that the transport properties (D_i, μ_i) are uniform in the solution bulk, and hence are independent of c_i, the concentration change in the absence of a chemical reaction is:

$$\frac{\partial ci}{\partial t} = D_i \nabla^2 c_i - \vec{v} \nabla c_i + F n_i m_i \nabla (c_i \nabla E) \tag{25}$$

where *v* is the velocity of the liquid, D_i the diffusion coefficient of species *i*, m_i the mobility of *i*, n_i the charge number of *i*, and *E* the electric potential. Thus the concentration is modified under the simultaneous influence of diffusion (first term), convection (second term) and migration (third term). If the transport properties are not independent of the concentration a chemical source term (x_i) needs to be added to eqn (25).

If the electro-neutrality of the solution is assured, in the presence of major ionic species which are assumed not to take part in the reaction (supporting electrolyte), one can neglect the migration term. Generally, calculation of concentration in the presence of convection is difficult unless very particular hydrodynamic conditions are fulfilled. The well known example of the rotating disc electrode gives rise to a constant concentration gradient at the electrode (uniformly accessible electrode [23]). However, in other cases, calculation of concentration is simple only if one can disregard convection. This happens when Schmidt's number, v/D_i, (v is the kinematic viscosity), is sufficiently high (several thousands). The concentration gradient is then located in a layer, called the Nernst layer, of thickness δ_N, within which the liquid is nearly motionless (v = 0). The transport equation can then be reduced to Fick's equation with a good accuracy:

$$\frac{\partial c_i}{\partial t} = D_i \nabla^2 c_i \tag{26}$$

Convection is implicitly taken into account by applying the boundary conditions on c_i, that is $c_i = c_i^*$, at a finite distance δ_N from the electrode surface instead of at infinity. If the assumption is made that the diffusion layer has an infinite thickness in integrating eqn (26), the solutions obtained may not be satisfactory at low frequencies (see § 1.3.2).

1.2.3 Separation of the Faradaic Current from the Charging Current of the Double Layer

Strictly speaking, there is a close coupling between the Faradaic current I_F and the charging current I_C of the double layer. Full calculation of the impedance with no separation of the electrode impedance into Faradaic and double layer components has been attempted but the analytical expression of the impedance is particularly complicated [24-27]. Hence, in most models, it is assumed that the two components can be separated. Then the overall current I is:

$$I = I_f + I_c \tag{27}$$

and the interface can be represented, in the case of srnall perturbations, by the equivalent circuit shown in Fig 1.3, where the double layer behaviour is represented by a capacitance C_d.

However, the danger in applying analysis based on *a priori* separation could be particularly great for processes involving specific adsorption of reactant and product, or for any process in an insufficiently concentrated supporting electrolyte [27].

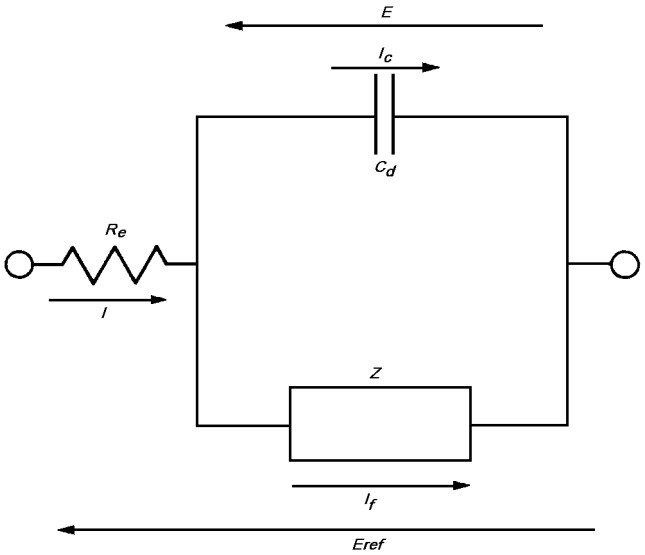

Fig 1.3 General equivalent circuit of an electrochemical cell

Re = electrolyte resistance

Cd = double layer capacitance

Z = Faradaic impedance

1.2.4 Heterogeneous Reactions at the Interface

In applying the laws of heterogeneous chemical kinetics to the adsorbed species involved in electrochemical kinetics, the mass-balance equation for a species *i* can be written:

$$\frac{\partial c_{Si}}{\partial t} = x_i + D_{Si} D c_{Si} \tag{28}$$

where x_i, the source term, can be either positive or negative and in eqn (28) represents the electrochemical or chemical surface reactions, the adsorption or the desorption. D_{Si} is the surface diffusion coefficient of species *i*. The surface concentration c_{Si}, is generally considered as being proportional to the coverage fraction q_i. of the electrode surface by species *I*

$$c_{Si} = b_i q_i \tag{29}$$

where b_i is the maximum surface concentration of species *i*.

By analogy with gas phase adsorption, an expression for the value of q_i is obtained by choosing an isothermal law expressing the occupation of the surface, the interactions between adsorbed species, and the distribution of adsorption energy between the various sites. The shape of the isotherm chosen has a considerable influence on the laws relating the reaction rate to the potential and the bulk concentration of the species. The most commonly adopted isothermal law is the Langmuir isotherm [28-29].

1.2.5 Charge-transfer at the Interface

The charge balance gives the Faradaic current I_F which is a function of several quantities:

$$I_F = I_F(c_i^*, E_{ref}, T, P, A, W) \tag{30}$$

c_i^* concentration of species *i* in the bulk of the solution

E_{ref} potential difference between the reference electrode and the working electrode

T absolute temperature

P pressure

A area of the electrode

W rotation speed of the electrode.

These last six quantities, which can play the role of experimental control quantities, enable the experimenter to act on the state of the system and hence on the current. Techniques where E or I are varied for analysis, while c_i^* T, P, A, and W are maintained constant, are classified as electric techniques. But, all the other quantities can be used as control quantities, thus constituting other types of techniques for analysing electrochemical systems. These techniques are described in § 4.

In order to demonstrate these concepts a few examples of simplified models are given in the next paragraph.

1.3 Models of the Electrochemical Interface

The first case considered is one in which a quasi-reversible charge transfer is controlled by mass transport. The only reaction taking place at the interface is the Redox reaction:

$$Ox + ne \underset{k_b}{\overset{k_f}{\rightleftharpoons}} \text{Red} \tag{31}$$

where k_f and k_b. are the forward and backward reaction rates.

The concentrations c_R and c_O, of species Red and Ox which diffuse from and towards the solution bulk, are ruled by the following equations (known as the second Fick's law) which are deduced from eqn (26)

$$\frac{\partial c_O}{\partial t} = D_O \frac{\partial^2 c_O}{\partial z^2} \tag{32}$$

$$\frac{\partial c_R}{\partial t} = D_R \frac{\partial^2 c_R}{\partial z^2} \tag{33}$$

If species Ox and Red are assumed to diffuse linearly in the direction z perpendicular to the electrode surface, with coefficients D_O and D_R, then the following initial and boundary conditions are imposed:

i) initial conditions: the solution is homogeneous before establishing current.

$t = 0; \quad z \geq 0; \quad c_O(z,0) = c_O^*; \quad c_R(z,0) = c_R^*$

ii) boundary conditions at an infinite distance from the electrode: at a sufficiently large distance from the electrode the concentration of the species attain the bulk concentration.

$t \geq 0; \quad z \rightarrow \infty; \quad c_O(z,t) \rightarrow c_O^*; \quad c_R(z,t) \rightarrow c_R^*$

iii) boundary conditions at the electrode surface : since there is no adsorption, the fluxes of Ox and Red are the same and equal to the Faradalc current because of mass and charge balances (known as the first Fick's law).

$$t \geq 0; z = 0; D_O \frac{\partial c_O}{\partial z}(0,t) = -D_R \frac{\partial c_R}{\partial z}(0,t) = \frac{I_F(t)}{nFA} \quad (34)$$

In addition, the current I_F is given by the heterogeneous kinetic law:

$$I_F(t) = nFA\,(k_f c_O(0,t) - k_b C_R(0,t)) \quad (35)$$

where the surface concentration is assumed to be equal to the bulk concentration of the species near the surface (z = 0).

In eqn (35) :

$$k_f = k_f^o \exp(-anFE / RT) \quad (36)$$

$$k_b = k_b^o \exp((1-a)nFE / RT)$$

where k_f^o and k_b^o are constants independent of E.

At the standard (or normal) electrode potential E^o, the rate constants of the forward reaction (k_f) and of the backward reaction (k_b) are equal to each other. Hence:

$$k_f^o \exp(-anFE^o / RT) = k_b^o \exp((1-a)nFE^o / RT) = k_S \quad (37)$$

and therefore

$$I_F = nFAk_S\left[c_O(0,t)\,exp\left(\frac{anF\left(E - E^o\right)}{RT}\right) - c_R(0,t)\,exp\left(\frac{(1-a)nF\left(E - E^o\right)}{RT}\right)\right] \quad (38)$$

$$\text{and } E^o = \frac{RT}{nF} ln \frac{k^o{}_f}{k^o{}_b} \quad (39)$$

At the equilibrium potential *Eeq* where the electrode is at rest the overall Faradaic current is zero (I_F = 0), and the apparent exchange current I_0 is given by

$$\frac{I_o}{nFA} = k_f\left(E_{eq}\right)c_O(0,t) = k_b\left(E_{eq}\right)c_R(0,t) \quad (40)$$

In that case, there is no concentration gradient at the electrode surface:

$$I_F = nFAD_O \frac{\partial c_O}{\partial z}(0,t) = -nFAD_R \frac{\partial c_R}{\partial z}(0,t) = 0 \quad (41)$$

hence

$$c_O(0,t) = c_O^* \text{ and } c_R(0,t) = c_R^* \text{ at } E = E_{eq} \quad (42)$$

and

$$I_O = nFAk_f^o c_O^* \exp\left(-anFE_{eq} / RT\right) = nFAk_b^o c_R^* \exp\left((1-a)nFE_{eq} / RT\right) \quad (43)$$

Consequently

$$E_{eq} = \frac{RT}{nF}\left(ln\frac{k_f^o}{k_b^o} + ln\frac{c_O^*}{c_R^*} \right) \tag{44}$$

$$E_{eq} = E^o + \frac{RT}{nF} ln\frac{c_O^*}{c_R^*} \tag{45}$$

By dividing eqn (35) by eqn (43), we obtain:

$$I_F = I_O\left[\frac{c_O}{c_O^*} exp\left(-\frac{anF\left(E - E_{eq}\right)}{RT} \right) - \frac{c_R}{c_R^*} exp\left(\frac{(1-a)nF\left(E - E_{eq}\right)}{RT} \right) \right] \tag{46}$$

In opposition to k_S, the exchange current alone cannot characterise the electrochemical reaction kinetics because it depends on the concentrations of the reacting species.

For an ideally reversible system the rate constants k_f and k_b, as well as the exchange current I_o, can be considered as infinitely high. Therefore, if charge transfer is assumed to be sufficiently fast, with respect to diffusion, for the condition of virtual or quasi-equilibrium to be maintained at the electrode surface, then the boundary condition at the electrode surface is given by the Nernst equation instead of eqn (35).

$$\frac{c_O(0,t)}{c_R(0,t)} = exp\frac{nF}{RT}\left(E - E^o\right) \tag{47}$$

However, one has to be careful when applying this relation to out-of-equilibrium conditions because it is valid only at equilibrium, or for ideally reversible systems.

Supposing a small perturbation $\Delta E exp(jwt)$ is applied to the system, the corresponding current change $\Delta I_F exp(jwt)$ is obtained by differentiating eqns (35), (32), and (33), and after eliminating the exp(jwt) terms one has

$$\frac{\Delta I_F}{nFA} = \frac{-anF}{RT} k_f \overline{c_O(0)} \Delta E + k_f \Delta c_O(0) - \frac{(1-a)nF}{RT} k_b \overline{c_R(0)} \Delta E - k_b \Delta c_R(0) \tag{48}$$

$$jw\Delta c_i(z) = D_i \frac{\partial^2 \Delta c_i(z)}{\partial z^2} \tag{49}$$

where Δc_i is a small variation in c_i, and i represents the suffices O and R. $c_i(z)$ is the concentration of species for dc polarisation, such that:

$$c_i(z,t) = \overline{c_i(z)} + \Delta c_i(z) exp(jwt)$$

Eqns (48) and (49) lead to two important concepts: the charge transfer resistance and the Warburg impedance [30].

1.3.1 The Charge Transfer Resistance R_{ct}

The charge transfer resistance is defined by:

$$1/R_{ct} = \left(\partial I_f / \partial E\right)_{c_i} \tag{50}$$

which becomes by virtue of eqn (35)

$$1/R_{ct} = \frac{nF}{RT}\left(-ak_f\overline{c_O} - (1-a)k_b\overline{c_R}\right)nFA \tag{51}$$

where $\overline{c_i} = c_i(0, t \to \infty)$

This value generalises, under non-equilibrium conditions, the concept of charge transfer resistance at equilibrium [9]. As a matter of fact, under equilibrium conditions, eqn (43) applies and by substituting these values in eqn (51) the well-known value of R_{ct} is found again.

$$R_{ct} = (RT/nF)(1/I_o) \tag{52}$$

For an ideally reversible process I_o is infinitely high, therefore, from eqn (52), R_{ct} tends to zero.

1.3.2 The Warburg Impedance

The resulting concentration perturbation $Dc_i(0, t)$ is obtained from the general solution of eqn (49), i.e. from the following equation obtained after eliminating the exp(jwt) terms:

$$Dc_i(z) = M_i\ exp\left(z\sqrt{jw/D_i}\right) + N_i\ exp\left(-z\sqrt{jw/D_i}\right) \tag{53}$$

The integration constants M and N can be calculated from the boundary conditions, following two hypotheses on the thickness of the diffusion layer.

1.3.2.1 Diffusion Layer of Infinite Thickness

In this case M = 0 and hence:

$$Dc_i(z) = N\ exp\left(-z\sqrt{jw/D_i}\right) \tag{54}$$

and by eqn (34)

$$DI_F(t) = -N_O nFAD_O\sqrt{jw/D_O}\ exp(jwt) = N_R nFAD_R\sqrt{jw/D_R}\ exp(jwt) \tag{55}$$

After eliminating the integration constant N, the equation becomes:

$$\frac{Dc_O(0)}{DI_F} = -\frac{1}{nFA\sqrt{jwD_O}} \tag{56}$$

$$\frac{Dc_R(0)}{DI_F} = \frac{1}{nFA\sqrt{jwD_R}} \tag{57}$$

combining eqns (56), (57) and (48):

$$DI_F = \frac{1}{R_{ct}} DE - \left(\frac{k_F}{\sqrt{D_O}} + \frac{kb}{\sqrt{D_R}} \right) \frac{DI_F}{\sqrt{jw}} \tag{58}$$

Hence one obtains for the impedance

$$Z(w) = \frac{DE}{DI_F} = R_{ct} \left(1 + \frac{l}{\sqrt{jw}} \right) \quad \text{where} \quad l = \frac{k_F}{\sqrt{D_O}} + \frac{k_b}{\sqrt{D_R}} \tag{59}$$

In eqn (59), $R_{ct}\, l \,/\, \sqrt{jw}$ is usually called the Warburg impedance [9, 31]. It can be seen that the high frequency limit of $Z(w)$ is equal to R_{ct}.

Taking into account the double layer capacitance, leads to the Randles equivalent circuit of the electrochemical impedance (Fig 1.4a) [32]. It has been shown in [33] that the high frequency limit is a semi-circle similar to that depicted in Fig 1.1a (where $R_1 = R_e$ and $R_2 = R_{ct}$) and the low frequency limit is a Warburg impedance such that:

$$Re(Z) = R_e + R_{ct} \left(1 + \frac{l}{\sqrt{2w}} \right) = R_{ct}^2\, l^2 C_d \tag{60}$$

$$Im(Z) = \frac{R_{ct}\, l}{\sqrt{2w}} \tag{61}$$

So, as depicted in Fig 1.4b, extrapolation of the 45° straight line representing the Warburg impedance in the complex plane intersects the real axis at:

$$R_{WO} = R_e + R_{ct} - R_{ct}^2\, l^2 C_d \tag{62}$$

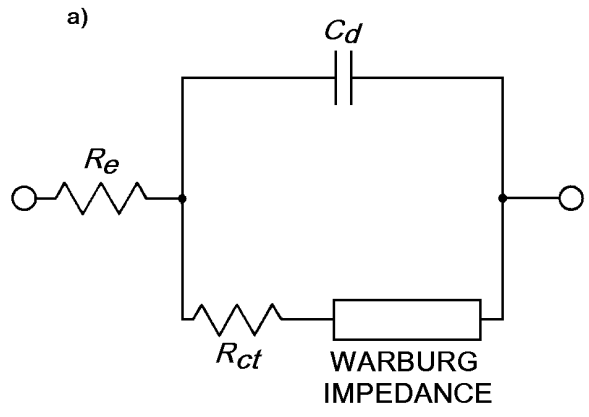

Fig 1.4a Randles equivalent circuit

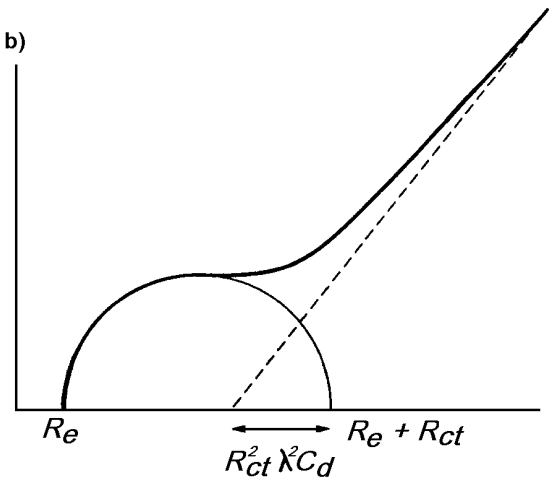

Fig 1.4b Electrochemical impedance in the case of a diffusion layer of infinite thickness: scheme of the impedance of the Randles equivalent circuit in the complex plane.

Depending upon the relative values of the charge transfer and the diffusion parameters, various shapes can be obtained for the impedance diagram. Hence, obtaining electrochemical quantities by simple extrapolation of the 45° straight line can be difficult.

1.3.2.2 Diffusion Layer of Finite Thickness

The Nernst hypothesis is then considered, i.e.

$$\left.\begin{aligned} c_i(z,t) &= c_i(0,t) + \left(c_i^* - c_i(0.t)\right)\frac{z}{d_N} \qquad \text{for } z < d_N \\ c_i(z,t) &= c_i^* \qquad\qquad\qquad\qquad\quad \text{for } z \geq d_N \end{aligned}\right\} \tag{63}$$

where d_N is the thickness of the Nernst diffusion layer. By using the boundary conditions at $z=d_N$, the following equations can be obtained from eqn (53):

$$\left.\begin{aligned} Dc_i(z) &= -2N_i\, exp\left(-d_N\sqrt{jw/D_i}\right)sh\left[(z-d_n)\sqrt{jw/D_i}\right] \\ Dc_i(z) &= 0 \end{aligned}\right\} \tag{64}$$

Thus by eqn (34)

$$\left.\begin{aligned} DI_F(t) &= -2N_O nFAD_O\sqrt{jw/D_O}\, exp\left(-d_N\sqrt{jw/D_O}\right)chd_N\sqrt{jw/D_O}\, exp(jwt) \\ DI_F(t) &= 2N_R nFAD_R\sqrt{jw/D_R}\, exp\left(-d_N\sqrt{jw/D_R}\right)chd_N\sqrt{jw/D_R}\, exp(jwt) \end{aligned}\right\} \tag{65}$$

and hence:

$$\frac{Dc_O(0)}{DI_F} = -\frac{1}{nFAD_O}\frac{thd_N\sqrt{jw/D_O}}{\sqrt{jw/D_O}} = -\frac{1}{nFA}N_O(w) \tag{66}$$

$$\frac{Dc_R(0)}{DI_F} = \frac{1}{nFAD_R}\frac{thd_N\sqrt{jw/D_R}}{\sqrt{jw/D_R}} = \frac{1}{nFA}N_R(w) \tag{67}$$

Substituting eqn (66) and (67) in eqn (48), one obtains:

$$DI_F = \frac{1}{R_{ct}}DE - \left(\frac{k_f}{\sqrt{D_O}}thd_N\sqrt{jw/D_O} + \frac{k_b}{\sqrt{D_R}}thd_N\sqrt{jw/D_R}\right)\frac{DI_F}{\sqrt{jw}} \tag{68}$$

Hence, in that case

$$Z(w) = R_{ct}\left(1 + \frac{k_f thd_N\sqrt{jw/D_O}}{\sqrt{D_O}\sqrt{jw}} + \frac{k_b thd_N\sqrt{jw/D_R}}{\sqrt{D_R}\sqrt{jw}}\right) \tag{69}$$

This impedance is schematised in Fig1.5. It should be noted that

i) if $\delta_N \to \infty$ we obviously find again the Warburg impedance.

ii) If $\omega \to \infty$, as $\frac{thd_N\sqrt{jw/D}}{\sqrt{jw/D}}$ is equivalent to $1/\sqrt{jw/D}$, we find the behaviour of the Warburg at high frequencies.

Hence if the double layer capacitance is considered, the coalescence problem of the semi-circle and of the 45° straight line of the Randles circuit still holds.

In Fig 1.5 the oscillation above the Warburg straight line (at frequencies between 0.4 and 0.14kHz) is related to the Nernst hypothesis. Numerical calculation taking account of the convection term in eqn (25) has shown that the curve representing the impedance, in the case of control by both reaction and diffusion, is below the Warburg impedance [34].

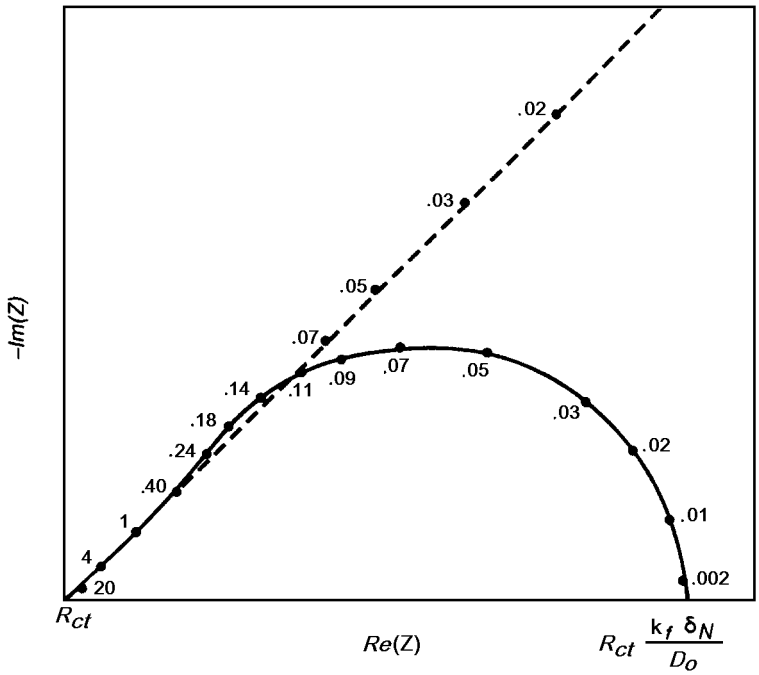

Fig 1.5 Electrochemical impedance in the case of the diffusion of species Ox in a diffusion layer of finite thickness (Nemst hypothesis) from [33]. (Frequency in kHz)

1.3.3 Impedance in the Case of Heterogeneous Reactions

Several methods have been developed for obtaining an expression for the impedance in the case of heterogeneous reactions. Each of these methods follows one of two very similar approaches. The first approach was used by Gerisher and Mehl [35] in their study of the impedance due to adsorbed intermediates in the hydrogen evolution reaction, and was later used extensively by Epelboin et al in the study of various electrochemical phenomena. The second approach was originally used by Frumkin and Melik-Gaikazyan [36], and later by Armstrong et al. It is more formal than the first approach and needs less assumptions in defining the model.

1.3.3.1 The Method of Epelboin et al [37 – 41]

Species *B* arrives at the surface by diffusion, adsorbs and reacts at the electrode surface giving species *P* in two reaction steps according to the scheme:

$$\left.\begin{aligned} B &\xrightarrow{k_1} X + e \\ X &\xrightarrow{k_2} P + e \end{aligned}\right\} \qquad (70)$$

The model is based on the following assumptions:

i) only adsorption and charge transfer processes occur on a two dimensional interface.

ii) adsorption of reaction intermediate X obeys a Langmuir isotherm and is characterised by a surface coverage θ.

iii) reactions are governed by heterogeneous kinetics

iv) reaction rates are exponentially potential dependent (Tafel's law):

$$k_i = k_i^o \exp b_i E \tag{71}$$

v) maximum number of sites per surface unit which can be occupied by the absorbate X is characterised by a coefficient β.

Mass and charge balances give:

$$b \frac{dq}{dt} = k_1 c_B (1-q) - k_2 q \tag{72}$$

$$I_F = FA[k_1 c_B (1-q) + k_2 q] \tag{73}$$

Solution of these equations for $\frac{dq}{dt} = 0$ gives, after elimination of q, the equation of the steady-state current-voltage curve:

$$I_F = \frac{2FAk_1 k_2 c_B}{k_1 c_B + k_2} \tag{74}$$

If a sine wave perturbation ΔE is superimposed on the polarisation voltage, the sine wave responses Δq, Δc_B and ΔI_F can be obtained by linearising the equations (72) and (73).

$$jwb\Delta q = [b_1 k_1 (1-q) c_B - b_2 k_2 q]\Delta E - (k_1 c_B + k_2)\Delta q + k_1 (1-q)\Delta c_B \tag{75}$$

$$\Delta I_F = FA([b_1 k_1 (1-q) c_B + b_2 K_2 q]\Delta E + (-k_1 c_B + k_2)\Delta q + k_1 (1-q)\Delta c_B) \tag{76}$$

Since species *B* diffuses towards the surface, one has

$$\frac{\Delta c_B}{\Delta I_F} = \frac{N(w)}{FA} \tag{77}$$

where N(ω) is defined by eqn (56) or by eqn (66), according to the hypothesis made on the thickness of the diffusion layer, and

$$(jwb + k_1 c_B + k_2)\Delta q = [b_1 k_1 (1-q) c_B - b_2 k_2 q]\Delta E + k_1 (1-q) N(w) \Delta I_F / FA \tag{78}$$

$$[1 - k_1 (1-q) N(w)]\Delta I_F = \frac{1}{R_{ct}} \Delta E + FA(-k_1 c_B + k_2)\Delta q \tag{79}$$

In that case the charge resistance is:

$$R_{ct} = \left(\frac{\partial E}{\partial I}\right)_{q, c_B} = \frac{k_1 c_B + k_2}{FAk_1 k_2 c_B (b_1 + b_2)} \tag{80}$$

After eliminating Δq in eqns (78) and (79) and replacing q by its steady state value the final expression for the impedance can be obtained:

$$Z(w) = \frac{1}{FA} \frac{k_1 c_B + k_2 - k_1 k_2 N(w)\left[1 + \frac{-k_1 c_B + k_2}{jwb + k_1 c_B + k_2}\right]}{k_1 k_2 c_B \left[b_1 + b_2 + \frac{(b_1 - b_2)(-k_1 c_B + k_2)}{jwb + k_1 c_B + k_2}\right]} \tag{81}$$

Hence $R_{ct} = Z\ (w \to \infty)$, the $w = 0$ limit leading to $R_P = \left(\frac{dE}{dI}\right)_{steady-state}$

In the particular case of a reaction controlled process the diffusion can be supposed as infinitely fast ($D_i \to \infty$, hence $N(w) = 0$) and therefore the new expression of the impedance is:

$$Z(w) = \frac{1}{FA} \frac{k_1 c_B + k_2}{k_1 k_2 c_B \left[b_1 + b_2 + \frac{(b_1 - b_2)(-k_1 c_B + k_2)}{jwb + k_1 c_B + k_2} \right]} \tag{82}$$

It can be shown that, according to the values of the parameters in eqn (82), this impedance can include either a capacitance or an inductance, as depicted in Fig 1.6. A great number of reaction mechanisms, among them some very complicated ones, have been analysed by the use of this method, as will be seen later.

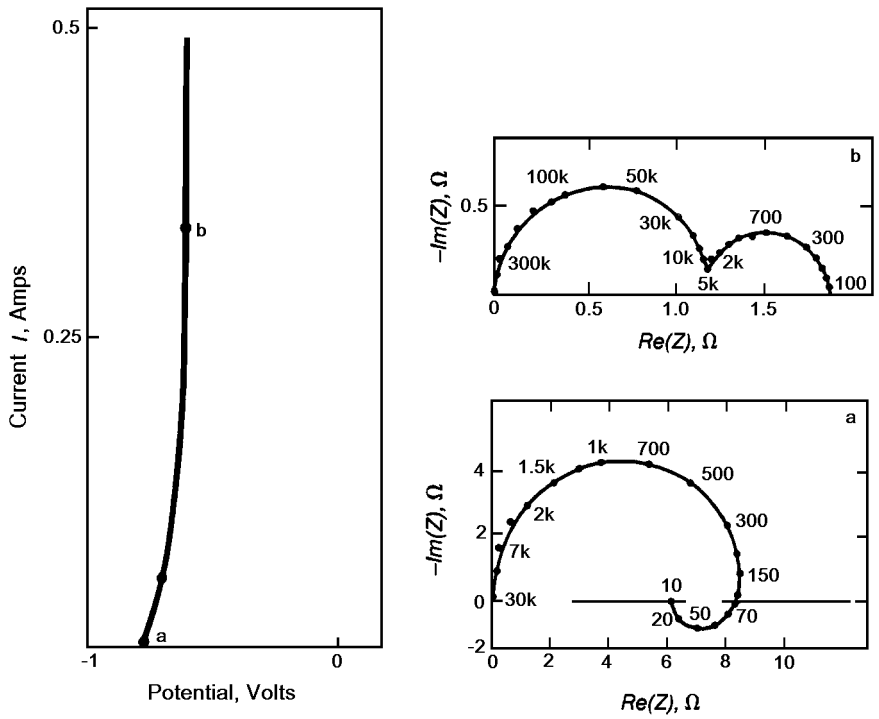

Fig 1.6 Simulated impedance in the case of heterogeneous reactions (eqn (82)). The kinetic parameters are $k_1 = 4.10^8$ exp 36E, $k_2 = 10^{-3}$ exp I0E, $\beta = 2.10^{-9}$, $C_B = 10^{-4}$ and $C_d = 20\mu F$. Impedances (a) and (b) are calculated at polarisation points corresponding to points a and b on the I- V curve. (from [41])

1.3.3.2 The Method of Frumkin and Armstrong [42 – 47]

In this method no assumptions are necessary, either for the isotherm law or for the reaction rate laws. Hence, for the same reaction mechanism as before (if diffusion effect is neglected), the reaction rates of the two steps are v_1 and v_2. The time variation of Γ, the surface concentration of X, is therefore

$$\frac{dG}{dt} = v_1 - v_2 \tag{83}$$

and $I_F = F(v_1 + v_2)$ (84)

The response of the system to a sine wave can be found from a Taylor series expansion

$$v_1 = v_{10} + \left(\frac{\partial v_1}{\partial G}\right)_E DG\ exp\ jwt + \left(\frac{\partial v_1}{\partial E}\right)_G DE\ exp\ jwt \tag{85}$$

$$v_2 = v_{20} + \left(\frac{\partial v_2}{\partial G}\right)_E DG\ exp\ jwt + \left(\frac{\partial v_2}{\partial E}\right)_G DE\ exp\ jwt \tag{85}$$

As $$jwDG = Dv_1 - Dv_2 \tag{87}$$

And $$DI_F = F(Dv_1 + Dv_2) \tag{88}$$

Elimination of $\Delta\Gamma$ between eqns (85), (86), (87) and (88) leads to:

$$DI_F = F\left\{\left[\left(\frac{\partial v_1}{\partial G}\right)_E + \left(\frac{\partial v_2}{\partial G}\right)_E\right]\frac{\left(\frac{\partial v_1}{\partial E}\right)_G - \left(\frac{\partial v_2}{\partial E}\right)_G}{jw - \left(\frac{\partial v_1}{\partial G}\right)_E + \left(\frac{\partial v_2}{\partial G}\right)_E} + \left(\frac{\partial v_1}{\partial E}\right)_G + \left(\frac{\partial v_2}{\partial E}\right)_G\right\}DE \tag{89}$$

If the time constant of the addmittance is:

$$t = \left[\left(\frac{\partial v_2}{\partial G}\right)_E - \left(\frac{\partial v_1}{\partial G}\right)_E\right]^{-1} \tag{90}$$

then:

$$Y(w) = \frac{1}{R_{ct}} + \left[\left(\frac{\partial v_1}{\partial G}\right)_E + \left(\frac{\partial v_2}{\partial G}\right)_E\right]\left[\left(\frac{\partial v_1}{\partial E}\right)_G - \left(\frac{\partial v_2}{\partial E}\right)_G\right]\cdot\frac{tF}{1 + jwt} \tag{91}$$

An additional resistance at zero frequency is then defined:

$$\frac{1}{R_0} = t\left[\left(\frac{\partial v_1}{\partial G}\right)_E + \left(\frac{\partial v_2}{\partial G}\right)_E\right]\left[\left(\frac{\partial v_1}{\partial E}\right)_G - \left(\frac{\partial v_2}{\partial E}\right)_G\right]F \tag{92}$$

which is related to the polarisation resistance *Rp* by

$$\frac{1}{R_P} = \frac{1}{R_{ct}} + \frac{1}{Ro} \tag{93}$$

This impedance is described in terms of an equivalent RC parallel circuit. The component values of this circuit are determined by comparison with the experimental data. Various reaction mechanisms have been analysed by this method: two step reaction with an adsorbed intermediate, limited or not by diffusion, adsorption coupled with an homogeneous reaction in solution, and reaction with a solution soluble intermediate. A survey of these models has been recently published [46].

1.3.3.3 The method of De Levie [48-50]

This method of calculation of the electrochemical impedance is very similar to the previous one. In this case the concentration appears explicitly in the reaction rate.

$$v_i = k_i c_i(0) \tag{94}$$

Hence the impedance is written in terms of $\frac{\partial k_i}{\partial E}$. In a series of papers, De Levie *et al* have discussed various models, in particular the generalised expression for the impedance of the coupling of interfacial and diffusional processes for a simple one-step (or pseudo one-step) first order reaction.

REFERENCES FOR CHAPTER 1

1. P DELAHAY *New Instrumental Methods in Electrochemistry*, Interscience, New York, 1954
2. P DELAHAY, *Advances in Electrochemistry and Electrochemical Engineering*, (P Delahay and C W Tobias, ed), Vol 1, pp 233 - 318, lnterscience, New York, 1961
3. B B DAMASKIN, *Principles of Current Methods for the Study of Electrochemical Reactions,* McGraw Hill, New York, 1967
4. E YEAGER and J KUTA, *Physical Chemistry, an Advanced Treatise* (H Eyring, D D Henderson and W Jost ed) Vol 9A, pp 356 - 462, Academic Press, New York, 1970
5. H R THIRSK and J A HARRISON, *A Guide to the Study of electrode Kinetics*, Academic Press, London, 1972
6. E YEAGER and A S SALKIND, *Techniques of electrochemistry* (2 volumes), Wiley, Interscience, New York, 1973
7. D D MacDONALD, *Transient Techniques in Electrochemistry*, Plenum Press, New York, 1977
8. D K ROE, *Anal Chem (Annual Reviews)* 44, pp 85R - 96R (no. 5), 1972, and 48, pp 9R - 17R (no. 5), 1976
9. K J YETTER, *Electrochemical Kinetics*, Academic Press, New York, 1967
10. J O'M BOCKRIS and A K N REDDY, *Modern Electrochemistry* (2 volumes), Plenum Press, New York, 1970
11. E YEAGER, B E CONWAY, J O'M BOCKRIS, *Comprehensive Treatise on Electrochemistry*, Vol 5, Plenurn Press, New York, 1981
12. I M HODGE, M D INGRAM, and A R WEST *J Electroanal Chem* 74, pp 125 - 143, 1976
13. J W WHITE, *Proc IEEE 59*, pp 98 - 99, 1971
14. J W WHITE, *Proc of the 6th Annual Princeton Conference on lnfomation Sciences and Systems*, pp l73-175, 1972
15. J RICHALET, A RAULT and R POULIQUEN*, Identification des Processus par la Methode du Modele*, Gordon & Breach, London, 1971
16. S K RANGARAJAN *J Electroanal Chem* 41, pp 459 - 471, 1973
17. S K RANGARAJAN, *J Electroanal Chem* 55, pp 297 - 327, pp 329 - 335, pp 337 – 361, pp 363 - 374, 1974
18. J P BADIALI and C GABRIELLI *J Chim Phys*, pp 1725 - 1732, 1972
19. J R MacDONALD, *Phys Rev* 92 pp 4 - 17,1953
20. J R MacDONALD, *J ChemPhys* 58, pp 4982 - 5001, 1973. 60, p 343, 1974
21. J R MacDONALD, *J Chem Phys* 61 pp 3977 – 3996, 1974
22. J NEWMAN, *J Electrochem Soc* II3, pp l235-1241, 1966

23. V D LEVICH, *Physicochemical Hydrodynamics* Prentice Hall, New York, 1962

24. P DELAHAY and G G SUSBIELLES, *J Phys Chem* 70 pp 3150 - 3157, 1966

25. P DELAHAY and K HOLUB, *J Electroanal Chem* 16 pp 131 - 136, 1968

26. G G SUSBIELLES and P DELAHAY, *J Electroanl Chem* 17 pp 289 - 292, 1968

27. K HOLUB, G TESSARI and P DELAHAY, *J Phys Chem* 71 pp 2612-2618, 1967

28. B E CONWAY, *Theory and Principles of Electrode Processes*, Ronald Ed, New York, 1965

29. S SRINIVASAN, H WROBLOWA and J O'M BOCKRIS, *Advances in Catalysis* (D D ELEY, H PINES and P B WEISZ Ed) Vol 17, pp 351 - 418, Academic Press, New York, 1967

30. D C GRAHAME, *J Electrochem Soc* 99 pp 370C - 385C, 1952

31. J LLOPIS and F COLOM, *Proc of the 8th meeting of the CITCE*, (Madrid 1956), Butterworths Scientific Pub, London, pp 414 - 427, 1958

32. J E B RANDLES, *Pans Faraday Soc* 44 pp 327 - 338, 1948

33. M SLUYTERS-REHBACH and J H SLUYTERS, *Electroanalytical Chemistry*, Vol 4 A J Bard Ed, Marcel Dekker, New York, 1970

34. E LEVART and D SCHUMANN *Int J Heat Mass Transfer* 17, pp 555 - 566, 1974

35. H GERISHER and W MEHL, *Z Elektrochem* 59 pp 1049 - 59, 1955

36. A N FRUMKIN and V I MELIK-GAIKAZYAN, *Dokl Akad Nauk*, USSR, 77 p 855, 1951

37. D SCHUMANN, *J Electroanal Chem* 17 pp 45 - 59, 1968

38. I EPELBOIN and M KEDDAM, *J Electrochem Soc* 117, pp 1052-1056, 1970

39. I EPELBOIN and R WIART, *J.Electrochem Soc* 118, pp 1577 - 1582, 1971

40. I EPELBOIN, M KEDDAM and J C LESTRADE, *Faraday Disc of the Chem Soc* 56, pp 265 - 275, 1973

41. I EPELBOIN, C GABRIELLI, M KEDDAM and H TAKENOUTI, *Electrochim Acta* 20 pp 913 - 916, 1975

42. R D ARMSTRONG, W P RACE and H R THIRSK, *J Electroanal Chem* 16, pp 5I7 - 529 1968

43. R D ARMSTRONG, *J Electroanal Chem* 22, pp 49 - 53 1969

44. R D ARMSTRONG and M HENDERSON, *J Electroanal Chem* 39, pp 81-90, 1972

45. R D ARMSTRONG and R E FIRMAN, *J Electroanal Chem* 45, pp 3 - 10, 1973

46. R D ARMSTRONG, M F BELL and A A METCALFE, *Specialist Periodical Reports - Electrochemistry* Volume 6, pp 98 - 127, The Chemical Society, London, 1978

47. R D ARMSTRONG, R E FIRMAN and H R THIRSK, *Faraday Disc of the Chemical Soc* 56, pp 244 - 263, 1974

48. R de LEVIE and A A HUSOVSKY, *J Electroanal Chem* 22, pp 29 - 48, 1969

49. R de LEVIE and L POSPISIL, *J Electroanal Chem* 22, pp 277 - 290, 1969

50. H MOREIRA and R de LEVIE, *J Electroanal Chem* 29, pp 353 - 374, 1971

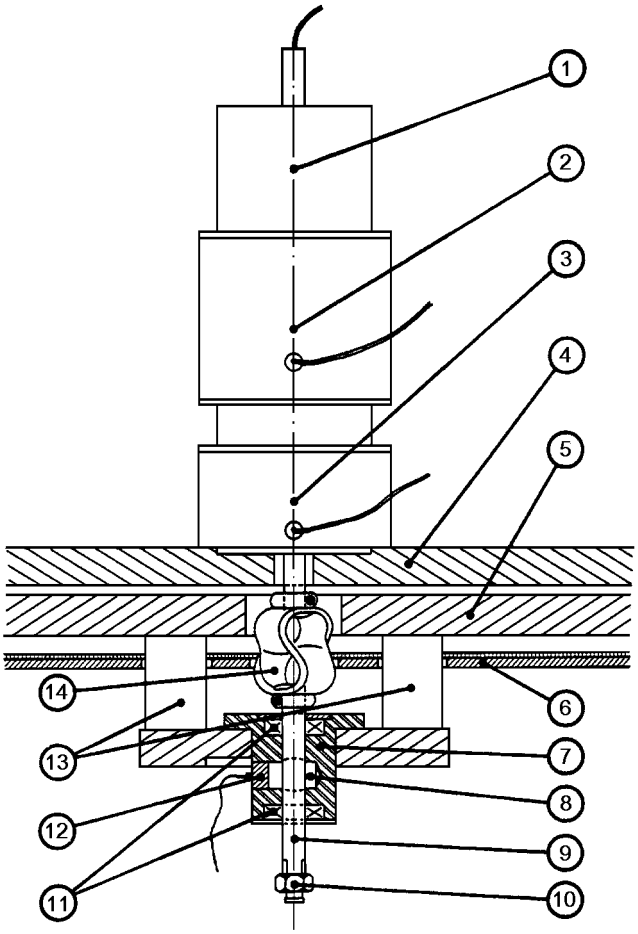

Fig 2.2 Specially constructed rotating disk electrode from [18 § 4]

1. incremental coder
2. tachometer dynamo
3. dc motor (80W)
4. motor support
5. support of the electrode holder bearing
6. cage made of μ-metal
7. contactor bearing
8. mercury chamber
9. titanium axle
10. conical holder of the electrode
11. mercury tight ball bearing
12. titanium roller for electric connection
13. insulating supports
14. Oldham coupling, for mechanical coupling and electrical insulation

2 Impedance Measurement Techniques

Before using any non steady-state technique the steady-state polarisation point of interest has to be established. Therefore, after some general considerations related to the electrochemical cell, the polarisation control principles will be examined.

2.1 The Electrochemical Cell

The electrochemical cell can consist of 2, 3 or 4 electrodes immersed in an electrolytic solution contained in a vessel (Fig 2.1). The electrochemical interface whose impedance is measured is generally located between the electrolyte and the working electrode (W.E.). When mass transport needs to be controlled a rotating disc electrode is often used. The rotation speed of the disc is carefully monitored or even electronically controlled. For measuring the current flowing through the rotating electrode a mercury rotating contact (e.g. Vibrometer) has to be used. A specially constructed arrangement is shown in Fig 2.2. In polarography the interface currents are minute, especially in analytical electrochemistry applications, hence dropping or hanging mercury electrodes are used.

A counter (auxiliary, or secondary) electrode (C.E.) is used to allow a current to flow through the cell. This is essentially a large surface area electrode (a long wire or mesh), often made of platinum, in order to have a very low impedance. The simplest form of cell (2 electrodes) consists of a working electrode and a secondary electrode immersed in an electrolytic solution (Fig 2.1a).

Where the potential difference across the interface needs to be very well defined and reproducible, however, a reference electrode (R.E.) is used (Fig2.1b). The reference electrode has a constant and reproducible potential when no current flows through it. The saturated calomel electrode (S.C.E.) is the most common type of reference electrode in aqueous media, but when chloride ions have to be avoided the saturated sulphate electrode (S.S.E.) is employed. Depending on the electrolyte, other types of reference electrode can be used.

The output impedance of the reference electrode can cause artefacts in high frequency impedance measurements and instability in the feedback loop of the regulating device. The resistance part of the output impedance (between 100Ω and a few kΩ) depends very much on the construction of the electrode (one or more compartments separated by sintered glass) [1] and stray capacitances of 1nF are common.

When the ion transport through a membrane has to be studied a four-electrode cell can be used (Fig 2.1c). Two auxiliary electrodes allow the current to flow. The potential difference across the membrane is measured by means of two reference electrodes, one on each side of the membrane.

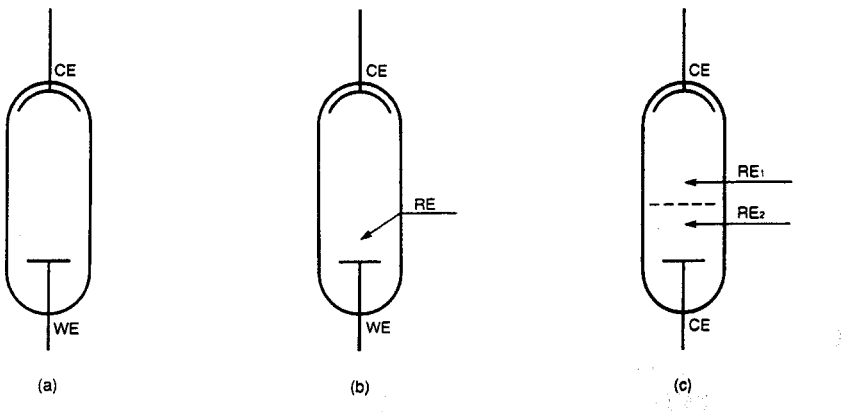

Fig 2.1 Scheme of experimental electrochemical cells:

(a) 2-electrode cell
(b) 3-electrode cell
(c) 4-electrode cell

WE Working electrode
CE Counter electrode
RE reference electrode

2.2 Polarisation Control

2.2.1 Principles of Polarisation Control [2]

The first galvanostatic supplies imposing a direct current allowed out-of-equilibrium electrochemical systems to be studied. A difficulty soon arose, however, in the case of metal-electrolyte interfaces whose current-potential characteristic had a part with a negative slope (Fig 2.3b), because this part was inaccessible. An important improvement was achieved when potentiostats began to be used, because they allowed control of the complete characteristic. With such devices many experimental problems encountered in electrochemistry have been solved satisfactorily and are still being solved. However, it has been observed that oscillation and commutation phenomena sometimes persist even when a potentiostat is used; certain electrochemical systems remain inaccessible even with a potentiostatic regulation. To solve this problem, it is necessary to consider the principle of regulation in a different way, in particular by taking account of the role of the load-line.

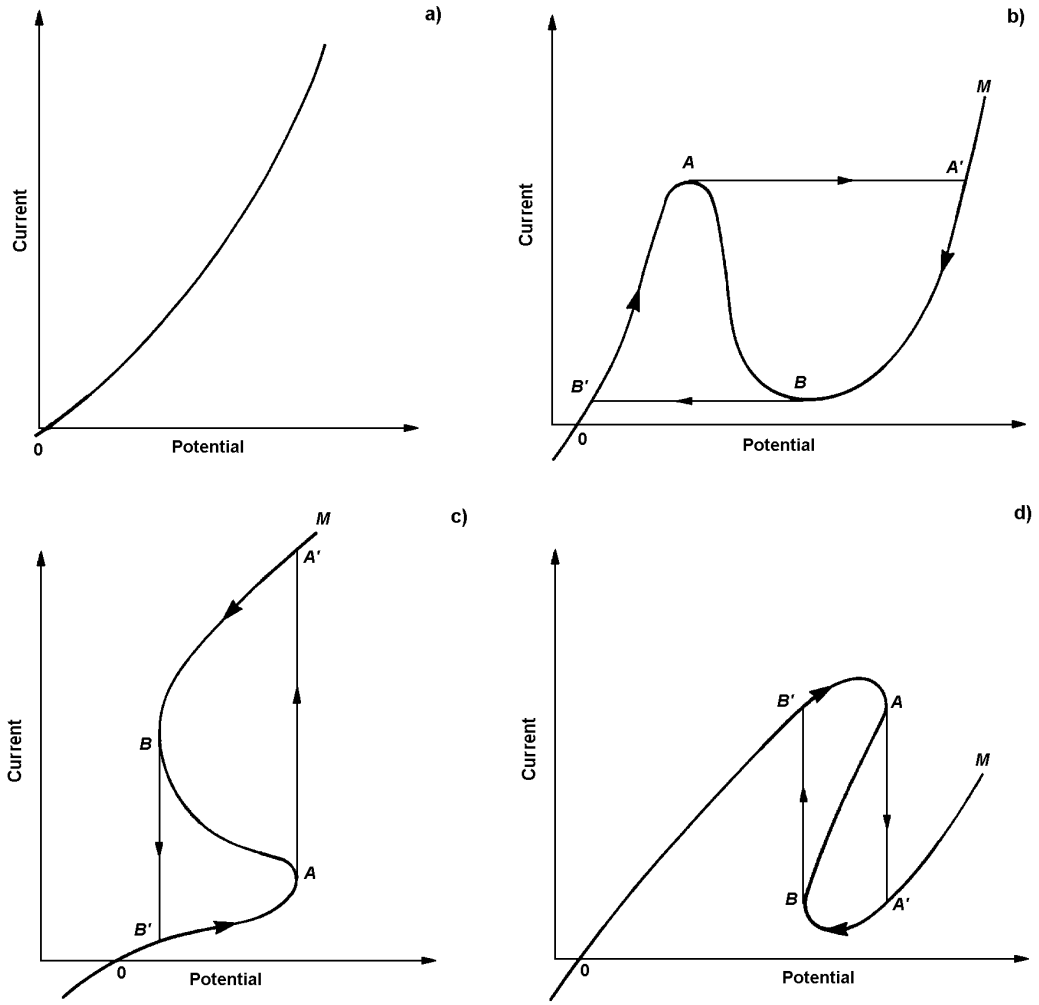

Fig 2.3 Examples of non-linear current-potential curves (from [2]):

(a) Exponential-shaped curve: potential or current-controlled interface

(b) N-shaped curve: potential-controlled interface

(c) S-shaped curve: current-controlled interface

(d) Z-shaped curve: O-A-A'-M-B-B'-O hysteresis observed on the current-potential curve for multi-steady state interfaces.

2.2.2 Suitability of the Polarisation Method

In general, oscillations and commutations seem to be related to phenomena that appear when a system is far from its equilibrium state. These phenomena are directly related to the interactions between the system and its environment, which arise from the type of constraint imposed on the system being studied. The environment is usually described as an independent variable (for example, the potential in electrochemistry), because it is considered that the system does not react with its environment, constituted by the reservoir, thermostat, ambient medium, the regulation device … as the case may be. Therefore the control quantity, which is governed by the experimenter, is transmitted to the system without any modification, and the system-environment interactions can be neglected. The steady-state characteristic is plotted by varying the constraint imposed and by measuring the change of a quantity characterising the state of the system. When electrical quantities are used, the characteristic represents the overall current, I, passing through the interface considered, to which a potential E_{ref} (i.e. the potential difference between the reference electrode and the working electrode) is applied.

Fig 2.3 shows some definitive examples of non-linear current-potential curves. For all the values on a particular type of curve to be determined unambiguously, an appropriate method of polarisation control must be used. Two variables can be used to control the system: the potential for curves of type a) and b), and the current for curves of type a) and c). If, however, an attempt is made to determine curves of type b) by controlling the current, curves of type c) by controlling the potential, or curves of type d) with either system then three possible states are attainable for each value of the constraint imposed and a multi-steady-state system is obtained.

Using the usual regulation (potentiostat, galvanostat) the results obtained from a multi-steady-state system do not, in general, follow the curves indicated by the thick lines shown in Figs b), c) and d).

The constraint is imposed as an independent variable and, where it is not matched precisely with the system, potential (or current) jump phenomena are observed, leading to hysteresis loops. Thus, when the constraint (current for b), potential for c) and d)) is increased a steep jump occurs in the value of the observed quantity (point A). When a decreasing constraint is imposed a similar phenomenon is observed in the opposite direction (point B). Experimentally, a hysteresis loop O-A-A'-M-B-B'-O is obtained which is often characteristic of a multi-steady-state system. It is noteworthy that the states characterised by the branch AB are inaccessible in that case.

2.2.3 Matching the Imposed Constraint with the System

When the results of an experiment exhibit the hysteresis effect it may be that part of the system characteristic (i.e. the part between A and B in Fig 2.3) is being obscured. This can, of course, make it very difficult to determine the properties of the process under investigation.

The most critical case is where the system is characterised by a curve of type d) (Fig 2.3), since the system states cannot be determined unambiguously by varying either the current I which flows through the system or the potential difference E_{ref} developed across it. There are also problems associated with dynamic stability, which cannot be neglected in practice, but which, for the sake of simplicity, are disregarded in the present study.

Generally, the initial state is assumed to be the state of the system in the absence of any constraint ($I = 0$). This state of rest (which is sometimes the thermodynamic equilibrium state) will be supposed unique and stable. The problem now is how to reach experimentally the state to be studied and how to control it. This is done using an external constraint described by a set of equations called the control law. This law is subject to the input quantities which are themselves controlled by the experimenter. In the case where the system and its environment presents several possible equilibrium states, it is necessary to establish, using this control law, which are the states that can be reached starting from the state of rest (point O, in Fig 2.3). As a matter of fact, only the accessible *and* stable states can be studied experimentally.

In the case of systems characterised by the Z-shaped characteristic shown in Fig 2.3d the states are defined by both I and E_{ref}, Therefore, both of these two quantities must be acted on in order to control a particular state. Hence the control law will be a function of both I and E_{ref}.

In general, a regulation which imposes a time-independent control law has to be realised. In that case the control law is reduced to a relationship between I and E_{ref} which depends neither on the derivatives nor on the integrals of these quantities with respect to time and which, for the sake of simplicity, will be taken as linear:

$$E_o = E_{ref} + \Re I \qquad (1)$$

where E_o is the input quantity and $\Re$ a controlled parameter.

This type of constraint is usually called a load line (Fig 2.4a).

Load lines representative of the various types of polarisation control are shown in Fig 2.4b. The lines are plotted in a plane E_{ref}, I, together with the Z-shaped characteristic $f(I, E_{ref}) = 0$. Each line is a graphical representation of equation (1) for a specific polarisation control method:

Load line d_1 ($\Re > 0$) : potentiometric supply

Load line d_2 ($\Re = 0$) : potentiostatic regulation

Load line d_3 ($\Re = \infty$) : galvanostatic regulation

Load line d_4 ($\Re < 0$) : negative output impedance regulation

For a load line to be effective, the working point $m(E_{ref},I)$ should be chosen such that the line is not tangential to the characteristic curve; if it is then the system becomes destabilised and jumps can occur in the experimental plots. Furthermore, to ensure the accessibility of the working point, it is necessary that a continuous succession of stable states can be established between the working point and the state of rest. It should be possible to do this by varying E_o or $\Re$ or both.

If a system, characterised by a curve similar to that shown in Fig 2.4b, is polarised using a potentiostat (d_2 parallel to the current axis), at points A and B the load line becomes tangent to $f(I, E\text{ref}) = 0$ at the polarisation point imposed, and there is destabilisation (see Fig 2.3d). The new polarisation point establishes at A' or B', i.e. two stable equilibrium points of the interface-regulation system.

It can be seen that, by realising a supply imposing a load line such as d_4, it is possible to explore the branch AB (Fig 2.3). An electronic supply having this property can be realised using a negative irnpedance converter [3, 4] which allows a complete investigation of systems exhibiting such a characteristic.

2.3 Regulating Devices

The first polarisation supplies used in clectrochemistry were of the potentiometric type, consisting of a potentiometer connected in series with a voltage source. When the potentiometer had a high impedance this arrangement was often called 'galvanostatic'. These early supplies, however, were unregulated. Truly galvanostatic (constant current) supplies, and potentiostatic (constant voltage) supplies, were later developed by employing the principle of negative feedback. Negative feedback ensures that the polarisation of an clectrochemical interface follows precisely a reference quantity set by the experimenter. The regulated quantity - interface potential or interface current - is compared with the reference quantity by a differential amplifier: any difference between the two quantities causes the regulated quantity to be adjusted by a change in the amplifier output, such that the difference approaches zero. With this system the reference quantity provides the positive input and the regulated quantity the negative (feedback) input.

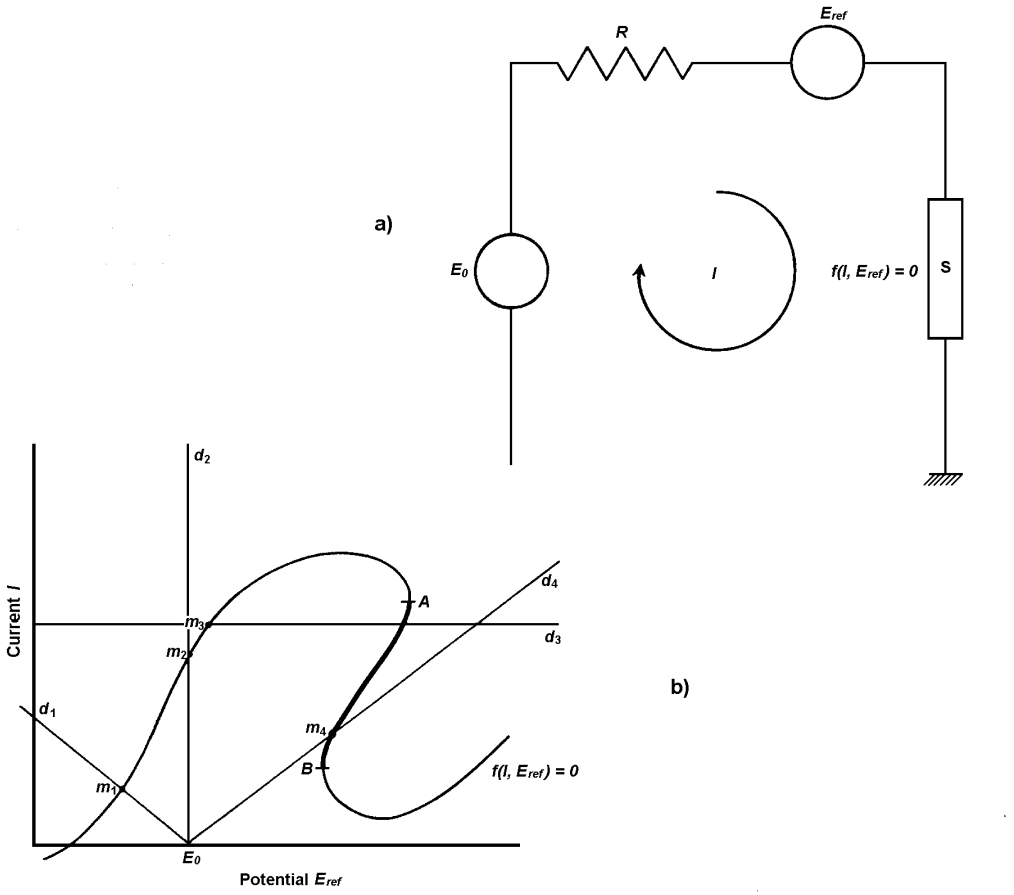

Fig 2.4 Regulation of the polarisation of a multi-steady state system S, characterised by a current-potential relationship $f(I, E_{ref}) = 0$ (from [2]):

(a) equivalent circuit of a regulator controlling the polarisation of the system S (E_o is the voltage supply and $\Re$ the internal resistance)

(b) polarisation curve of the multi-steady state system S with the four typical positions of the load-line:

d_I defined by $\Re > 0$ (potentiometric supply)

d_2 defined by $\Re = 0$ (potentiostatic regulation)

d_3 defined by $\Re$ infinite (galvanostatic regulation)

d_4 defined by $\Re < 0$ (negative impedance regulation)

To comply with the requirements of an electrochemist, the design of a polarisation supply must conform to the following criteria:

- The accuracy of the regulation is dependent on the gain of the amplifier. The accuracy demanded in electrochemical impedance measurement is such that the amplifier gain must be $>10^5$.
- For accuracy of resolution under dynamic conditions amplifier response time and bandwidth are important: high frequency impedance measurements demand a correspondingly wide bandwidth from the regulating circuit.
- For the reference electrode to be maintained at a constant voltage, only minute currents should flow through it. Therefore, the input impedance for the reference electrode must be $>10^7\Omega$.
- To allow measurements to be made with low amplitude signals (as are required in quasi-linear measurements) parasitic noise in the regulating circuit must be low.

2.3.1 Examples of potentiostatic and Galvanostatic Regulation

Schematic diagrams are given in Figs 2.5 and 2.6 of regulation circuits used for polarising a 2,3 or 4 electrode electrochemical cell, in potentiostatic or galvanostatic mode. These circuits are contained in the Solartron 1286 Electrochemical Interface (ECI).

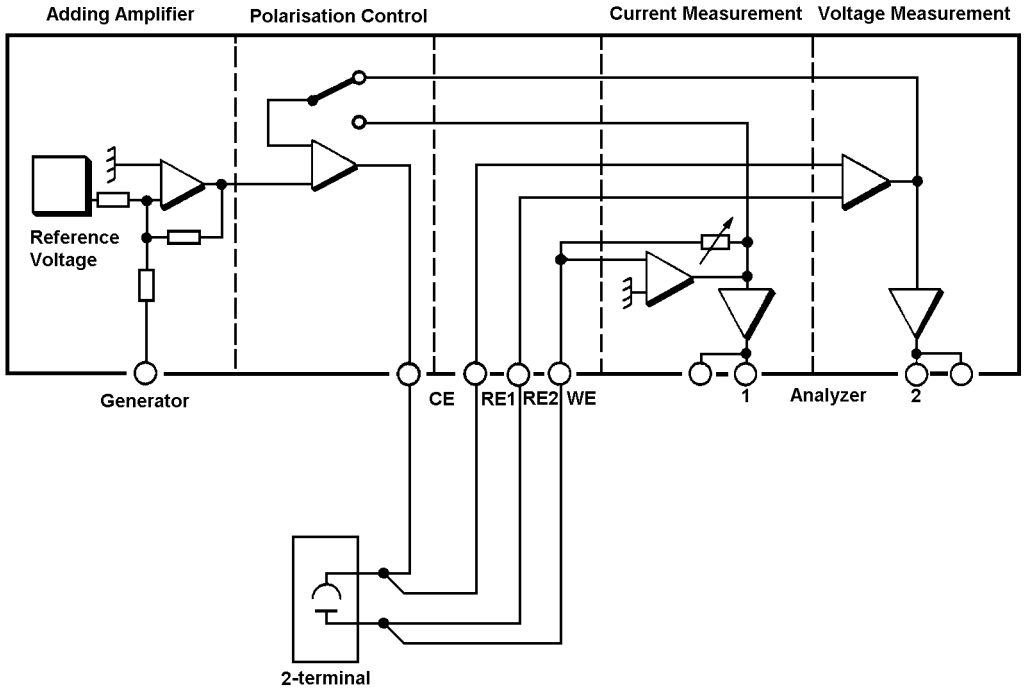

Fig 2.5a

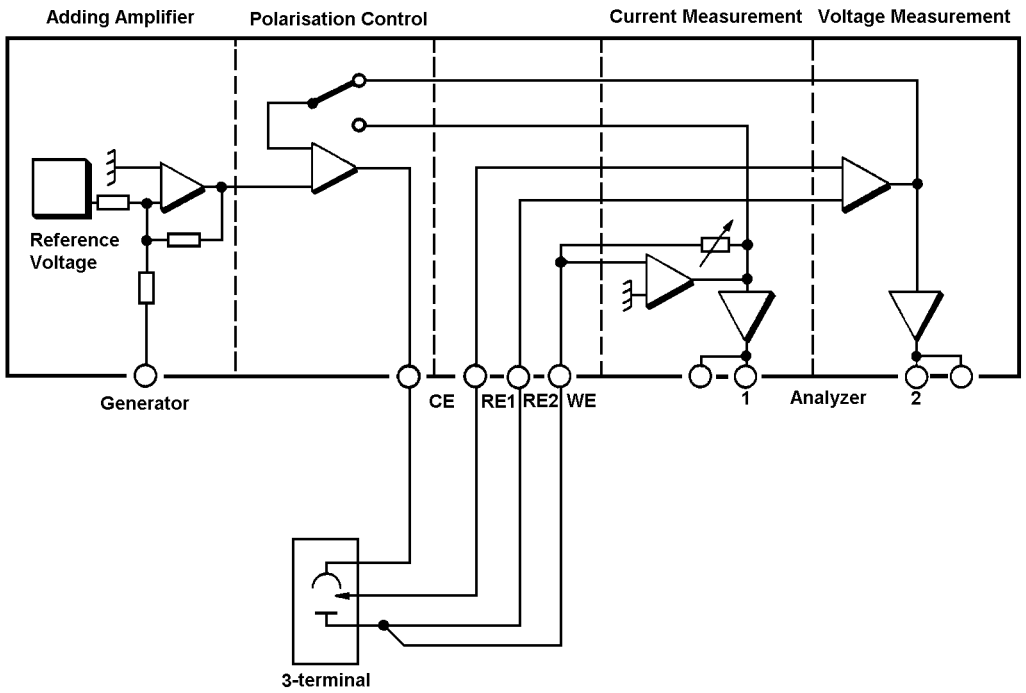

Fig 2.5b

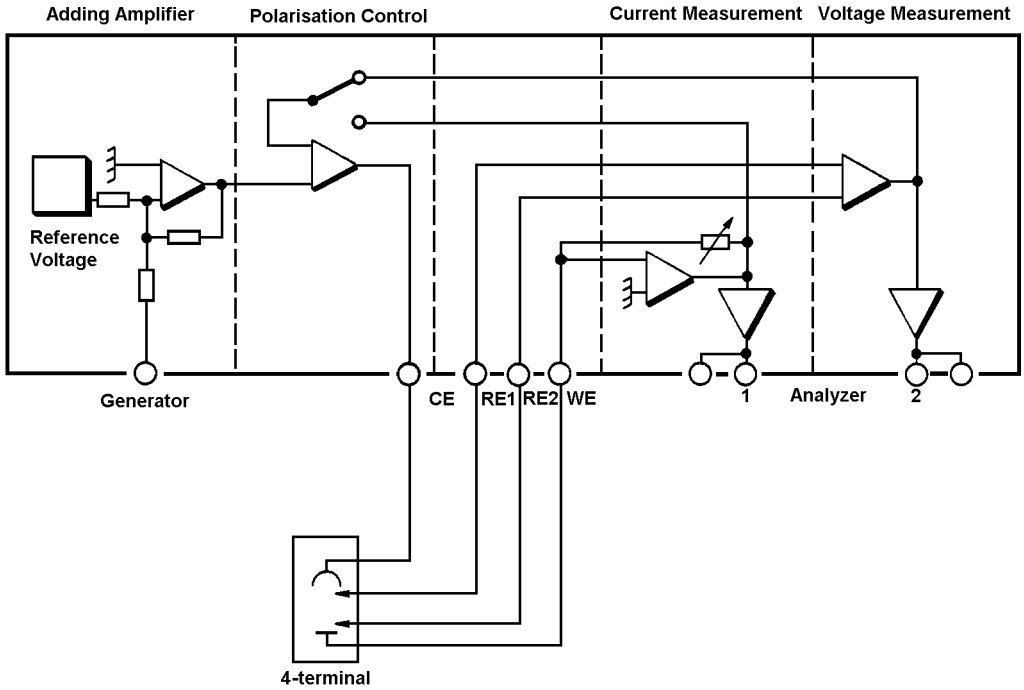

Fig 2.5c

Fig 2.5 Examples of potentiostatic regulation using the Solartron 1286 ECI

(a) two-electrode cell control
(b) three-electrode cell control
(c) four-electrode cell control

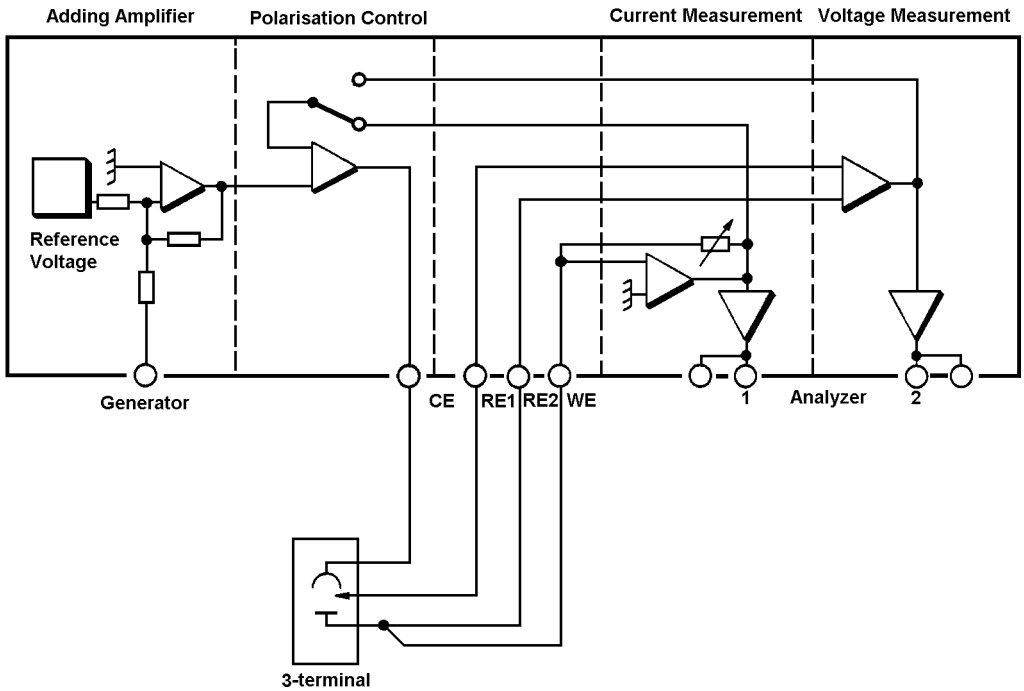

Fig 2.6 Example of galvanostatic regulation using the Solartron 1286 ECI

2.3.2 Example of Negative Output Impedance Regulation

This device permits domains such as AB in Fig 2.3d to be investigated, using positive feedback. It is equivalent to a generator having a voltage source, E_s, in series with an output impedance Z_s variable from $Z_s = 0$ (equivalent to a potentiostat) to some negative value [3, 4].

The part of the curve between the rest potential O and a point between O and B in Fig 2.3d is plotted using potentiostatic regulation ($Z_s = 0$, i.e. load line d_2 in Fig 2.4). Then negative output impedance regulation ($Z_s < 0$, i e load line d_4 in Fig 2.4) is selected to plot that part of the curve between points A and B. After point B is reached, potentiostatic regulation ($Z_s = 0$) is again used to plot the remainder of the curve.

For these devices an obvious problem of stability arises for the whole call regulation system. It can be shown that if such devices have a very wide bandwidth the whole system is unstable. Hence, it is necessary to use positive feedback with a narrow bandwidth: in this way Z_s is given a negative value which is high at low frequencies and low at the higher frequencies. This is achieved by filtering the positive feedback signal (e.g. by introducing a filter in the current feedback).

Other examples and more detailed schemes of the various regulating devices can be found in [5].

2.4 Electrochemical Impedance Measurement

2.4.1 General Considerations

An impedance value is usually represented, like any complex number, either by a pair of Cartesian co-ordinates or by a pair of polar co-ordinates. The decision on which type of co-ordinates to use is not without importance. From the Kramers-Kronig equations [6] there is a one-to-one relationship between real and imaginary parts with Cartesian co-ordinates, but the same relationship does not always apply between modulus and phase with polar co-ordinates. For example, the Bode equation is not satisfied for a non-minimal phase shift system: therefore as the nature of the electrochemical impedance is not known *a priori* measurements must include both polar co-ordinates. Measurements which include both Cartesian co-ordinates over the whole frequency range produce redundant data, but it is better to include both co-ordinates throughout, since this increases the measurement accuracy.

The characteristics of electrochemical interfaces demand a quite rigorous specification in the instruments used to measure cell impedance. Various aspects of impedance measurement are discussed below and these include frequency range, linearity, and signal-to-noise ratio.

2.4.1.1 Frequency Range

Due to the high frequency capacitive effect attributed to the double layer, impedance measurements must be made over a wide range of frequencies (sometimes up to several hundred kHz) in order to attain the high frequency limit of the impedance equal to the electrolyte resistance. The lowest frequency at which measurements need to be made, according to experimental results published over the last two decades, lies between the sub-acoustic frequencies 10^{-2}Hz and $I0^{-3}$Hz. The result at this frequency equals the slope of the current-voltage curve (equal to the polarisation resistance R_P).

2.4.1.2 Linearity

For an electrochemical impedance to be defined correctly, it is necessary to use a perturbating signal of low amplitude. The limits between which the amplitude may lie define a 'linearity range', which depends on the polarisation point. The low limit is determined by the signal-to-noise ratio which can be accepted by the measuring instrument. The high limit is determined by the onset of non-linear distortion.

The linearity domain for an electrochemical system can be depicted as shown in Fig 2.8a. From this it can be seen that the maximum permissible amplitude of a perturbating signal is smaller at a low frequency than it is at a high frequency. For convenience, a constant amplitude perturbating signal is used over the whole frequency range, the amplitude being determined by the high limit at the most critical frequency point [7].

It is possible to check that the amplitude ΔE of the perturbating signal is sufficiently small for linear conditions by measuring the variation of the modulus or, better, the variation of both modulus and phase, of the impedance with respect to ΔE. As long as the measured quantity (modulus and / or phase) does not vary with increase in ΔE (Fig 2.8b), the measurement is actually in a linear regime; when this quantity varies the measurement is no longer in the linear regime. Measurement of higher harmonics, of order 2, 3, 4.... can also be used as a check.

2.4.1.3 Signal-to-noise Ratio

The task of data acquisition and signal processing becomes more exacting when very accurate measurements have to be made, especially in the case of small signal analysis [8]. Information theory shows that optimum accuracy, for a given signal-to-noise ratio, is achieved when signals are detected by means of a correlation process. This is the technique used with synchronous detectors [9, 10] and digital transfer function analysers [11]. Where such devices are not available other techniques can still be used, but these will have certain limitations regarding the accuracy, processing time, and bandwidth of the measurement.

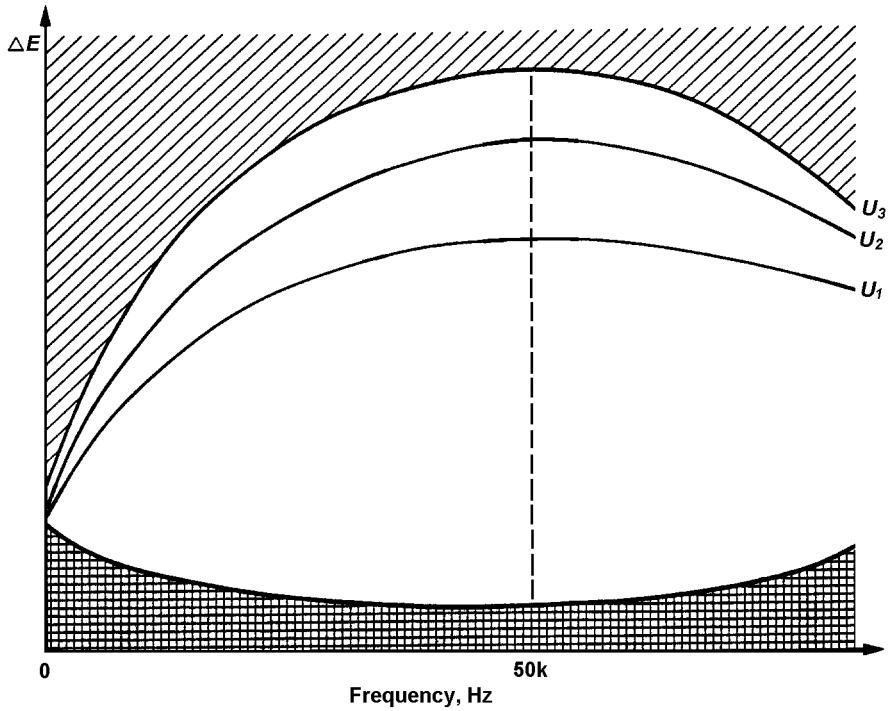

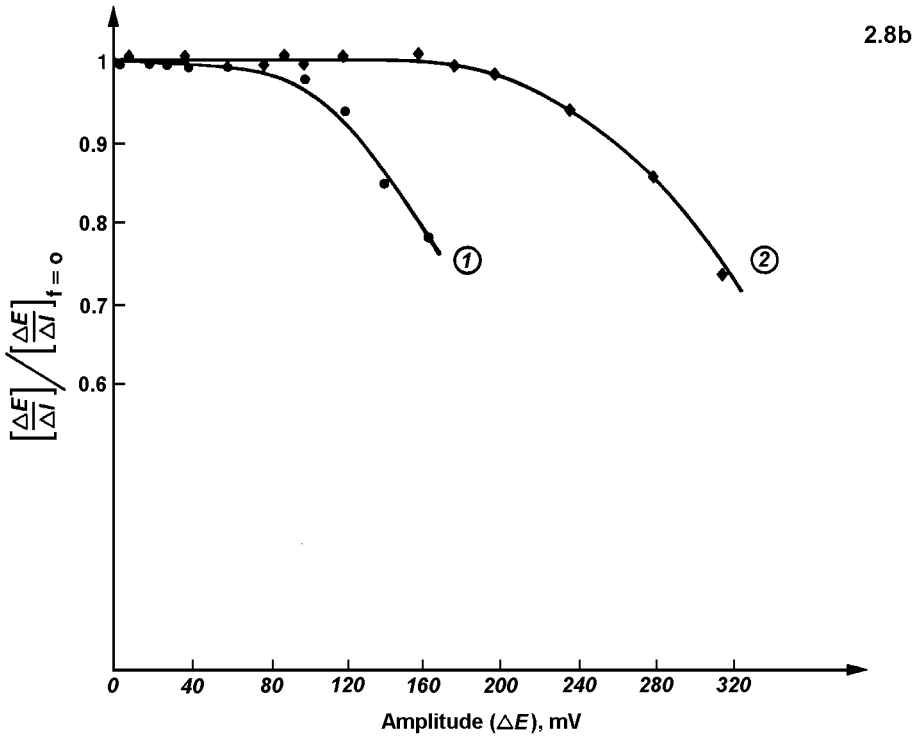

Fig 2.8 Definition and checking of the linear regime (from [2, 7]):

a) linear domain (the amplitude of the measurement signal has to be in the white region at a given frequency) for various polarisation points U_1, U_2, U_3

b) Variation of the modulus of the impedance versus the amplitude of the perturbating signal

1) active iron in sulphuric medium at 10 Hz

2) passive nickel in sulphuric medium at 40 Hz

2.4.2 Measurement Techniques

2.4.2.1 A C Bridges [12]

AC bridges, inherited from electrolyte conductivity measurements, have been used to measure electrochemical impedance for a long time. Their availability is such in some laboratories that numerous experimenters still use them. They were improved in order to be compatible with the electrochemical cell. However, although they are very accurate, their use is very time-consuming. In addition, their useful frequency range (f≥10Hz) is too limited for many electrochemical studies. By balancing the ac bridge (Fig 2.9a), it is possible to lower the non-equilibrium signal measured by the detector D down to zero, when

$$Z_1 Z_4 = Z_2 Z_3 \qquad (2)$$

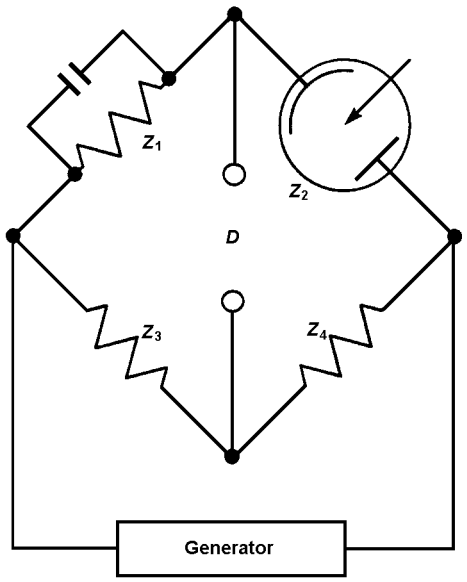

Fig 2.9a Impedance measurement: ac bridge method

2.4.2.2 Lissajous Figures [7]

This very simple method allows the impedance to be measured over a wide frequency range, provided that an XY oscilloscope is available for higher frequencies (f ≥5Hz) and a storage XY oscilloscope or an XY recorder is available for lower frequencies (f <5Hz).

If $e(t) = \Delta E \sin \omega t$ is used as a perturbating signal of an electrochemical system of impedance

$$Z = |Z| \exp(-jf) \qquad (3)$$

then a current

$$i(t) = \frac{DE}{|Z|} \sin(wt + f) \qquad (4)$$

can be observed.

If $e(t)$ is connected to the horizontal plates of an oscilloscope and $i(t)$ to the vertical plates, the ellipse depicted in Fif 2.9b is observed on the display. Characteristic quantities can then be determined.

$$OA = e\left(wt = \frac{p}{2}\right) = DE \tag{5}$$

$$OB = i\left(wt = \frac{p}{2} - f\right) = \frac{DE}{|Z|} \tag{6}$$

$$OD' = e(wt = -f) = -DE \sin f \tag{7}$$

Hence, the modulus and the phase of the impedance can be calculated:

$$|Z| = \frac{AA'}{BB'}; \qquad \sin f = \frac{DD'}{AA'} \tag{8}$$

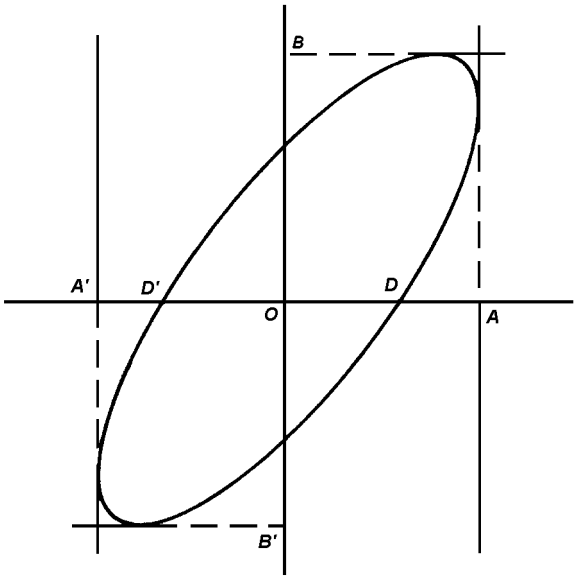

Fig 2.9b Impedance measurement: Lissajous figure method

2.4.2.3 Simultaneous Plotting of the Current and the Voltage [7]

An XY recorder can be used to analyse low and very low frequencies (f<1Hz, or above, limited by the bandwidth of the recorder) by simultaneously plotting the current and the voltage (Fig 2.9c). Comparison of the two recordings gives directly the rnodulus and the phase of the impedance.

$$|Z| = \frac{DE}{DI}; f = DF \tag{9}$$

2.4.2.4 Phase Sensitive Detection (Lock-in Amplifier) [9, 10]

The in-phase and out-of-phase components of the cell response to the perturbating signal are successively analysed by various techniques. For example, the perturbating signal is applied simultaneously to the cell and a reference channel (Fig 2.9d). The cell response is successively compared using a phase sensitive detector, with the perturbating signal shifted by $\Delta\phi$ and $\Delta\phi + \pi/2$. The analysis results depend very much on the phase detector technique used, but it is not normally possible to measure irnpedances with a perturbating frequency below 1Hz.

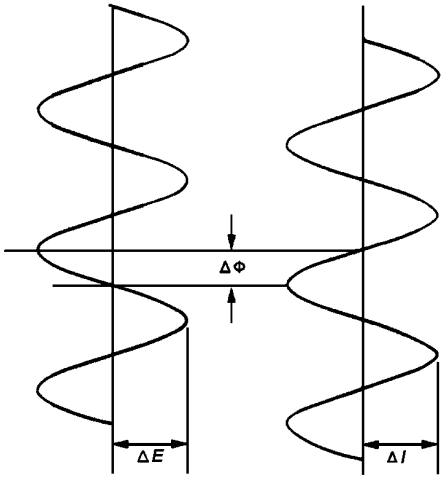

Fig 2.9c Impedance Measurement
Simultaneous plotting of current and voltage

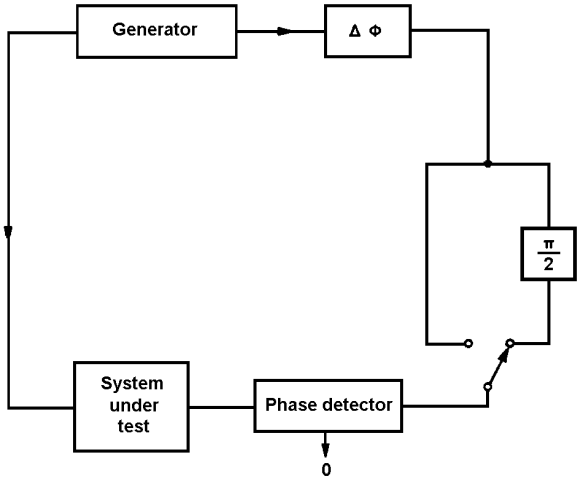

Fig 2.9d Impedance Measurement
phase sensitive devices

2.4.2.5 Digital Frequency Response Analyser

The principle of transfer function measurement is schematised in Fig 2.10. The cell response $S(t)$ to the perturbating signal

$$x(t) = X_o \sin \omega t \qquad (10)$$

is correlated with two synchronous reference signals, one in phase with $x(t)$ and the other 90° out of phase, i.e. sin wt and cos wt, in order to calculate:

$$Re = \frac{1}{T}\int_0^T S(t) \sin wt dt \qquad (11)$$

$$Im = \frac{1}{T}\int_0^T S(t) \cos wt dt \qquad (12)$$

where $S(t) = X_o K(w) \sin[wt + f(w)] + \sum_m A_m \sin(mwt - f_m) + n(t)$ (13)

is the sum of the various harmonics and parasitic noise for a cell with a transfer function

$$K(w)e^{jf(w)} \qquad (14)$$

T, the integration time, equals an integer number of periods of the perturbating signal.

Considering harmonics, the only non-zero integral is given by the first harmonic (fundamental); all other harmonics are rejected. With noise, however, total rejection is possible only if the integration time T is infinite. The equivalent filter would have an infinitely narrow bandwidth, centred on the generator frequency. Hence:

$$Re = \lim_{T \to \infty} \frac{1}{T}\int_0^T S(t) \sin wt dt = X_o K(w) \cos f(w) \qquad (15)$$

$$Im = \lim_{T \to \infty} \frac{1}{T}\int_0^T S(t) \cos wt dt = X_o K(w) \sin f(w) \qquad (16)$$

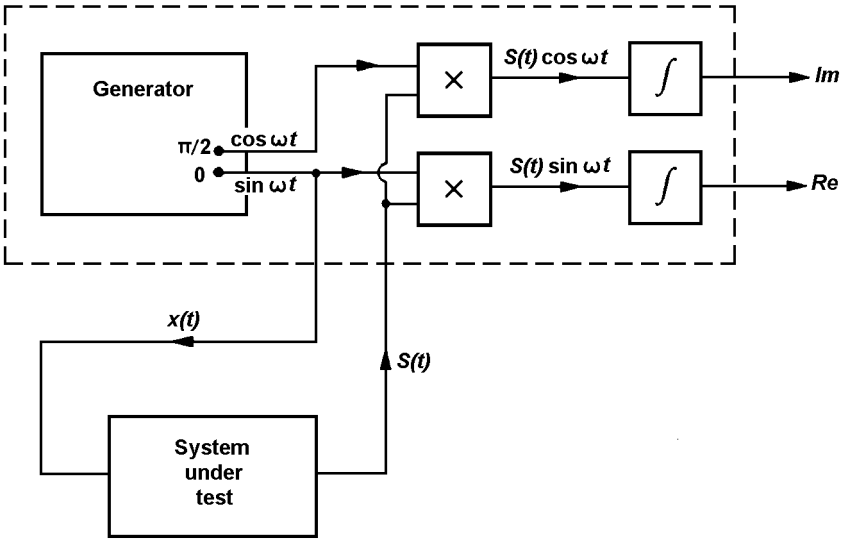

Fig 2.10 Frequency Response Analyser – working principle
Im: imaginary part
Re: real part
$x(t)$: perturbating signal; $S(t)$: cell response signal

These two quantities, proportional to the real part and to the imaginary part of $S(t)$, are obtained, and hence the impedance is known.

However, the measurement time T cannot, in practice, be infinite and hence the equivalent filter has a bandwidth dependent on T. The improvement in the signal-to-noise ratio can be calculated. The parasitic noise, which is assumed to be white with power spectral density b, is reduced to a bandwidth $Df = \frac{1}{T}$ with the same spectral density. The uncorrelated noise is then rejected as the integration time is T increased. Hence the equivalent filter has a selectivity:

$$\frac{Df}{f_1} = \frac{1/T}{f_1} = \frac{(1/N)f_1}{f_1} \qquad (17)$$

$$\frac{Df}{f_1} = \frac{1}{N} \qquad (18)$$

where f_1 is the analysed frequency and N the period number. Using this signal processing technique, an exceptional performance can be obtained, e.g. for impedance measurement at 1 Hz, with integration over 100 periods, the equivalent bandwidth is 0.01Hz.

For studies on fast enough processes (0.1 to 50kHz), an entirely analog instrument can be designed on the same principle [13]. However, for most electrochemical studies, where very low frequencies need to be analysed, digital techniques have to be used. Digital frequency response analysers (FRA) are quite adequate to perform such measurements.

Example of Experimental Arrangement

An example of an experimental arrangement is given in Fig 2.11. It should be noticed that this arrangement would be very similar if, instead of using a FRA, an oscilloscope was employed to display Lissajous figures, or a lock-in arnplifier was used.

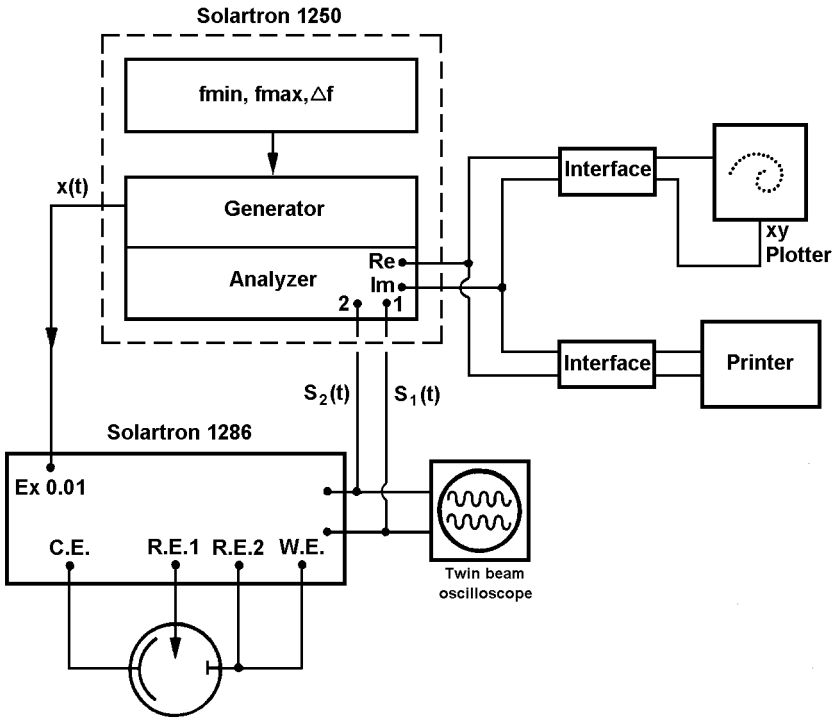

Fig 2.11 Electrochemical impedance measurement

Example of experimental arrangement based on:

- Solartron 1250 FRA with frequency programming: f_{min} = minimum frequency, f_{max} = maximum frequency, Δf = frequency increment (i.e. log or lin) defining the measurement frequency range.
- Solartron 1286 Electrochemical Interface

The Solartron two channel 1250 series FRA automatically and simultaneously measures the in-phase (or real) and out-of-phase (or imaginary) components, with reference to the perturbating signal x(t). The real and imaginary parts of the transfer function, H_{12} between the two channels can then be automatically calculated from these components (denoted A and jB respectively) using the relationship

$$H_{12}(w) = \frac{S_2(w)}{S_1(w)} = \frac{A_2 + jB_2}{A_1 + jB_1} \tag{19}$$

$H_{12}(\omega)$ is directly related to the irnpedance of the cell without any influence of the regulating device Examples of potentiostatic and galvanostatic measurements follow.

In the potentiostatic mode, if $S_1(t)$ is the current and $S_2(t)$ is the voltage across the cell, one has (from Fig 2.5b)

$$S_1(w) = G_I R \frac{K_1 X_o}{Z} \tag{20}$$

$$S_2(w) = G_V K_1 X_o \tag{21}$$

$$H_{12}(w) = \frac{G_V}{G_I} \frac{Z}{R} \tag{22}$$

In galvanostatic mode, if $S_1(t)$ is the current and $S_2(t)$ is the voltage across the cell, one has (from Fig 2.6)

$$S_1(w) = G_I \frac{K_2 X_o}{R} R = G_I K_2 X_o \quad (23)$$

$$S_2(w) = G_V Z \frac{K_2 X_o}{R} \quad (24)$$

$$H_{12}(w) = \frac{G_V}{G_I} \frac{Z}{R} \quad (25)$$

where K_1 and K_2 are, respectively, the transfer functions of the potentiostat and the galvanostat, R the standard resistor used for measuring the current, and G_V and G_I the gains of the voltage and current amplifiers. Hence, if R is chosen so that there are no inductive or capacitive components over the frequency range of interest and if the amplifiers are such that $G_V = G_I = 1$ at low frequencies and they are balanced for higher frequencies, i.e. the amplifiers have the same phase shift at a given frequency, the impedance is equal to

$$Z(w) = RH_{12}(w) \quad (26)$$

In the present state of the art it is possible to measure and plot the electrochemical impedance automatically. With the Solartron 1250 Series FRA, the generator can be programmed to sweep from a minimum frequency (f_{min}) to a maximum frequency (f_{max}) in a number of steps Δf in the required frequency range. Thus the measurement frequency is changed automatically and hence the total measurement time for one experiment can be reasonably short. Table 2.1 shows the measurement time for various frequency ranges, using 5 frequency steps per decade.

Frequency Range	**Measurement Time**
50kHz to 0.1Hz	31s
50kHz to 0.01Hz	5m 25s
50kHz to 0.001Hz	53m 20s

Table 2.1

Automatic plotting of the experimental data can be performed in two ways, depending on the availability, or non-availability, of a computer. Thus a digital or analogue X-Y recorder allows direct plotting of impedance diagrams and a printer provides a copy of digital data. Alternatively, the digital data are transferred to the memory of a computer, which allows any graphical representation or subsequent digital processing (e.g. parameter identification).

Further devices are used to measure electrochemical impedances. The summing amplifier is used with a gain of 0.01 for the analysing signal (this gain is necessary because digital generators have a low signal-to-noise ratio at very low level and it is better to use a 1V signal reduced by a factor of 100 than a 0.01V signal).

The voltage and current amplifiers should have a high common mode rejection and a wide bandwidth. In addition, they need to have an offset capability in order to eliminate the dc component of the analysed signal.

It is also necessary to use an oscilloscope (bandwidth ≥10MHz) that is sufficiently sensitive (e.g. 1mV/div.) for monitoring the measurement signals. Its use avoids many experimental problems due to regulation instabilities, signal distortion when the signal level is too large, or an excessive parasitic noise level.

2.4.2.6 High Frequency Measurements

For f ≥10^5Hz further consideration must be given to the aspects of cell impedance measurement discussed in § 2.4.1. In relation to the frequency range, the general structure of the experimental arrangement is of importance (e.g. short electrical leads) because of leakage components (inductive or capacitive). For very low impedance measurements (IZI<1Ω), the same care must be taken where f ≤10^5Hz.

For very high frequencies (f ≥1MHz) coaxial structures have been used [14, 15]. In the $10^5 \le f \le 10^6$ Hz range in potentiostatic mode it can be advantageous to use two different reference electrodes: one for the regulation, the other for measuring the analysing signal.

2.4.2.7 Impedance Determination Using a Computer

Progress in digital algorithms and in circuit design has led to an increase in the use of on-line computers in electrochemistry. With this method the fast Fourier transform (FFT) algorithm is used to calculate the electrochemical impedance.

As $$Z(w) = \frac{E(w)}{I(w)} \qquad (27)$$

Hence $$Z(w) = \frac{E(w) \cdot E^*(w)}{I(w) \cdot E^*(w)} \qquad (28)$$

where $E(\omega)$ or $I(\omega)$ are the Fourier transforms of the low amplitude voltage and current, respectively, (either one being the perturbating signal) and $E^*(\omega)$ the complex conjugate of $E(\omega)$. As small amplitude techniques can lead to the impedance regardless of the specific excitation waveform used, various types of perturbating signal have been used [16]: step [17, 18], pseudo-random white noise [19 – 22], multi-frequency [23 – 25].

The main reason for using a broad band perturbating signal and FFT analysis is one of time saving over the frequency by frequency method. However, due to the inherent noise encountered in signal measurement, the FFT analysis has to be repeated a number of times to enable the effect of noise on the impedance measurement to be averaged out. Although, in a noisy environment, it is necessary to average over a few signal periods with the FRA also, it seems that the difference between the two methods is not as great as was originally believed. A thorough comparison is lacking but, in practice, the following general rule seems to apply. When the system being measured is steady-state over a reasonably long time then FRA analysis is better to use, since it is more accurate and convenient. When the system state is time varying, however, the demand for measurement accuracy is not too stringent and the system response is known to be linear then FFT analysis may be used.

The frequency by frequency measurement allows the frequencies to be chosen. Generally these values are chosen in order to keep $\frac{\Delta f}{f}$ constant (where Δf is the frequency step and f the frequency of measurement). Conversely, the FFT algorithm gives a constant Δf over the whole frequency range. Hence, in order to obtain a good resolution in the lowest part of the frequency range, redundant frequency measurements are obtained in the highest part. This often leads to the use of a large number of signal samples, and necessitates the use of a computer with a large memory.

2.4.2.8 Ohmic Drop Measurement and Correction

A severe limitation of the non steady-state techniques comes from the electrolyte resistance R_e located between the equipotential surface defined by the reference electrode and the working electrode. The finite conductivity of the electrolyte limits the use of these techniques by adding a parasitic ohmic drop in series with the Faradaic overvoltage. When this ohmic drop is large compared with the latter it is difficult to obtain accurate results of the Faradaic processes. Potentiostatic modes are basically affected. The Habber-Luggin capillary technique could be used to diminish ohmic drop, but not to cancel it completely.

Electrolyte Resistance Measurement

Electrolyte resistance, R_e, can be evaluated either by high frequency impedance measurement or by an interruptor technique. The first method is based on the fact that the high frequency limit of the impedance is generally equal to R_e, e.g. R_e is often obtained for a 50kHz measurement in aqueous medium. When the polarisation current I_o is suddenly cut, the voltage, observed on a wide bandwidth oscilloscope, shows a steep drop ΔE (Fig 2.12a). This drop is followed by an exponential-shaped relaxation due to the double layer capacitance and to the Faradaic processes. It is assumed that ΔE is equal to the global ohrnic drop located between the reference electrode and the working electrode [26].

$$R_e = \frac{DE}{I_o} \tag{29}$$

However, this is an approximation, because the ohrnic drop is characteristic only of the primary distribution of the current on the surface of the electrode, i.e. that involved for extremely fast interfacial processes (no electrochemical overvoltages). The ohmic drop characteristic of the secondary distribution is not measurable [27]. Also, due to the current distribution on the electrode surface the measured ohmic drop is global and is only rigorously valid at one point of the electrode.

The interruption of the polarisation current can be done in three ways (Fig 2.12):

i) by using a relay with a very short break time (e.g. 10^{-9} s for a wetted contact mercury relay) [26].

ii) by using a fast diode, rapidly polarised in reverse by an impulse [28, 29]

iii) by using a metal oxide semiconductor field effect transistor (MOSFET) switch, as in the Solartron 1286.

With these techniques, if the current is interrupted for a few hundreds of μs at a frequency within the range tens of Hz to low kHz, the signal can be conveniently observed on an oscilloscope without undue perturbation of the steady-state polarisation and, hence, of the studied process. The Solartron 1286 uses a sample and hold technique enabling the compensated impedance to be determined from the measurement of I_o and E_o - ΔE, as defined in Fig 2.12.

Electrolyte Resistance Compensation and Correction

Various circuits have been proposed to compensate for ohmic drop [30]. These circuits are based on a positive feedback principle (e.g. Fig 2.7 without the filter on the current feedback).

With this, however, instability problems arise if the electrolyte resistance is compensated at more than 80%. Exact compensation or overcompensation yields to instability.

In order to study slow processes, i.e. low frequency processes in terms of impedance, frequency-dependent over-compensation can be used. However, the stability problem can be avoided by correcting the ohmic drop out of the feedback loop of the potentiostat. An analog quantity, KI, proportional to the current flowing through the cell, is subtracted from the potential difference, E_{ref} between the reference and working electrodes, and a voltage

$$E_c = E_{\text{ref}} - KI \tag{30}$$

is obtained. Hence the electrolyte resistance can be corrected exactly ($K = R_e$), overcorrected ($K > R_e$), or partially corrected ($K < R_e$), without any influence on the stability of the potentiostatic regulation Fig 2.13 [31]. This real part control of the impedance allows the impedance to be measured with a better accuracy, especially for the phase, because the phase of the measured impedance varies much more than without correction, e.g. over more than 180° in Fig 2.14, instead of about 10°.

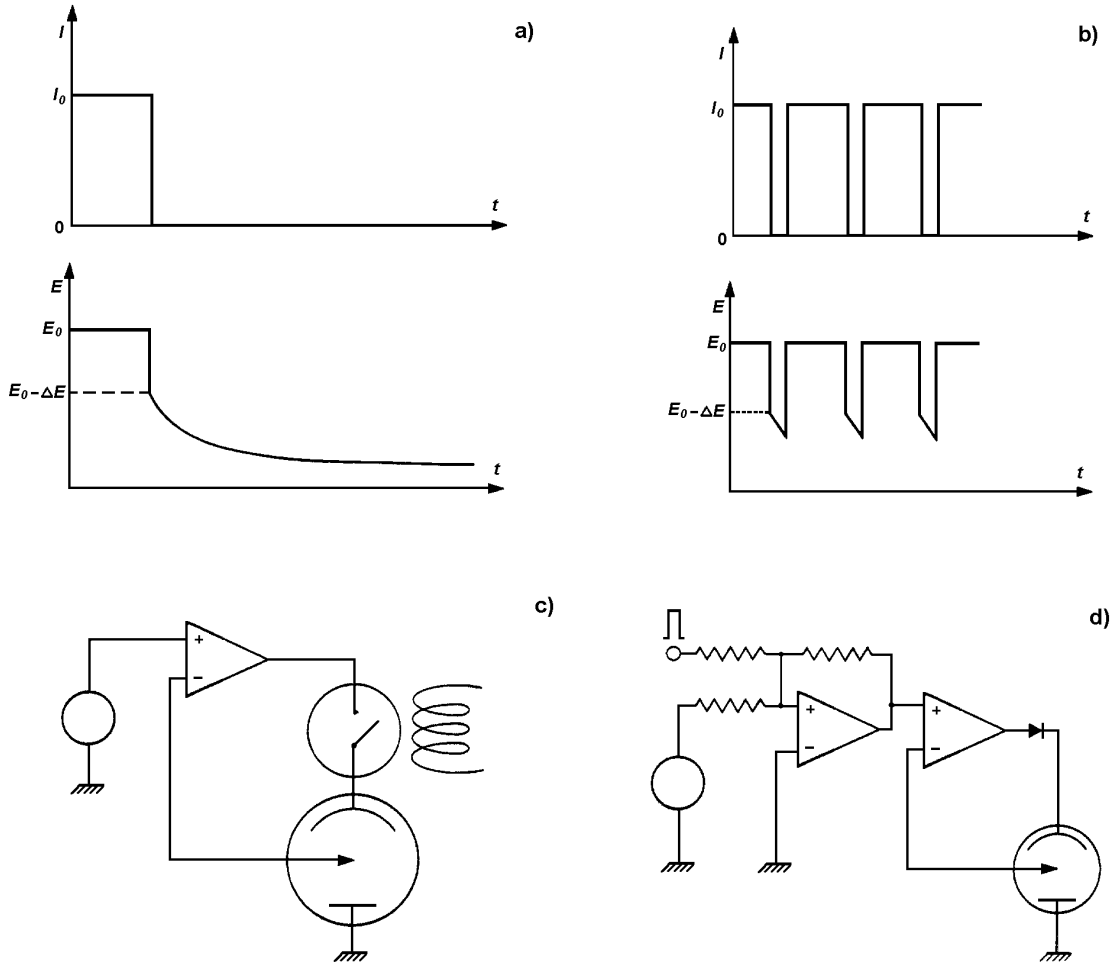

Fig 2.12 Ohmic drop measurement:

(a) Single interruption technique, ΔE: ohmic drop
(b) Periodic interruption technique
(c) Use of a relay
(d) Use of a diode

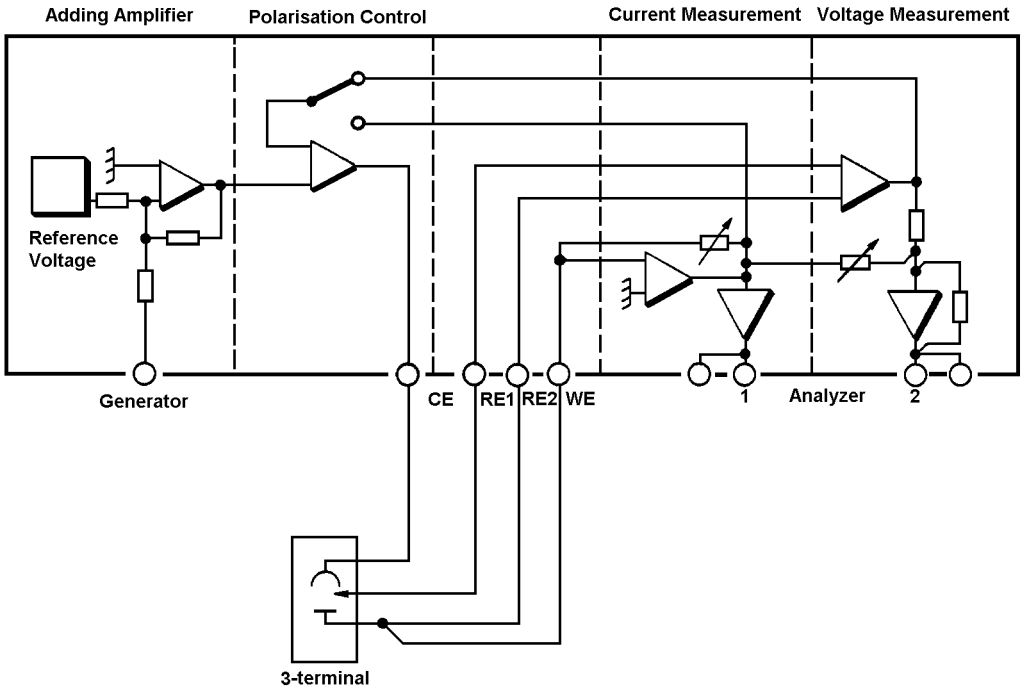

Fig 2.13 Circuit for real part correction of the impedance measurement (Solartron 1286)

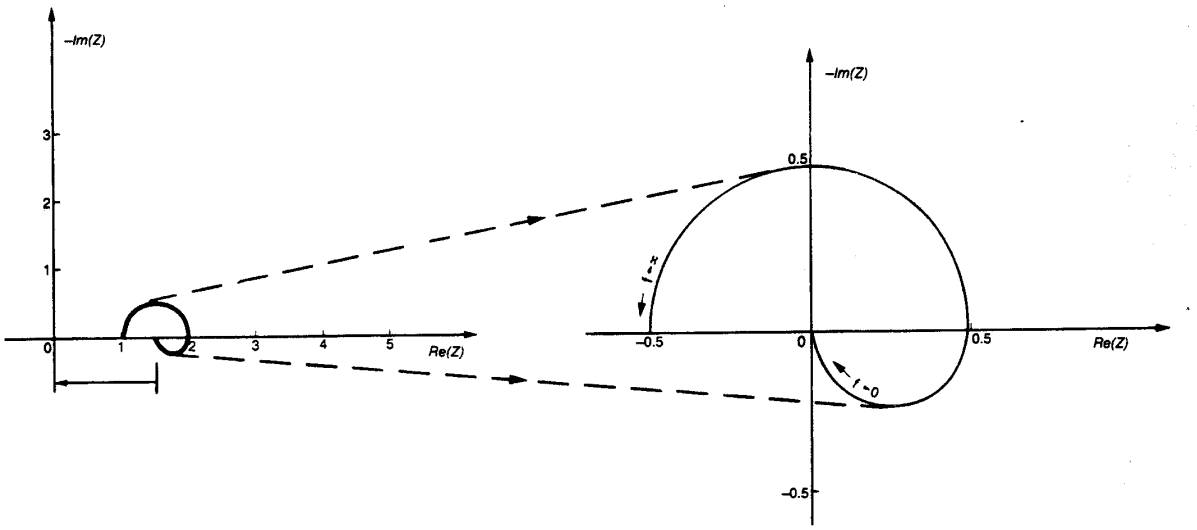

Fig 2.14 Improvement of the impedance measurement accuracy by the use of real part correction of the impedance (Solartron 1286)

REFERENCES FOR CHAPTER 2

1. L RAILLON, *These Paris*, 1979
2. C GABRIELLI, *These Paris, 1973 Metaux, Corrosion Industrie* No 573 pp 171 - 184, No 574 pp 223-244, No577 pp309-327, No578 pp356-369, 1973
3. I EPELBOIN, C GABRIELLI, J C LESTRADE, M KEDDAM and H TAKENOUTI, *J Electrochem Soc* 119, pp 1632 - 1637, 1972
4. D DEROO, J P DIARD, J GUITTON and B LE GORREC, *J Electroanal Chem* 67, pp 269 - 276, 1976
5. C GABRIELLI, *Cinetique Electrochimique, Instrumentation Electrique, Techniques de l'Ingenieur* D901,1980
6. R L VAN MEIRRAEGHE, E C DUTOIT, F CARDON and W P GOMES, *Electrochim Acta* 20, pp 995 - 999, 1975
7. M KEDDAM, *These Paris* 1968
8. G M HIEFTJE, *Anal Chem* 44, No 6 pp 81A - 88A, and No 7 pp 69A - 78A, 1972
9. R de LEVIE and A A HUSOVSKY, *J Electroanal Chem* 20, pp 181 - 193, 1969
10. R D ARMSTRONG and M HENDERSON, *J Electroanal Chem* 40, pp 121 – 131, 1972
11. C GABRIELLI and M KEDDAM, *Electrochim Acta* 19, pp 355 - 362, 1974
12. R D ARMSTRONG, W P RACE and H R THIRSK, *Electrochim Acta* 13, pp 215 – 239, 1968
13. C CACHET, H CACHET and J C LESTRADE, *Electrochim Acta* 19, pp 891 - 894, 1974
14. R DURAND, *These Grenoble* 1978
15. R DURAND, J AMOSSE and M J BARBIER, *Electrochim Acta* 19, pp 207 – 214, 1974
16. S C CREASON, J W HAYES and D E SMITH, *J Electroanal Chem* 47 pp 9 - 46, 1973
17. H B SIERRA-ALCAZAR, A N FLEMING and J A HARRISON, *J Electroanal Chem* 87, pp 339 - 345, 1978
18. D E SMITH, J W HAYES and S C CREASON, *J Electroanal Chem* 101, pp 253 – 256, 1979
19. S C CREASON and D E SMITH, *J Electroanal Chem* 36, App 1 – 7, 1972
20. G BLANC, I EPELBOIN, C GABRIELLI and M KEDDAM, *Electrochim Acta* 20, pp 599 – 601, 1975
21. W H SMYRL, *Proc of the ASTM Symposium*, San Francisco, May 1979 (to be published)
22. M ICHISE, Y NAGAYANAGI and T KOJIMA, *J Electroanal Chem* 70, pp 245 – 252, 1976
23. S C CREASON and D E SMITH, *J Electroanal Chem* 40, App 1 - 5, 1972
24. R J SCHWALL, A M BOND, R J LOYD, J G LARSEN and D E SMITH, *Anal Chem* 49 pp 1797 - 1805, 1977
25. R de LEVIE, J W THOMAS and K M ABBEY, *J Electroanal Chem* 62, pp 111 - 125, 1975
26. Ph MOREL, *These Paris*, 1968
27. W H TIEDEMAN, J NEWMAN and D N BENNION, *J Electrochem Soc* 120, pp 256 - 258 1973
28. D BRITZ and W A BROCKE, *J Electroanal Chem* 58, pp 301 - 311, 1975

29. J D E McINTYRE and W F PECK, *J Electrochem Soc* 117, pp 747 - 751,1970

30. D BRITZ, *J Electroanal Chem* 88, pp 309 - 352, 1978

31. C GABRIELLI, M KSOURI and R WIART, *Electrochim Acta* 22, pp 255 - 260, 1977

3 Applications of Electrochemical Impedance Measurement

3.1 Mass Transfer

The rate of an electrochemical process is governed both by the electron transfer at the interface and by the mass transfer rate of the reactants towards the interface, which are due to migration, convection and diffusion, as shown in § 1.2.2. Where the influence of the mass transfer can be neither neglected nor eliminated, it has to be carefully controlled by governing the hydrodynamic conditions, in order to study the coupling between the Faradaic and transport processes by impedance measurements (e.g. by using a rotating disc electrode). Alternatively, electrochemical techniques, and particularly impedance measurements, can be used to obtain information on fluid mechanics. These two complementary aspects are examined below.

3.1.1 Diffusion and Convection Processes

As already indicated in § 1.2.2 the influence of migration can easily be obviated and in that case only diffusion and convection act. The impedance has been measured when the rate of the reduction step (or oxidation step) of a Redox system is limited, or partially limited, by the transport of the ions towards the electrode in diluted solution, using a rotating disc electrode. Experimental results (between 0.15Hz and 180Hz) are shown in Fig 3.1 [1, 2], together with calculated impedance values. The calculated values were obtained in two ways: curve 'a' by the use of Nernst's approximation (see § 1.3.2.2), and curve 'b' by taking into account the convection term (see § 1.2.2). From these measurements the diffusion coefficients of the reacting species can be determined. Measurements have been made in concentrated media but full interpretation is still lacking, e.g. in Fig 3.2 the diffusion impedance is the lowest frequency loop [7, § 2].

Other types of cell geometry have been used. Thin layer cells contain a minute volume Of solution and the ohmic drop is very low due to the small distance (some tens of μm) between the two electrodes. Hence this cell can be attractive for electroanalysis [3, 4].

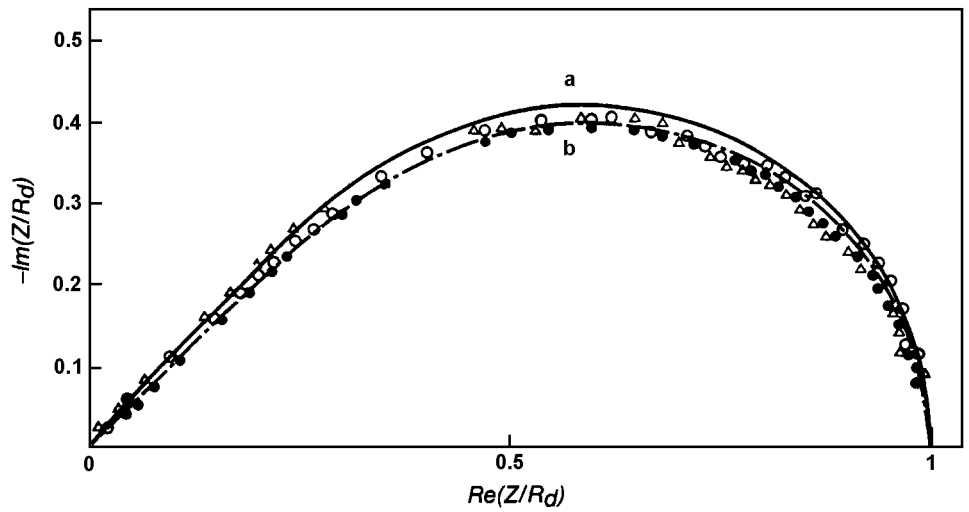

Fig 3.1 Impedance measurement in normalised coordinates [$R_d = Z(f \rightarrow 0)$] for the reaction

$Fe(CN)_6^{3-} + e \rightarrow Fe(CN)_6^{4-}, [FE(CN)_6^{3-} = 10^{-3} M]$, with the disc electrode rotating at 1800 rpm and at a current $(o)\frac{3}{4} i_d, (D)\frac{1}{2} i_d, (\bullet)\frac{1}{4} i_d$, where i_d is the limiting current (from [1])

curve (a) calculated impedance under Nemst's approximation

curve (b) calculated impedance taking into account the convection term (from [2])

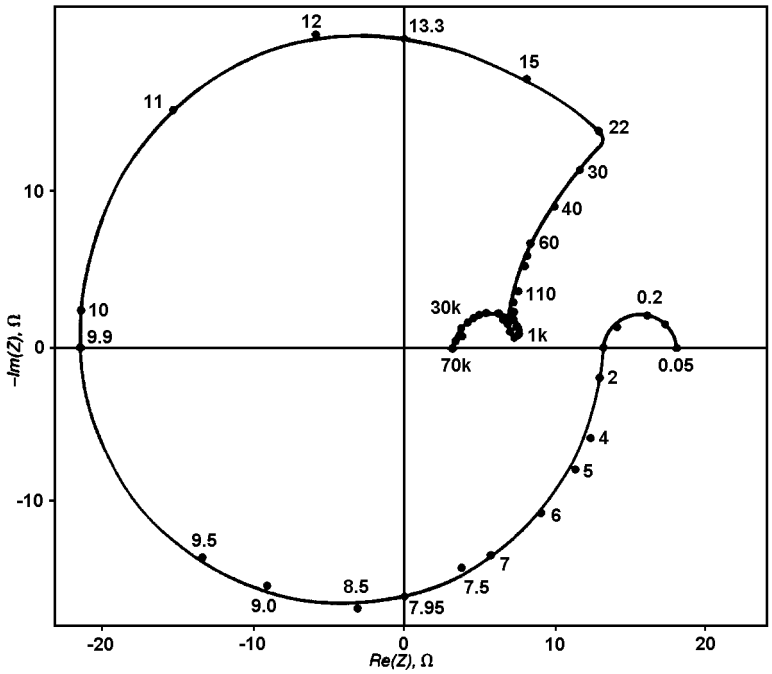

Fig 3.2 Impedance diagram of nickel in H_2SO_4, 20N at E_{ref} = 1.4V/SCE, with the disc electrode rotating at 400rpm (A=0.2cm^2) (from [7 § 2])

For intermediate kinetics on a uniformly active and accessible electrode surface the current *I* flowing through the interface is related to the rotation speed Ω of a rotating disc electrode by

$$I^{-1} = A + B^{-1}W^{-1/2} \qquad (1)$$

(A = 0 for a totally diffusion controlled process).

However, this behaviour (eqn 1) can also be explained by a diffusion controlled process on a partially active electrode (blocked electrode). The theory has been proposed that it is possible to obtain the values of coefficients A and B in eqn (1) by relating the dimensions of the active sites to the thickness of the Nernst diffusion layer [5, 6]. Experimental results seem to support this [7, 8].

3.1.2 Hydrodynamic Processes

Some hydrodynamic processes have been studied by using electrochemical techniques, particularly those of impedance measurement. For example, mass transport was studied for KCI, 1N medium containing polyethylenoxide (polymer) and a Redox couple. By measuring the impedance it was shown that, in laminar flow, the diffusional properties are modified only when the Newtonian behaviour of the solution is lost. In turbulent flow the radial component of the local drag reduction has been measured, in a layer whose thickness is about one μm [9] (Fig 3.3).

Similarly, by comparing experimental results with a theoretical calculation of the diffusion impedance in an Ostwald fluid, the molecular diffusion coefficient of the diffusing species has been shown to remain unchanged. This is with regard to that in pure solvent in solution, for which the apparent viscosity varies over a wide range [10].

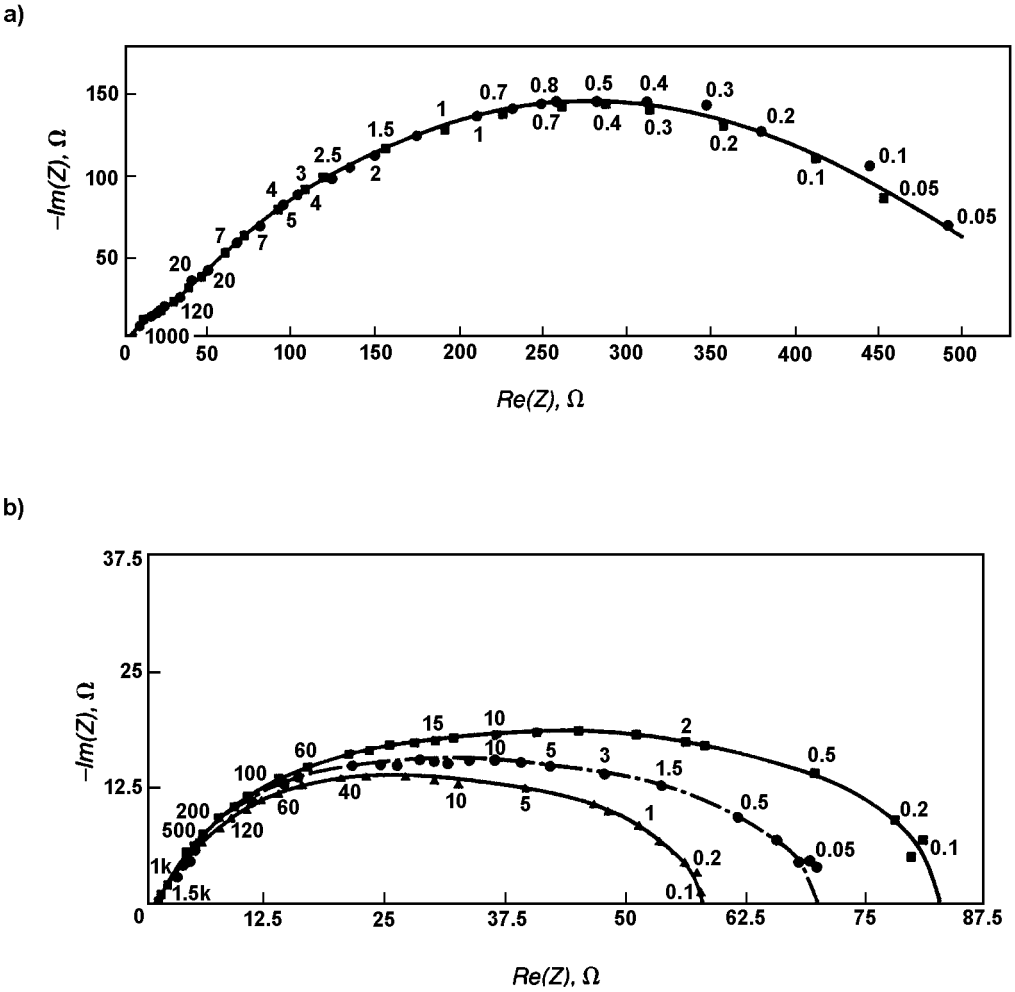

Fig 3.3 Impedance diagram of a rotating thin ring electrode (radius R = 34 mm, ΔR=0.1mm, made of platinum) for the ferri-ferrocyanide system in KCl, 1N, after adding a minute concentration of polyox WSR 301

(a) laminar region Reynold's number Re = 2.6 x 10^4 (■: 0 ppm; ●: 10ppm)

(b) turbulent regime Re = 5.1x10^5 (▲: 0 ppm; ●: 5ppm; ■: 40 ppm) (from [9])

Long chain linear polymers undergo an expansion in the water solvent and this results, for semi-dilute solutions, in an entangled network. This change in the medium structure has a large influence on the rheology of the fluid, which explains the viscosity increase, whereas the network mesh dimension remains large in relation to that of the diffusing species. Hence no variation is observed in the molecular diffusion coefficient.

3.1.3 Mass Transfer in Porous Electrodes

Some technological applications need a very large surface of contact between the electrode and the electrolyte (e.g. in battery devices) which leads to the use of porous electrodes. The complexity of the random structure of the porous electrode leads people to study simple single pore models. Of the possible shapes modelled the cylindrical pore has been most thoroughly investigated, both by analogy with the distributed electrical line and by direct integration of the equations describing the pore [11 – 14]. In order to take into account the random nature of a porous electrode a size distribution function of the pores can be considered.

The variation of the impedance with frequency has been examined for various geometries of a single pore, and the type of results obtained are shown in Fig 3.4 [15]. It can be shown that the more occluded the shape of a pore the more the impedance exhibits a pseudo transfer resistance. Hence, the form of the pore structure can be ascertained by comparing porous electrode impedance values (Fig 3.5) [16, 17]. From a general point of view it can be shown that if the local interfacial impedance on the wall of the pore is Z then the global impedance of the pore is $\sqrt{Z}$ [12], e.g. if the heterogeneous processes are diffusion limited in the pore, the impedance will, in theory, be a straight line with a $\frac{p}{8}$ slope. A practical example, with a slope of 38°, is shown in Fig 3.6. Various types of porous electrode have been analysed experimentally by the use of this method [18, 19].

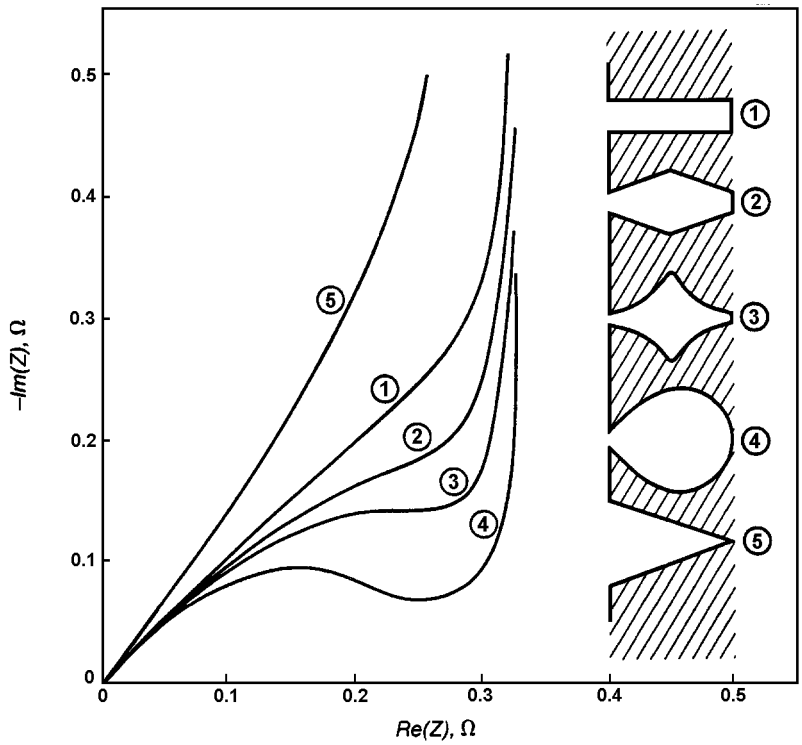

Fig 3.4 Calculated impedance for various shapes of a single pore (from [15])

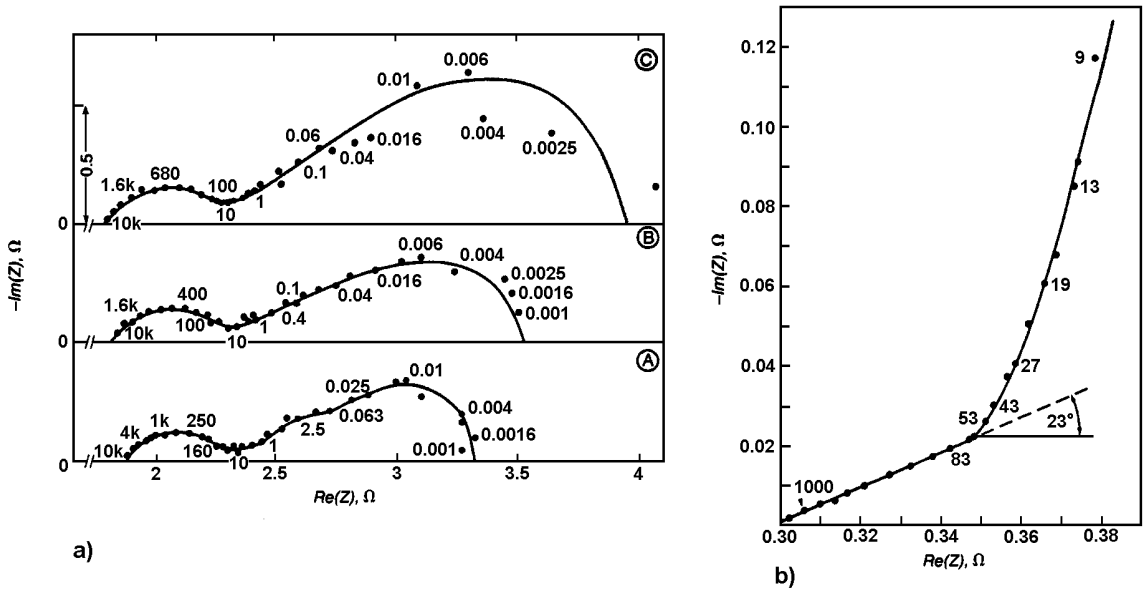

Fig 3.5 Impedance measurements on porous electrodes:

(a) hydrogen electrode made of Raney nickel (1cm^2) under a pressure of 1 atm at a current of A: 0mA, B:1mA; C:5mA (from [16])

(b) sintered plate cadmium electrodes in alkaline solution at –1000mV (from [17])

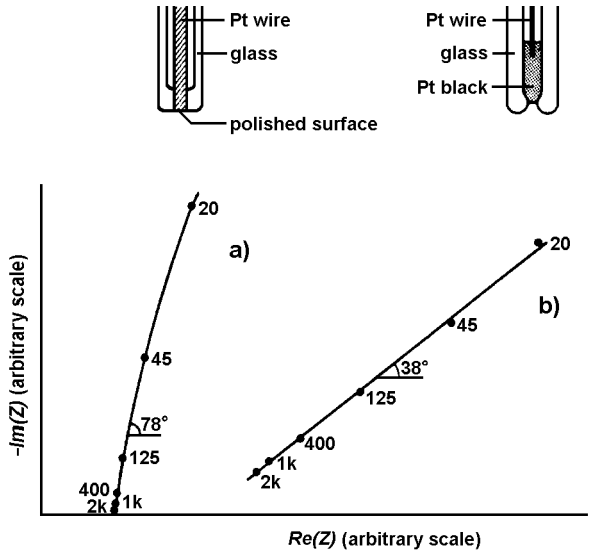

Fig 3.6 Impedance measurements on plane (a) and porous (b) Pt black electrode in 1M aqueous KCl (from [12])

3.1.4 Mass Transfer in Membranes

A membrane is a chemical entity that is interposed between two fluid media and allows a selective mass transfer between them. Among the various types, the ultrathin membranes are bimolecular lipid films which are good models of natural biological membranes. Thick membranes can be either solid or liquid and are used either as ion selective electrodes or as ionic filters. Due to their fundamental and practical interests, several studies using impedance techniques have been done in order to understand the complicated membrane phenomena.

Theoretical models have been proposed [20 – 22], to interpret the experimental results. Measurements performed on artificial ultrathin membranes (Fig 3.7) have made it possible to distinguish between the ion transport across the membrane itself and that across the water-membrane interface [23, 24].

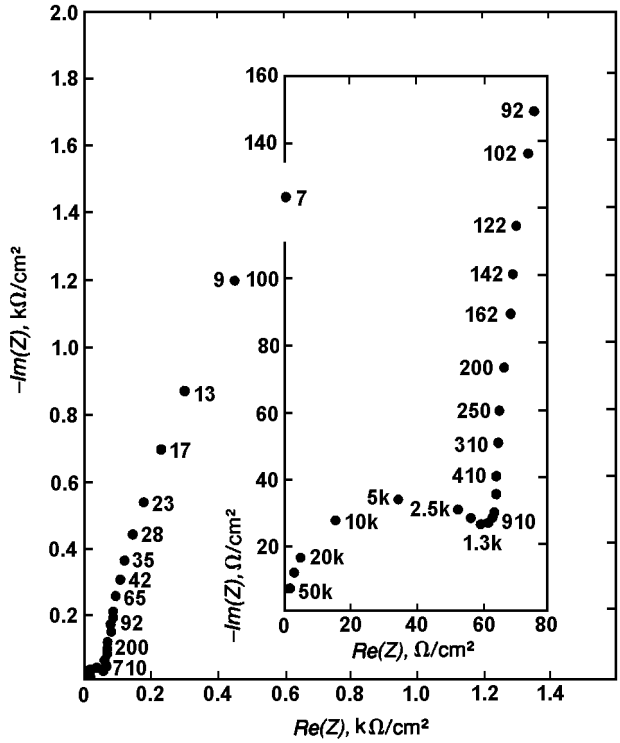

Fig 3.7 Impedance measurements on an ultrathin membrane in 10^{-5}M dipicrylamine in 0.1M NaCI. High frequency data are shown in detail in the insert (from [24])

Other measurements have been reported which relate to ion selective electrodes and provide. information on the kinetics and the mechanism of these sensors (see Fig 3.8; notice the magnitude of the impedances obtained) [25 – 28]. An example of the discoveries made in this field is the fact that, in the case of a glass membrane, the low frequency impedance is determined not by a diffusion controlled process but by a slow surface process [28].

Inherent difficulty in the study of the transport through the membrane is due to the fact that electrical quantities give information about both sides of the membrane at the same time. In the case of a liquid membrane this difficulty can be overcome by using two non-miscible media and hence studying one side at a time.

Three separate effects have been revealed by means of impedance measurements [29 – 31]:

i) ionic transfer polarisation

ii) diffusion polarisation

iii) charging of the diffuse layer

At low frequencies the slope of the impedance characteristic (linear part) obtained from these measurements is more than 45°, which is the slope for diffusion (see Fig 3.9). A model for this phenomenon has been suggested in [31] in which two adsorption states are considered, the two states corresponding to two different orientations of the adsorbed ion at the interface of the two liquids.

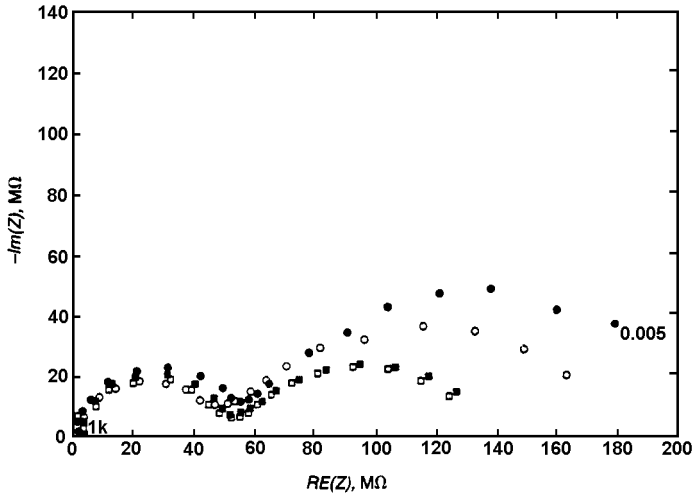

Fig 3.8 Impedance measurements on a Beckman E2 glass bulb electrode in 0.1M KCl (from [28])

● = before etching (KCl solution contact);

○ = before etching (hg contact);

■ = after 10% HF treatment (Hg contact);

□ = after 10% HF and 18M H_2SO_4 treatment (Hg contact)

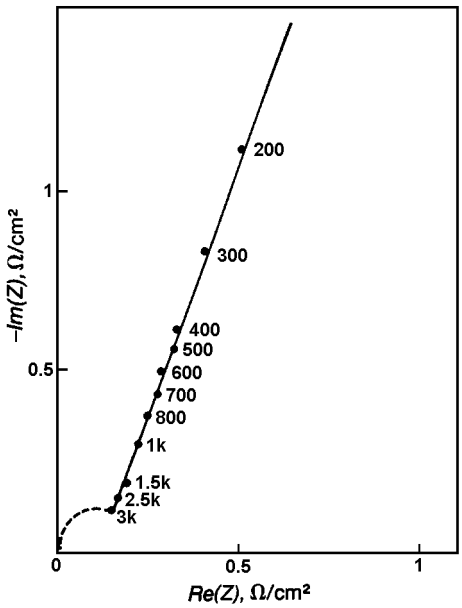

Fig 3.9 Impedance measurement at an interface between two non-miscible solutions containing organic ions of the alkyltrimethylammonium type (from [31])

3.2 Anodic Behaviour of Metals

Impedance measurements have frequently been used in the study of anodic behaviour of metals, either to obtain fundamental information on the active-passive behaviour (dissolution, passivation, passivity) or to obtain practical results related to the dielectric properties of the metal oxide, electrochemical machining, etc. A few examples of these applications follow.

3.2.1 Active-passive Transition of Metals

The behaviour of several metals has been studied in various aqueous media: acidic, neutral and basic [32]. Given its practical interest, iron has been extensively investigated, especially in acidic media as will be shown in the following examples.

3.2.1.1 Iron in Basic and Neutral Media

From pH = 14 to pH = 5 the current-voltage curve of an iron electrode is "bell-shaped", as shown in Fig 3.10 [32 – 36]. Impedances are similar for pH = 5 [32, 36] and pH 9.7 [33]: the lowest frequency capacitive loop in the activation range (positive slope of the current-voltage curve) transforms in the negative resistance loop characteristic of the passivation domain (negative polarisation resistance equal to the slope of the I-E curve). It can be seen that at least two reaction intermediates are involved in the active-passive transition, since at least two low frequency loops follow the high frequency loop. This latter is due to the charge transfer resistance and to the double layer capacitance. In the case of basic media, detailed reaction mechanisms have not been yet published and only qualitative analysis has been performed.

3.2.1.2 Iron in Sulphuric Acid Medium.

In the case of acidic medium (pH≤5) the main properties of the active-passive transition can be explained by the basic reaction sequence involving the three oxidation degrees of iron and species linked to hydroxyl ions. $Fe \xrightarrow{k_1} \underset{\downarrow k_2}{Fe(I)_{ads}} \underset{k'_3}{\overset{k_3}{\leftrightarrow}} Fe(II)_{ads} \underset{k'_4}{\overset{k_4}{\leftrightarrow}} Fe(III)_{ads}$ (Mechanism I)

$Fe(II)_{sol}$

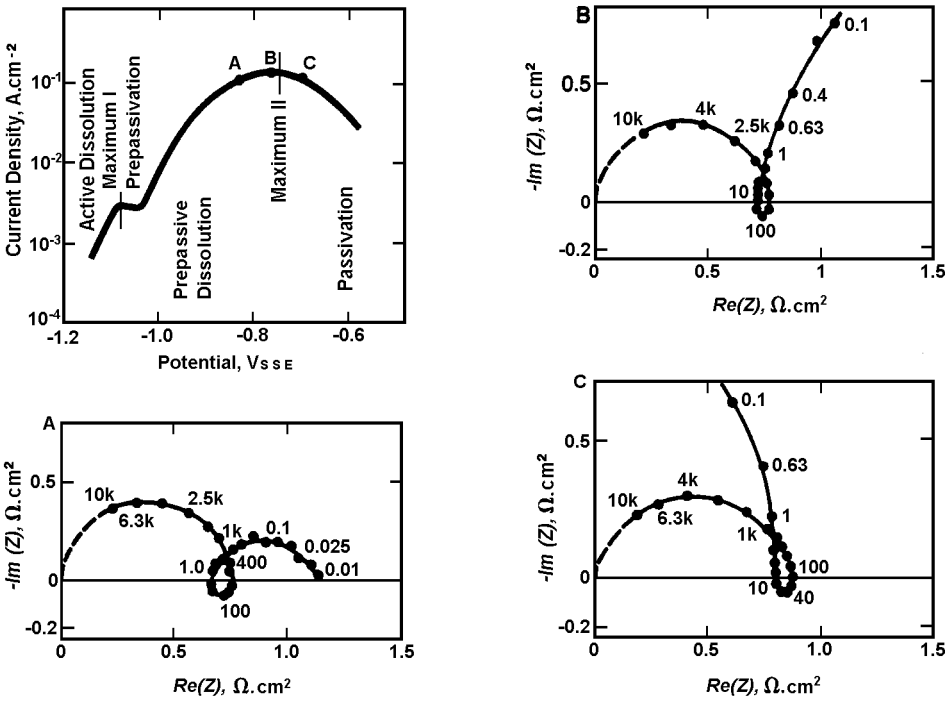

Fig 3.10 Steady-state current-voltage curve and potential dependence of impedance spectra for pure iron in sulphuric acid aqueous medium (pH = 5) disc electrode rotating at 1600 rpm (A = 0.2cm^2). (From [32, 36].)

For the full anodic behaviour of iron in sulphuric acid medium to be described, however, it is necessary to take into account other species with the same oxidation degree as in mechanism I but adsorbed onto the surface by other types of bonding. For example, the dissolution step involving sulphate anions is assumed to be catalysed by $Fe(OH)^-_2$ [37].

$$Fe \xrightarrow[k_1]{} (FeOH)_{ads} \xrightarrow[k_2]{} FeOH^+$$

$$\overset{OH^-}{k_5} \downarrow\uparrow \overset{H^+}{k_5} \qquad \text{(Mechanism II)}$$

$$\left(Fe(OH)^-_2\right)_{ads} \xrightarrow{HSO_4^-, SO_4^{--}} Fe^{++}$$

K_5 catal.

where the reaction rates k_1 and k_2 are the same as in mechanism I.

In the case of $0 \leq pH \leq 4$ diffusion of hydroxyl, or species incorporating hydroxyl, must be taken into account to interpret both the observed multi-steady state curve and the impedance diagrams (Fig3.11a). As an example of interpretation of potential dependence of impedance spectra the following simple model (mechanism III), is given with only one passivating intermediate in place of two [38-40].

$$Fe + OH^- \xrightarrow{k_1} (FeOH)_{ads} + e$$

$$(FeOH)_{ads} \xrightarrow{k_2} Fe(OH)^+ + e \underset{step}{\overset{fast}{\rightarrow}} Fe^{++}_{sol} + OH^- \qquad \text{(Mechanism III)}$$

$$(FeOH)_{ads} + OH^- \underset{k'_3}{\overset{k_3}{\leftrightarrow}} Fe(OH)_2 + e$$

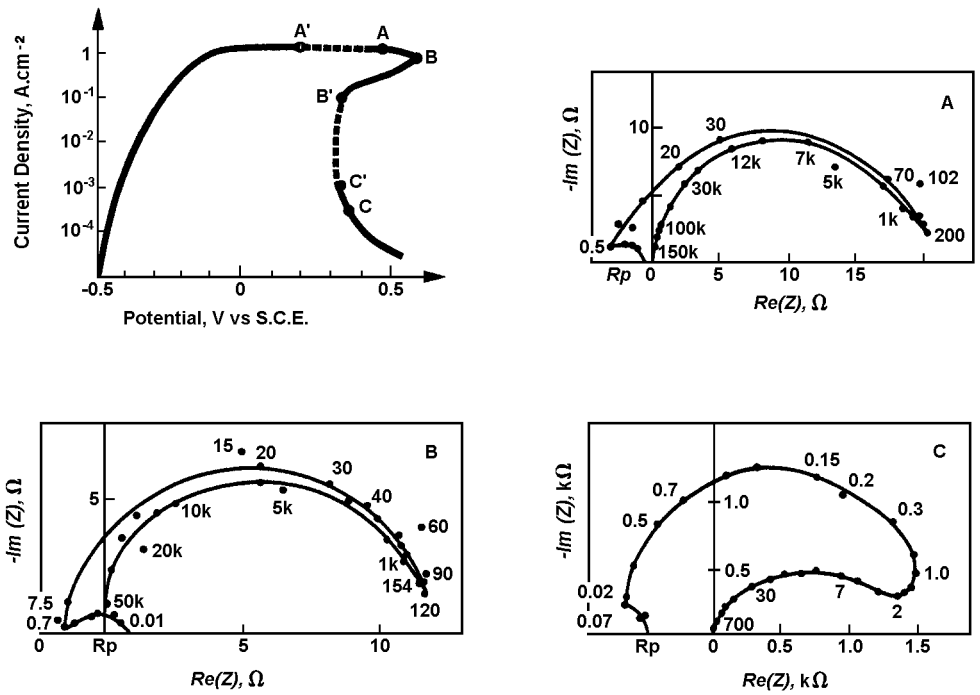

Fig 3.11a Steady-state current-voltage curve and impedance for pure iron in H2SO4, 2N (pH=0) electrode rotation speed = 750rpm: measurements (from [40]): ((A) and (B) ring (outer diameter 5mm, ΔR=0.75mm), (C) disc (diameter 5mm)).

If the hrdroxyl ion is assumed to diffuse towards the electrode surface the equations governing the model are given by:

i) the adsorbed intermediate balance

$$b_1 \frac{dq_1}{dt} = k_1 c(1 - q_1 - q_2) - k_2 q_1 - k_3 q_1 c + k_3' q_2 \qquad (2)$$

$$b_2 \frac{dq_2}{dt} = k_3 q_1 c - k_3' q_2 \qquad (3)$$

where θ_1, θ_2 are the surface coverages of $(FeOH)_{ads}$, $Fe(OH)_2$ and c is the concentration of OH^- at the electrode surface.

ii) the electrode balance

$$I_F = AF[k_1 c(1 - q_1 - q_2) + k_2 q_1 + k_3 c q_1 - k_3' q_2] \qquad (4)$$

iii) Fick's law

$$\frac{\partial c}{\partial t} = D \frac{\partial^2 c}{\partial z^2} \qquad (5)$$

with the assumption

$$c(z) = c - (c - c^*) \frac{z}{d_N} \text{ for } 0 \le z \le d_N \qquad (6)$$

By following the same rules as in § 1.3.3.1 the steady-state current-voltage relationship is

$$I_F = 2AF\frac{D}{d_N}(c^* - c) \tag{7}$$

where c is the solution of an equation of the third degree.

$$\frac{k_3}{k_3'}c^3 + c^2\left(1 - \frac{k_3}{k_3'}c^*\right) + c\left[k_2\left(\frac{d_N}{D} + \frac{1}{k_1}\right) - c^*\right] - \frac{k_2}{k_1}c^* = 0 \tag{8}$$

For adequate values of the parameters, this equation has three solutions for which $0 \le c \le c^*$ for one potential and hence gives three values of current for this one potential.

In the same way, the Faradaic impedance $Z_F(\omega)$ is:

$$Z_F(w) = \frac{1}{F}\frac{\begin{vmatrix} jwb_1 + k_1c + k_2 + k_3c & k_1c - k_3' & -\frac{k_1(k_2 - k_3c)}{2M}N(w) \\ -k_3c & jwb_2 + k_3' & -\frac{k_1k_3c}{2M}N(w) \\ k_1c - k_2 - k_3c & k_1c + k_3' & 1 - \frac{k_1(k_2 + k_3c)}{2M}N(w) \end{vmatrix}}{\begin{vmatrix} jwb_1 + k_1c + k_2 + k_3c & k_1c - k_3' & k_1c[k_2(b_1 - b_2) - k_3c(b_3 + b_3')] / M \\ -k_3c & jwb_2 + k_3' & k_1k_2c^2(b_3 + b_3') / M \\ k_1c - k_2 - k_3c & k_1c + k_3' & k_1c[k_2(b_1 + b_2) + k_3c(b_3 + b_3')] / M \end{vmatrix}} \tag{9}$$

where

$$M = k_1c(1 + kc) + k_2$$

$$k = \frac{k_3}{k_3'}$$

and $N(\omega)$ is given by eqn (66 § 1).

In Fig 3.11b the current-voltage curve and the impedances calculated from eqn (7) and eqn (9) are shown. The good agreement between the calculated and measured impedances leads the authors to the conclusion of the goodness of their model.

3.2.1.3 Iron in Nitric Acid Medium

The behaviour of iron in nitric acid media has fascinated researchers for a long time due to its similarity with the mechanism of the nervous impulse (Ostwald - Lillie's model). However, a lot of problems arose when studies began because of the strong coupling of the anodic process (iron dissolution) and the cathodic process (particularly NO_2 reduction). This coupling made it extremely difficult to measure current-voltage curves and impedances. Thanks to significant improvements in regulating the interface, however, measurements have been performed at zero current, thus allowing the spontaneous passivation of iron in concentrated nitric solution to be understood [41]. Stability analysis of the impedance diagram (Nyquist locus) shows that for low rotation speed of the electrode (no, or only weak, stirring) iron spontaneously passivates up to point E (Fig 3.12). With a high rotation speed (strong stirring) iron is polarised at point A and dissolves. Other points on the current-voltage curve are unstable [42].

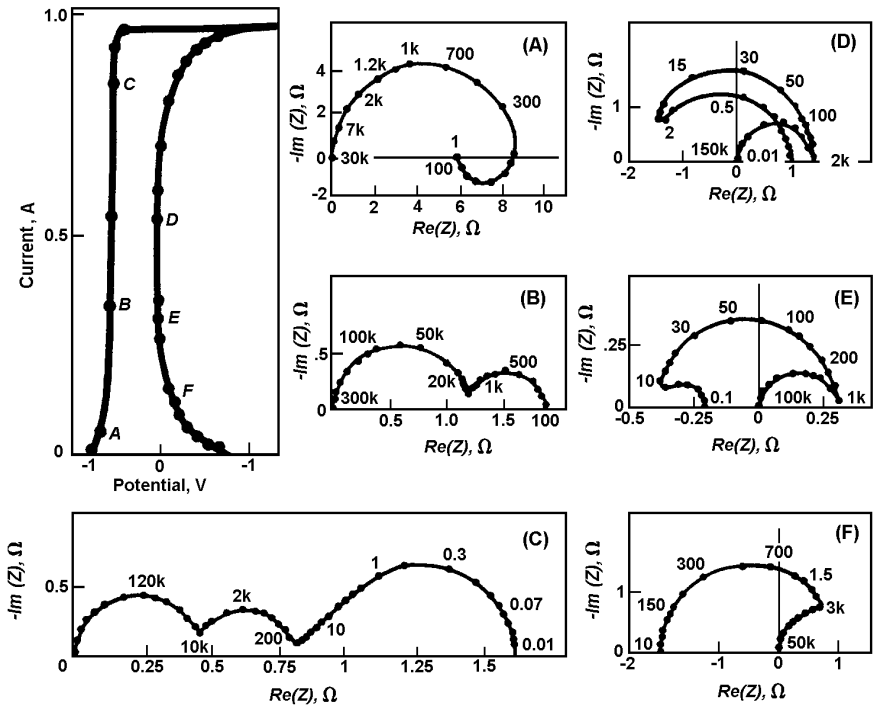

Fig 3.11b Steady-state current-voltage curve and impedance for pure iron in H_2SO_4, 2N (pH=0) electrode rotation speed = 750 rpm: calculated curves for $k_1=4 \times 10^8$ exp 36E, $k_2=10^{-3}$ exp 10E, $k_3=10^{-2}$ exp 12E,

$$k_3^{'} = 2x10^{-9}\ exp(-5E), \frac{d_N}{D} = 20, \frac{d_N^2}{D} = 1, b_1 = b_2 = 2x10^{-9}$$

$$c^* = 10^{-4}.(From[39])$$

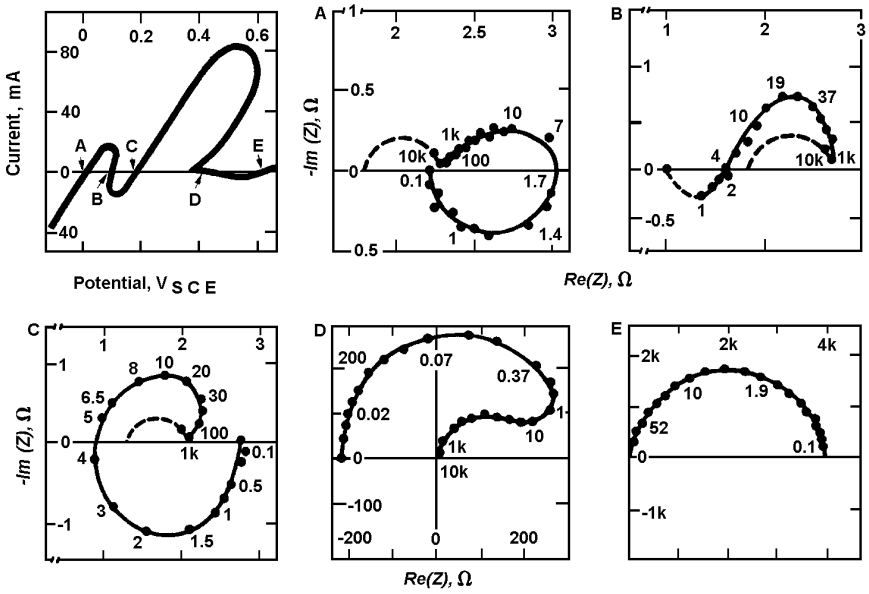

Fig 3.12 Steady-state current-voltage curve and impedance measurements for current zero (points A,B,C,D and E) pure iron in HNO_3, 12N, disc electrode rotation speed = 900rpm, A=0.2cm^2. (From [42])

The behaviour of iron has been thoroughly studied in the transpassive range and a model has been proposed [43]. This model is, formally, very similar to that describing the transpassive behaviour of nickel in sulphuric acid medium which is given below.

3.2.1.4 Nickel in Sulphuric Acid Medium

The Ni/H_2S0_4 interface has been known for a long time for its oscillatory behaviour in the transpassive range in a galvanostatic mode. Stability analysis of the impedance clearly shows that the whole transpassive range is stable only in potentiostatic mode. Based on impedance measurements [44, 45] (Fig 3.13) a reaction mechanism involving hydroxyl ions and anions has been proposed to interpret all the electric features (I-E curve and impedances) in the whole transpassive range [46]:

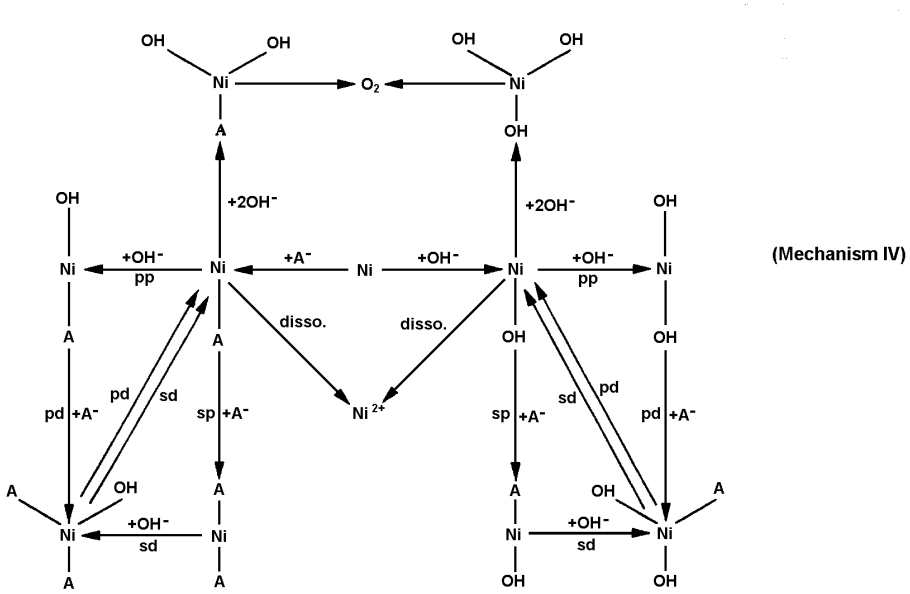

where A is the anion. pp is primary passivation, sp secondary passivation, pd primary depassivation, sd secondary depassivation, disso. dissolution.

The numerical simulation of this model fits the experimental results quite well.

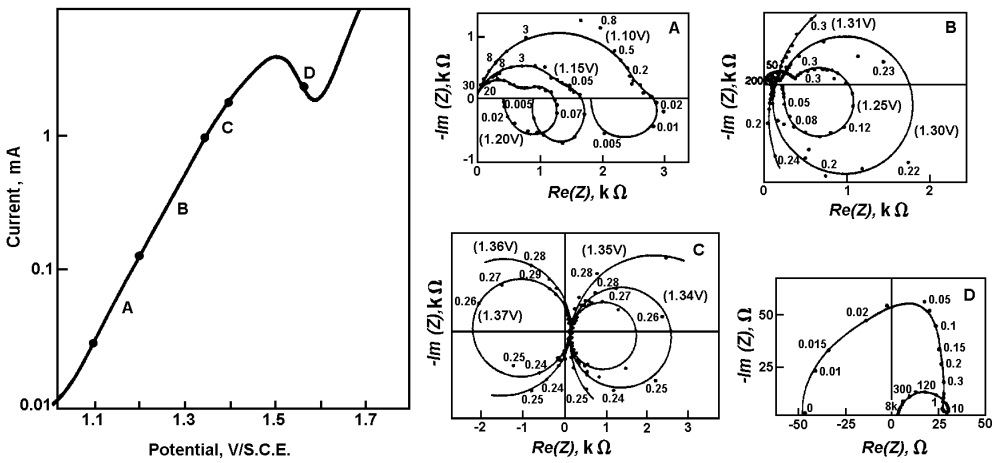

Fig 3.13 Steady-state current-voltage curve and impedance measurements between 1.2 V and 1.55 V vs SCE for nickel in H_2S0_4, 2N, disc electrode rotation speed = 2000 rpm (A = 0.2cm^2). The diagrams A, B, C and D are obtained in the voltage ranges A, B, C and D on the. I-E curve. (From [44])

3.2.1.5 Titanium in Fluorinated Sulphate Medium

Impedance measurements have been performed to study the active-passive transition of titanium [47, 48]. For example, in Fig 3.14, analysis of the diagram allows the charge transfer resistance R_{ct} to be obtained in order to calculate the product R_{ct} x I, which is potential independent when an exponential activation law is the rate determining step.

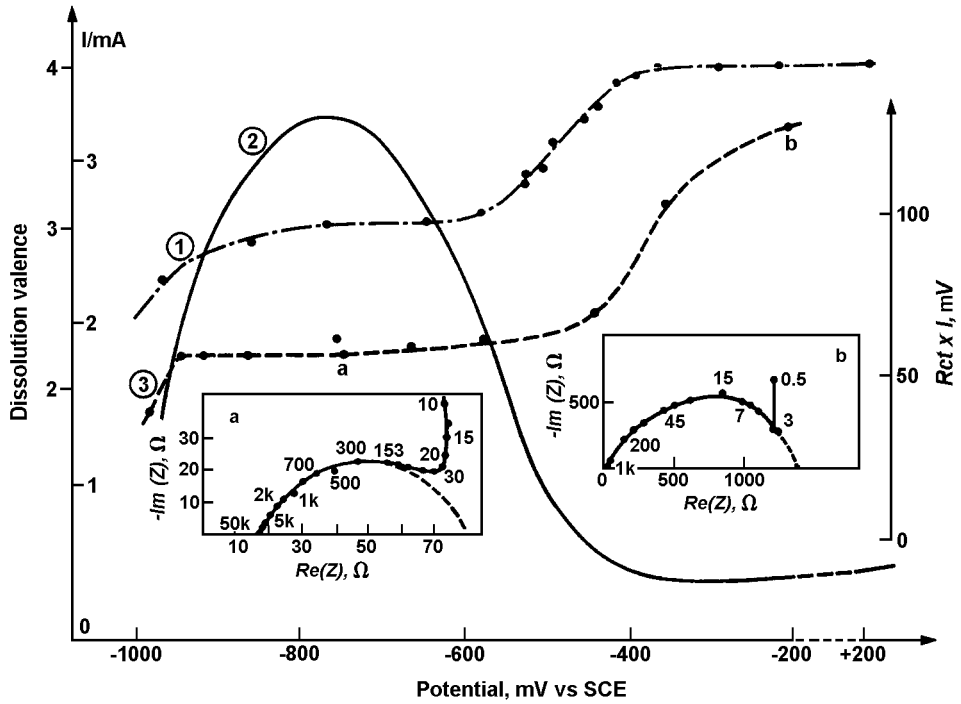

Fig 3.14 Anodic behaviour of titanium in deoxygenated 0.IM H_2S0_4 + 0.9M K_2S0_4 + 5 x 10^{-2} M HF solution, disc electrode rotation speed = 2000 rpm, (from [47]):

curve 1) variation of the apparent dissolution valency

curve 2) steady state current-voltage curve (ohmic drop corrected)

curve 3) R_{ct} x I product deduced from the impedance measurements.

The anodic behaviour of other metals has been studied by impedance techniques: Fe-Cr alloys [49], Cu-Ni alloy [50], chromium [51, 52], cadmium [53], zinc [54], molybdenum [55].

3.2.2 Electrochemical Machining

Electrochemical machining (etching or polishing) is based on high current density dissolution of metals. Very few studies have been done to date due to the complexity of the process and the experimental difficulties (especially very high current densities, which lead to time-varying systems).

Polishing of aluminium has been studied by this technique [56]. Impedances show a capacitive behaviour at low frequencies (Fig 3.15). The only result seems to be the existence of an anhydrous layer at the surface of the electrode.

3.2.3 Passivity of Metals

The thickness and the nature of the passivating layer are very metal-dependent. For example, striking differences exist between iron, where thin passivating layers evolve, and valve metals (Ti, Ta, W…), where passivating layers are rather thick.

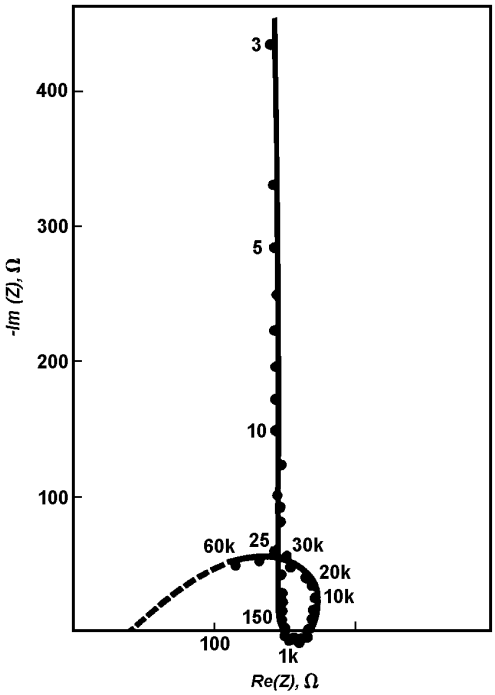

Fig 3.15 Impedance measurement for a vertical aluminium electrode (A = 28mm^2) T = 55°C, 20V polished in 100g/l $Hg(Cl0_4)_2$ in ethanol. (From[56])

3.2.3.1 Passivity of Iron

Passivity of iron has been extensively studied both in acidic [32, 57] and basic [58] rnedia, especially to gain an understanding of stainless steel protection. Very slow processes are involved which give a loop at very low frequencies and the low frequency limit is very difficult to achieve ($f_{lim} \leq 10^{-3}$Hz)

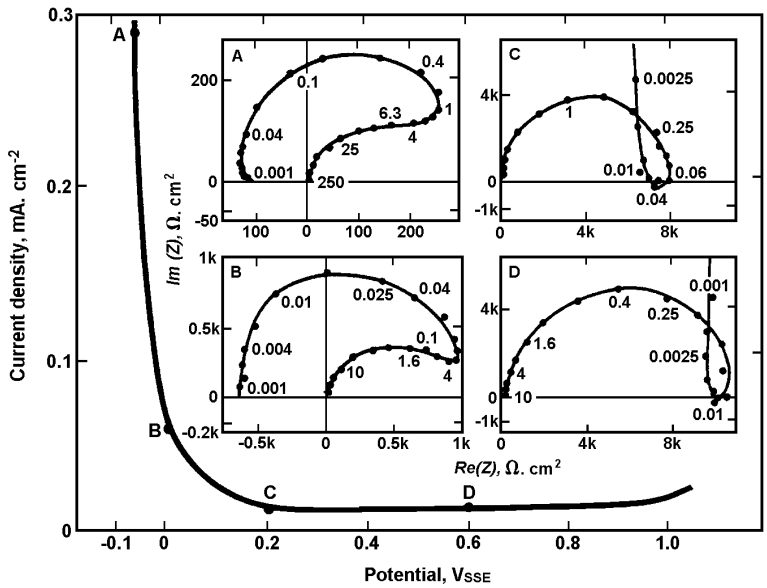

Fig 3.16 Steady-state curve and impedance measurements for passive pure iron in H_2S0_4, 2N. Diagrams A, B, C and D are measured for polarisation points A, B, C and D. Disc electrode rotation speed = 1600 rpm; 0.2cm^2. (From [32])

See Figs 3.16 and 3.17. In particular, infiltrations of electrolyte between the iron electrode and the insulator, leads to experimental artifacts. In sulphuric media it was shown that the adsorbed intermediates Fe (II) and Fe (III) give a thin passivating layer, which becomes more and more organised like a crystal as the potential becomes more anodic. The following sequence has been tested by the impedance technique (Fig 3.16) [57]:

$$Fe \rightarrow Fe(I)_{ads} \leftrightarrow \underset{\downarrow}{Fe(II)_{ads}} \leftrightarrow \underset{\downarrow}{Fe(III)_{ads}} \leftrightarrow oxide \qquad \text{(Mechanism V)}$$

$$Fe(II)_{sol} \qquad Fe(III)_{sol}$$

In the case of basic solutions or neutral solutions thicker layers are encountered. In the latter case results are still under discussion. For example, the high frequency loop (Fig 3.17) gives a capacitance value of 2.10^{-6} ($F.cm^{-1}$), which is too low for the double layer and too high for the space charge capacitance. The interpretation of the lowest frequency loop is not clear either [58].

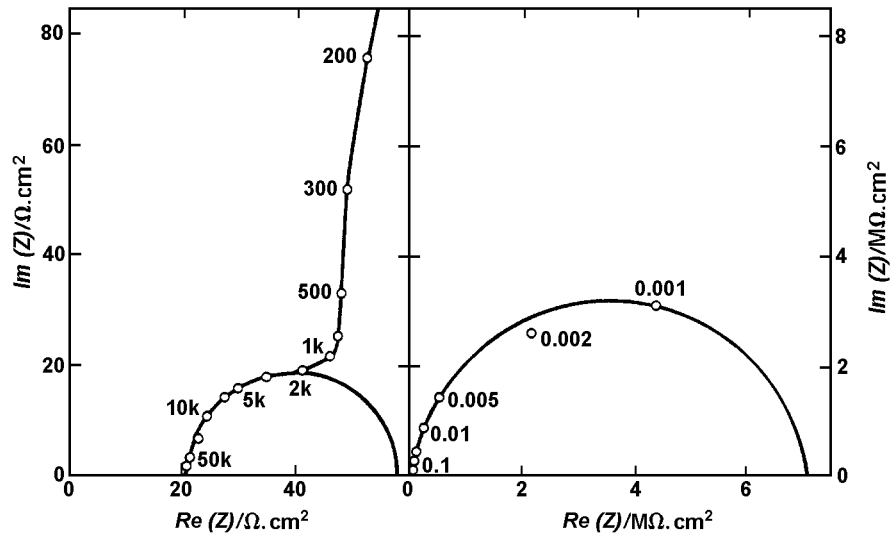

Fig 3.17 Impedance measurements for passive pure iron at 0.15 V (vs SCE) in borate buffer solution (pH = 8.39). (From [58])

3.2.3.2 Anodic Oxide Film Properties

Metal oxide films are often studied for practical applications. These oxides are used in capacitor technology. Concerning the anodic film on valve metals, the capacitive irnpedance found at high frequencies is well related to the thickness (several tens of A) and the dielectric constant of the film, although uncertainty still exists as to the dielectric dispersion. At low frequencies there are processes whose origins remain unknown [59].

Anodisation of aluminium, whose anodic film properties are similar to those of the valve metals, is used to protect against corrosion as will be seen later (§ 3.3.1.4).

To interpret passivating film behaviour, several authors claimed that semiconductive properties of the layer have an outstanding role and they used Mott-Schottky plots [60].

$$\frac{1}{C^2} = f(E) \qquad (10)$$

where C is the capacitance of the layer, in order to derive the flat band potential and to show that the capacitive behaviour originates from the space charge layer [61].

3.3 Corrosion

Corrosion of a metal in an aqueous medium is an electrochemical process. Hence electrochemical techniques, and particularly impedance techniques, are particularly suitable for estimating the corrosion rate, which is equal to

$$x = \frac{dW}{dt} = \frac{MI_a}{zF} \tag{11}$$

where W is the weight loss of the metal, M the atomic weight, z the valence of dissolution and I_a the anodic current of dissolution. In the past I_a was often determined by measuring the polarisation resistance (Impedance at $f = 0$) [62]. However, it has been shown that impedance measurements over the whole frequency range can give more accurate results [63, 64]. Various corrosion processes have been investigated by these techniques. Most of the studies have been done on uniformly corroding surfaces, but localised corrosion and stress corrosion cracking have begun to be analysed.

3.3.1 Estimation of the Rate of Uniform Corrosion

In this type of corrosion the dissolution of the metal is uniform all over the surface of contact with the electrolyte. The overall current I flowing through the interface is

$$I = I_a + I_c \tag{12}$$

where I_c is the cathodic current. In the case of spontaneous corrosion the net measurable current is $I = 0$; it is not possible to determine directly the dissolution current I_a in order to obtain x by eqn (11).

If I_a and I_c are assumed to be potential dependent and are able to follow instantaneously any variation of this potential, then differentiating eqn (12) gives:

$$\frac{\Delta I}{\Delta E} = \frac{1}{Z_F} = \frac{\Delta I_a}{\Delta E} + \frac{\Delta I_c}{\Delta E} = \frac{1}{R_p} \tag{13}$$

where E is the electrode potential corrected for ohmic drop.

Moreover, if I_a and I_c obey Tafel laws of slopes b_a and b_c:

$$\begin{aligned} I_a &= I_a^o \exp \frac{2.303}{b_a} E \\ I_c &= I_c^o \exp - \frac{2.303}{b_c} E \end{aligned} \tag{14}$$

similarly, for a true equilibrium potential ($I = 0$), the impedance is:

$$\frac{1}{Z_F} = \frac{1}{R_p} = 2.303 \left[\frac{I_a}{b_a} - \frac{I_c}{b_c} \right] \tag{15}$$

and at zero overall current, $I_a = -I_c = I_{corr}$, the relationship between impedance and corrosion current is:

$$\frac{1}{R_p} = 2.303 x I_{corr} \frac{(b_a + b_c)}{b_a b_c} \tag{16}$$

In this case, the polarisation resistance is identical to the charge transfer resistance and the Faradaic impedance is frequency independent. Basically, the frequency dependence of Z_F can be expressed by assuming that I_a or I_c, or both, are dependent not only on E but also on one or more parameters, each of which does not instantaneously follow E. As an example, if only one parameter p_a is involved in the anodic component:

$$\frac{\Delta I}{\Delta E} = \frac{1}{Z_F} = \left(\frac{\Delta I_a}{\Delta E}\right)_{p_a} + \left(\frac{\Delta I_c}{\Delta E}\right)_{p_a} + \left(\frac{\Delta I_a}{\Delta p_a}\right)_E . \frac{\Delta p_a}{\Delta E} \tag{17}$$

In contrast with eqn (13), only the first two terms on the right hand side of eqn (17) give a frequency independent contribution to Z_F. The third term is a function of the dynamic behaviour of p_a vs E, is time dependent, and is controlled by an equation of the general form:

$$\frac{d\Delta p_a}{dt} = l_a \Delta p_a + m_a \Delta E \tag{18}$$

If DE and, consequently, Dp_a are subjected to a sinusoidal time variation of small amplitude, from eqn (18) the frequency behaviour of Dp_a is:

$$jw\Delta p_a = l_a \Delta p_a + m_a \Delta E \tag{19}$$

or

$$\frac{\Delta p_a(w)}{\Delta E} = \frac{m_a}{jw - l_a} \tag{20}$$

At high frequencies p_a is frozen i.e. it can no longer follow the variation of the electrode potential in the way it does at sufficiently low frequencies, when the steady state is achieved:

$$\lim_{w \to \infty} \frac{\Delta p_a(w)}{\Delta E} = \left(\frac{\Delta p_a}{\Delta E}\right)_{st} = -\frac{u_a}{l_a} \tag{21}$$

where $\left(\frac{\Delta p_a}{\Delta E}\right)_{st}$ gives the steady state value of $\frac{\Delta p_a}{\Delta E}$

More generally eqn (17) becomes

$$\frac{1}{Z_F} = \frac{1}{R_{ct}} + \frac{\Delta Ia}{\Delta p_a}\frac{m_a}{l_a} \tag{22}$$

Eqn (22) accounts for the general features of the frequency dependence of Z_F stated above, namely:
for $w \to \infty . Z_F = R_{ct}$,

and for $w \to 0 . \frac{1}{Z_F} = \frac{1}{R_{ct}} + \frac{\Delta I_a}{\Delta p_a}\left(\frac{\Delta p_a}{\Delta E}\right)_{st} = \frac{1}{R_p}$ (23)

At finite frequency values, Z_F is frequency dependent according to eqn (22). Consequently, exploring a narrow potential domain around the corrosion potential does not eliminate, as is sometimes believed, the complications arising from surface changes with potential. From the view point of the estimation of the corrosion rate, it is worth considering the derivation given above in a number of particular cases.

It can be shown that eqn (17) is able to provide a relationship between I_{corr} and R_{ct} instead of R_p [65]. Obviously, both relationships tend to become identical in those cases where $R_{ct} \rightarrow R_p$. Table 3.1 gives, under different assumptions for the anodic and cathodic reactions, the relationships between R_p and I_{corr} on one side and R_{ct} and I_{corr} on the other. It is seen that I_{corr} can be related to R_{ct} in two cases of interest (partial diffusion control and multistep electron transfer) where the usual polarisation resistance technique would fail. The only case where R_p must preferably be used is that for passive electrodes.

Similarly, for R_p, the value of the technique is primarily to indicate changes of corrosion rate with respect to variables in the corrosive environment. Values of the Tafel slopes were successfully used for the corrosion of iron in acid media [65], where both anodic and cathodic reactions take place through a two-step reaction [66]. Usually the Tafel slopes of the steps which are not rate determining cannot be obtained easily and a calibration procedure, based for instance on weight loss data, must be used. The experimental data presented below illustrate the relevance of ac impedance measurement to corrosion rate estimation under various conditions.

3.3.1.1 Active Corrosion of Iron

Anodic and cathodic reactions both occur in two consecutive irreversible steps. Faradaic impedance measurements provide the values of $\sum_i \frac{1}{b_a^i}$ and $\sum_j \frac{1}{b_c^{ji}}$ which are involved in the relation between R_{ct} and I_{corr} (relation 4, table 3.1). A good agreement was found between weight-loss experiments, and the absolute value of the corrosion rate deduced from R_{ct} for either a high purity (Johnson-Matthey) iron (0.8mg cm^{-2} h^{-1}) or a pure iron of industrial origin (Holzer type) (2mg cm^{-2} h^{-1}) (Fig 3.18) [65].

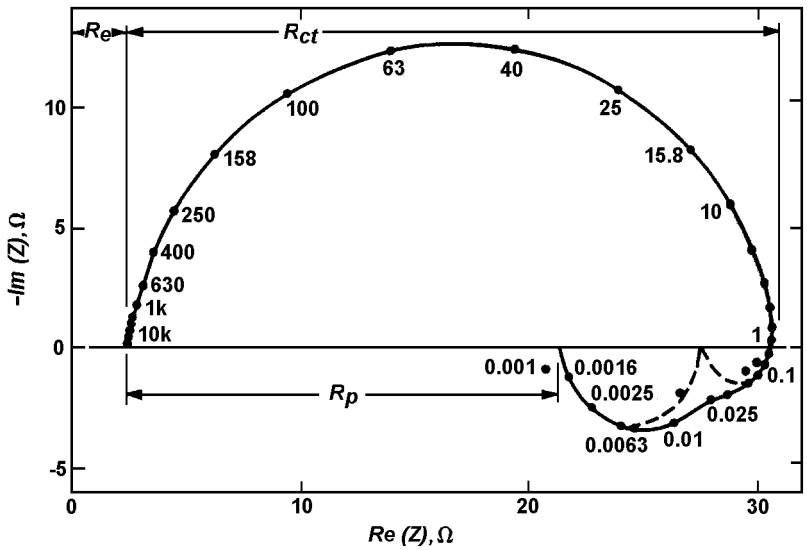

Fig 3.18 Impedance measurement of a corroding electrode: Holzer type iron in deoxygenated 1M, H_2S0_4; disc electrode rotation speed = 1600 rpm; A = 0.2cm^2. (From [63])

3.3.1.2 Inhibited Active Corrosion of Iron

Corrosion rate estimations based on R_{ct}, R_p and double layer capacitance C_d measurements were compared to weight loss data for a Holzer type iron in 0.5M H_2S0_4 as a function of an inhibitor (propargylic alcohol) concentration (Fig 3.19). Fig 3.19a shows the impedance diagram at the corrosion potential, for an inhibitor concentration of 2mM. As in the case of uninhibited iron corrosion (Fig 3.18), two inductive loops are found at low frequencies. They were proved to originate from the potential dependence of, respectively, the surface coverages by the inhibiting species (hydrogen or hydrogen bonded organic compound) at lower frequencies, and by the anodic intermediate species FeOH at higher frequencies [67-69]

Table 3.1 Theoretical relationship between the corrosion current and the charge transfer and Polarisation resistances, under various anodic and cathodic kinetics (from [63])

Kinetics Control of		Relation to Corrosion Current *Icorr*	
Anodic Reaction	Cathodic Reaction	Polarisation Resistance R_p	Charge Transfer Resistance R_{ct}
One step, tafelian electron transfer	One step, tafelian electron transfer	$\frac{b_a b_c}{2.303(b_a + b_c) I_{corr}}$	$\frac{b_a b_c}{2.303(b_a + b_c) I_{corr}}$
One step, tafelian electron transfer	Purely diffusional	$\frac{b_a}{2.303 x I_{corr}}$	$\frac{b_a b_c}{2.303(b_a + b_c) I_{corr}}$
One step, tafelian electron transfer	Mixed control, partly diffusional	Complicated equation, depends upon the degree of control by diffusion	$\frac{b_a b_c}{2.303(b_a + b_c) I_{corr}}$
n_a irreversible tafelian, consecutive steps $\left(b_a^i\right)$	N_c irreversible tafelian, consecutive steps $\left(b_c^i\right)$	Complicated equation, depends upon the whole set of rate constants	$\frac{1}{2.303\left(\frac{1}{n_a}\sum_{i=1}^{n_a}\frac{1}{b_a^i} + \frac{1}{n_c}\sum_{j=1}^{n_c}\frac{1}{b_c^i}\right) I_{corr}}$
Passive dissolution	One irreversible tafelian transfer on the passive area	$\frac{b_c}{2.303 x I_{corr}}$	Complicated equation, depends upon the kinetics of dissolution and passivation.

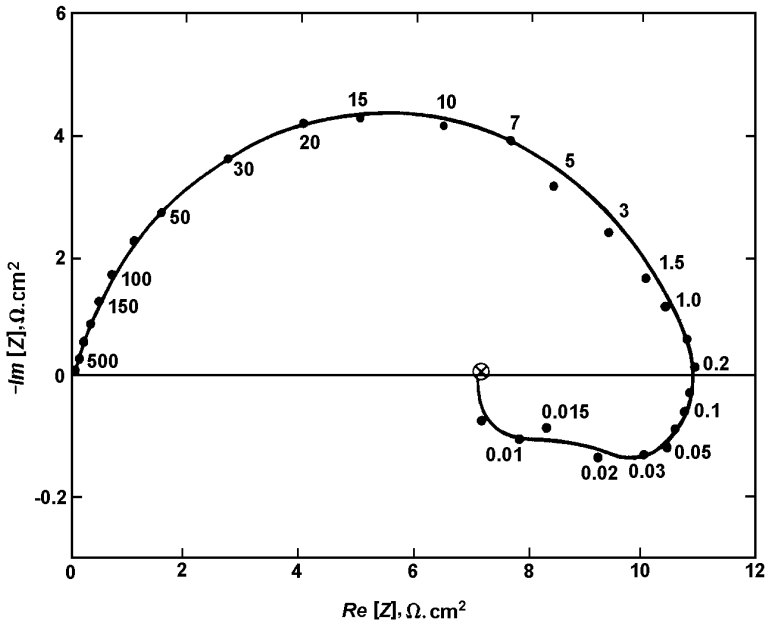

Fig 3.I9a Impedance measurement of a corroding electrode: Holzer type iron electrode in 0.5M, H_2S0_4 aerated + 2mM propargylic alcohol; disc electrode rotation speed = 1600 rpm. (From [65])

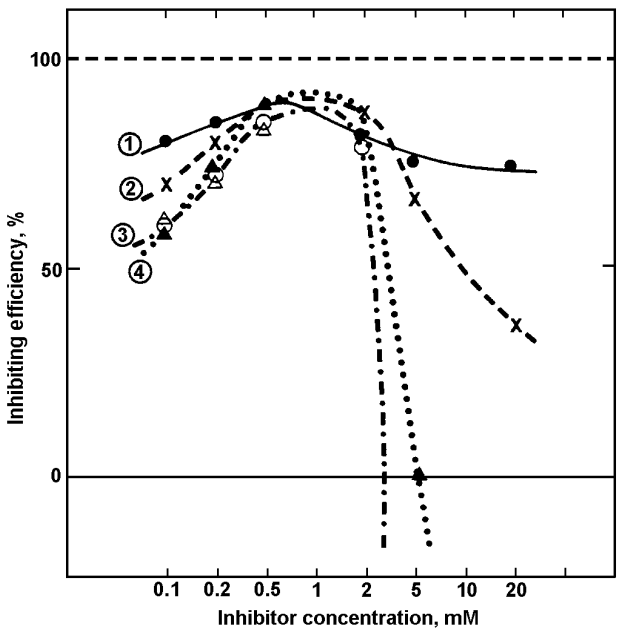

Fig 3.I9b Inhibiting efficiency with respect to the inhibitor (propargylic alcohol) concentration, determined by:

(1) weight loss, (2) R_{ct} measurements, (3) R_p measurements, and (4) double layer capacitance measurements (negative inhibiting efficiency indicates the acceleration of corrosion). (From [63])

Relative corrosion rates with respect to the uninhibited conditions can be expressed in terms of the dimensionless inhibiting efficiency:

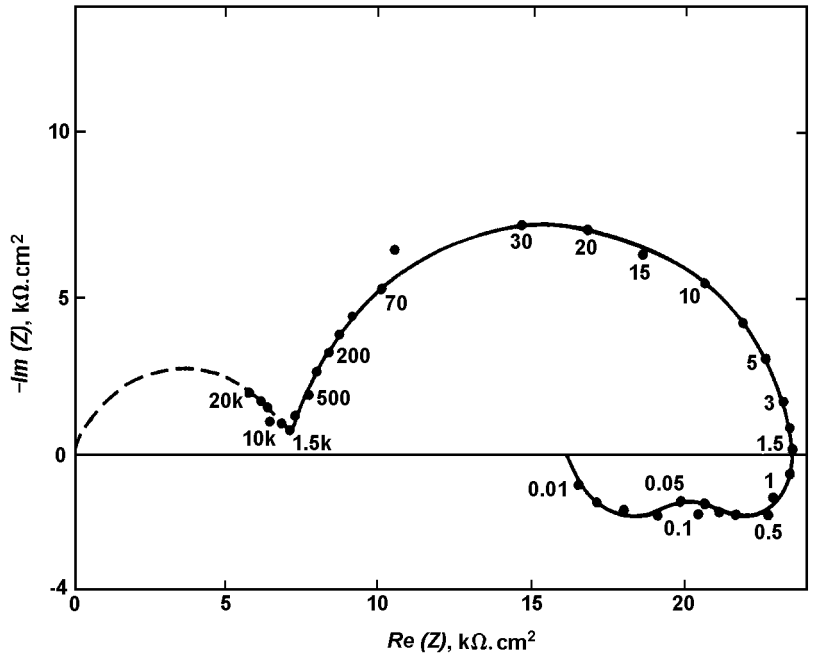

Fig3.20a Corrosion of iron coated with epoxy paint (from [73])

Impedance measurement of a corroding electrode: Armco iron (A = 60cm^2) covered by 40µm epoxy paint (ICI 5802022)

$$H = \frac{100(x_o - x)}{x_o} \tag{24}$$

where x_o is the corrosion rate in the absence of an inhibitor and x the corrosion rate in the presence of an inhibitor. x is either measured directly by weight loss (H_{dir}) or calculated from R_{ct} or R_p which are assumed inversely proportional to x. According to [70] H_{Cd} depends on a standardisation coefficient K_1:

$$H_{C_d} = 100K_1\left(\frac{C_{do} - C_d}{C_{do}}\right) \tag{25}$$

K_1 is chosen so that $H_{Cd} = H_{dir}$ at 0.5mM of propargylic alcohol.

As shown in Fig 3.19b, the values of H obtained from R_{ct} are in agreement with those of H_{dir} except at very high concentrations when indications become pessimistic. The values of H_{Rp} can be considered as acceptable, but, beyond an inhibitor concentration of 2mM, they predict a negative inhibition (i.e. an acceleration of the corrosion) in complete disagreement with direct measurements. According to the theoretical derivation given above, this discrepancy is related to the increasing size of the low frequency inductive arc as the inhibitor concentration is increased, resulting in a corresponding difference between R_p and R_{ct}.

As for the values of H_{Cd} they show the same type of error as H_{Rp} at high inhibitor concentrations.

3.3.1.3 Corrosion of Coated Metal

Faradaic impedance measurements on painted iron (Fig 3.20a) showed that the metal is corroded in the same way as when unprotected, but on a much reduced area at the place where the paint layer presents pore-like flaws [71, 72]. The isolating part of the paint layer gives rise to a characteristic capacitive behaviour at high frequencies.

Corrosion rates calculated from R_{ct}, data were compared to weight loss for a number of specimens protected with epoxy paint, from 0 to 80μm in thickness (Fig 3.20b). Coated thin foils of high purity Goodfellow iron were exposed to attack in a 0.5M H_2S0_4 solution for two to four days. The rate of corrosion continuously increased during the exposure and R_{ct}, was measured as a function of time. The average calculated corrosion rate was compared to weight loss at different layer thicknesses. As shown in Fig 3.20b a very good correlation is found: the thicker the layer, the better the protection [73]. Similar results were obtained for mild steel covered by porous concrete in sea water [74, 75].

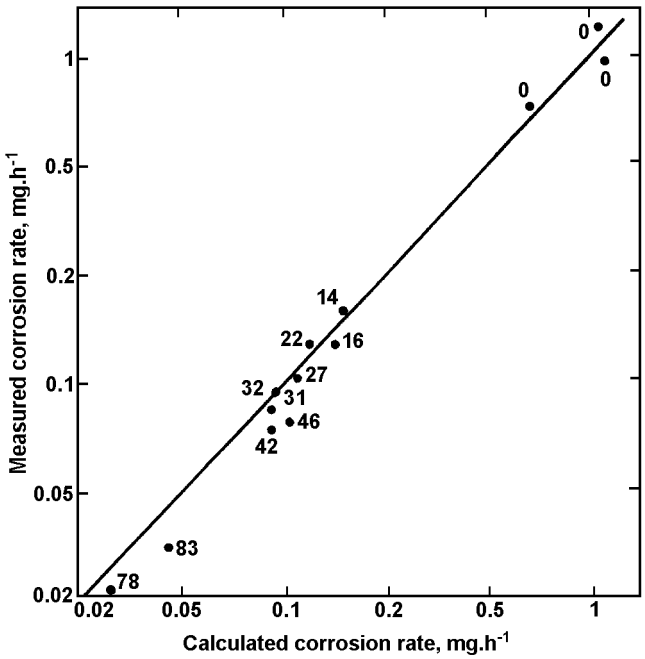

Fig 3.20b Estimated corrosion rate by R_{ct} measurement is compared with the results of the weight-loss measurement. Iron sheer (Goodfellow) covered by various thicknesses of epoxy paint film; parameter is film thickness in μm, 0 corresponds to the naked specimen.

3.3.1.4 Anodised Aluminium Alloys

The resistance against corrosion of aluminium based alloys protected by an anodic oxide layer is usually evaluated by a salt spray test, which needs a long time exposure. The ac impedance method is quicker and has the same degree of reliability [76 – 78]. The anodised sample to be tested is immersed in a 3% NaCI solution buffered at pH4 and deoxygenated by nitrogen bubbling. The impedance is measured at its free corrosion potential. Fig 3.21a shows the impedance diagram. Two capacitive contributions can be resolved when the high frequency behaviour is enlarged (Fig 3.21b). This shorter time constant probably arises from the dielectric property of the oxide layer. A correlation between corrosion susceptibility and impedance behaviour must reasonably be expected in the low frequency domain. In fact, a good correlation was found between the low frequency resistance R_{LF}, (Fig 3.21a) and the exposure time at which the first pit opened. The impedance technique being non-destructive, ac impedance and salt spray tests can be applied successively to the same sample so that a highly significant comparison can be made. No Faradaic model of corrosion is available in the case of aluminium, and R_{LF} can hardly be dealt with in terms of either R_{ct} or R_p. Therefore, the value of the test must be founded on a large number of experiments. Fig 3.21c gives, as an example, the selection made among 83 samples from the same batch on the basis of ac measurement or salt spray test. A "pass" in the salt spray test is recorded if no pits have appeared after 300h exposure to the spray. The "pass" / "fail" threshold value of R_{LF} (5.5MΩcm^2) was determined empirically. A similar correlation was found between the two techniques for different compositions of aluminium alloys and oxidising baths [78, 79].

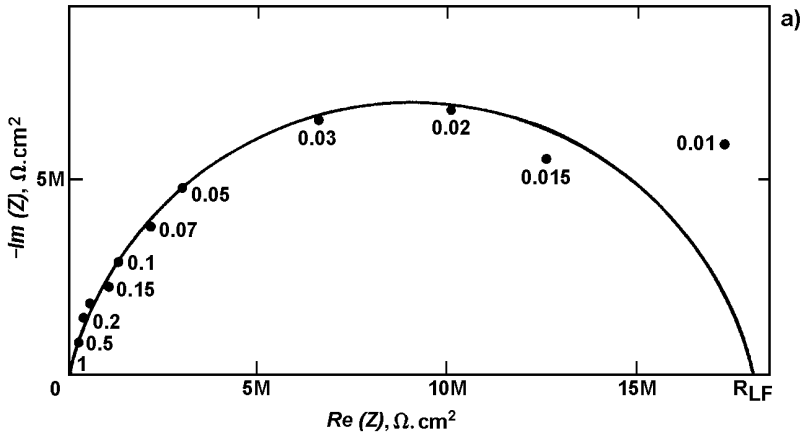

Impedance measurement of a corroding electrode: 2024T4 alloy anodized in chromic bath (A=50cm^2 – in 0.18M NaCl + 0.0115 CH_3COOH + 0.02M CH_3COONH_4.

Impedance given for a unit surface area.

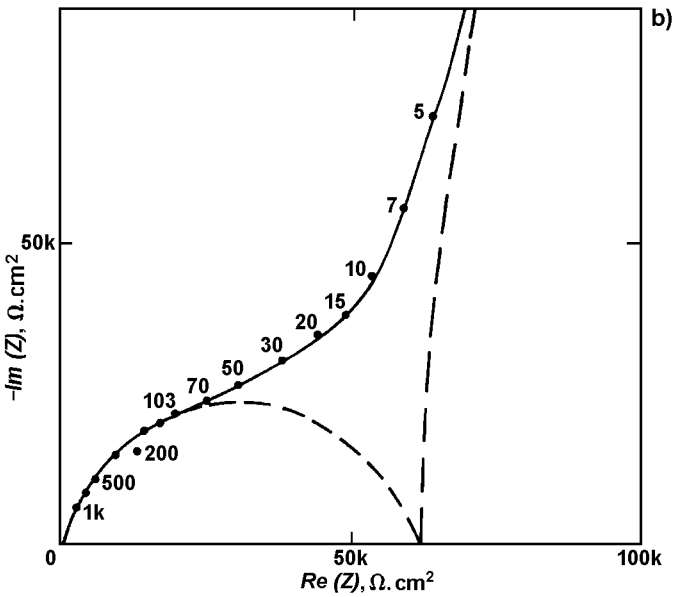

Enlarged diagram in the high frequency range of the diagram (a).

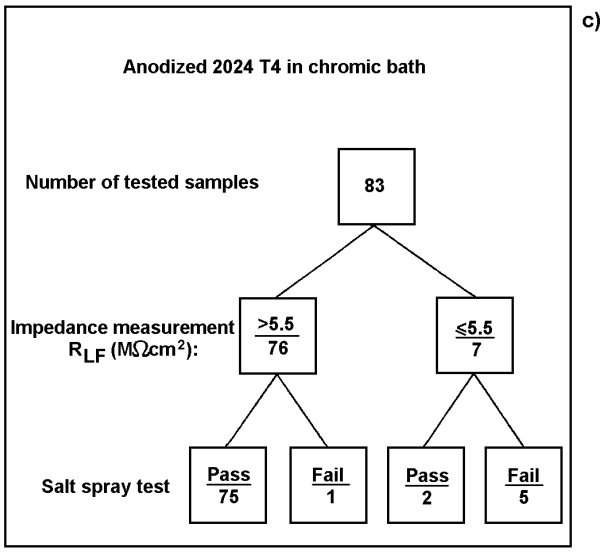

Comparison of impedance measurement and salt spray test.

Fig 3.21 Corrosion of an anodized aluminium alloy (from [78])

3.3.1.5 Stainless Steel

The corrosion of stainless steel occurs in the passive range. As shown in Table 3.1, the quantity used for estimating the corrosion rate in the passive range is the polarisation resistance R_p. This is only an assumption for stainless steel, because the actual dissolution mechanism is not known. However, experimental results have shown the relevance of such a choice [80]. As shown in Fig 3.22 the processes involved in the corrosion process of stainless steel are so slow that the low frequency limit, R_{LF}, can often be estimated only by extrapolation of a best-fitted half circle for the experimental values. R_p based corrosion rate estimation has also been used successfully for copper-nickel alloy in flowing sea-water for investigating the effect of oxygen [81] and for 18-8 stainless steel in IM, Na_2S0_4 [82].

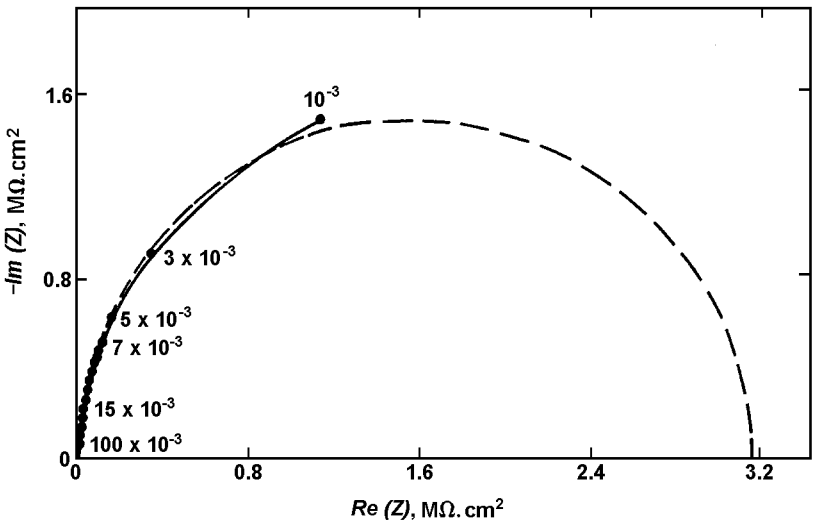

Fig 3.22 Impedance measurement of stainless steel corroding electrode Fe 17Cr 16Ni 5.5Mo 2.7Cu 0.03C in aerated 1.8M H_2S0_4 Solid line = experimental results; broken line = best-fitted half circle (from [80])

3.3.2 Localised Corrosion

In contrast with uniform corrosion, localised corrosion occurs in a few small places (pits, crevices, cracks). Hence the corroded surface can either be analysed as a whole, taking into account several corroding places, or each corroding place can be analysed in isolation. Both these approaches have been investigated.

Concerning the impedance measured on aluminium in a chloride solution, which is known to cause pitting if the potential is raised sufficiently in the anodic range, the onset of pitting is marked by a decrease in the modulus of the impedance, especially in the low frequency range [83]. Some analysis has been performed in vivo on implantable anode materials for heart pacemakers [84].

Impedance measurements have been performed for a pre-existing hole, made mechanically before immersing the sample in a H_2S0_4, 2N solution [38, 85]. In Fig 3.23a the polarisation curves give the anodic behaviour of the electrode for various geometries of the initial hole. A model taking into account a coupling through diffusion between dissolution and passivation is given in § 3.2.1.2 and this explains the main features of both the polarisation curve and the impedance diagrams (Fig 3.23b). However, it seems that the consideration of metal cation hydrolysis and migration is necessary. Hence the diffusion in the occluded cell is responsible for maintaining iron in an active state at a potential for which it should be passive.

The role of molydenurn additions to austenitic stainless steel in the inhibition of pitting has been similarly investigated [86]; the authors have shown that an adequate amount of chromium is necessary.

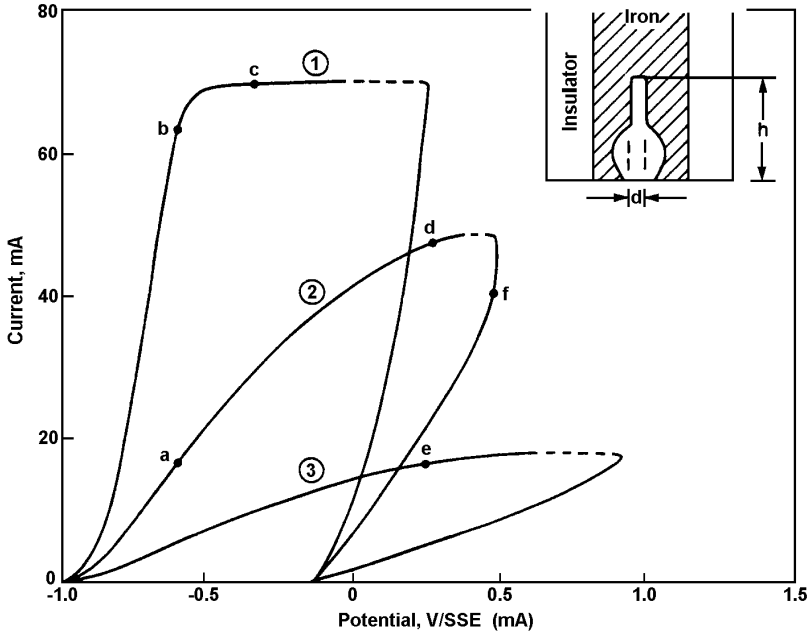

Fig 3.23a Polarisation curves (obtained by using negative output impedance regulation) of a fixed iron electrode with artificial pit in H_2S0_4, 2N. The schematic section of the electrode shows the shape taken by the initial artificial pit (diameter d, depth h) after dissolution: (1) flat electrode; (2) d = 2mm, h = 2.5mm; and (3) d = 1mm, h = 3mm. The fat part of the electrodes (2) and (3) are covered with inert coating.

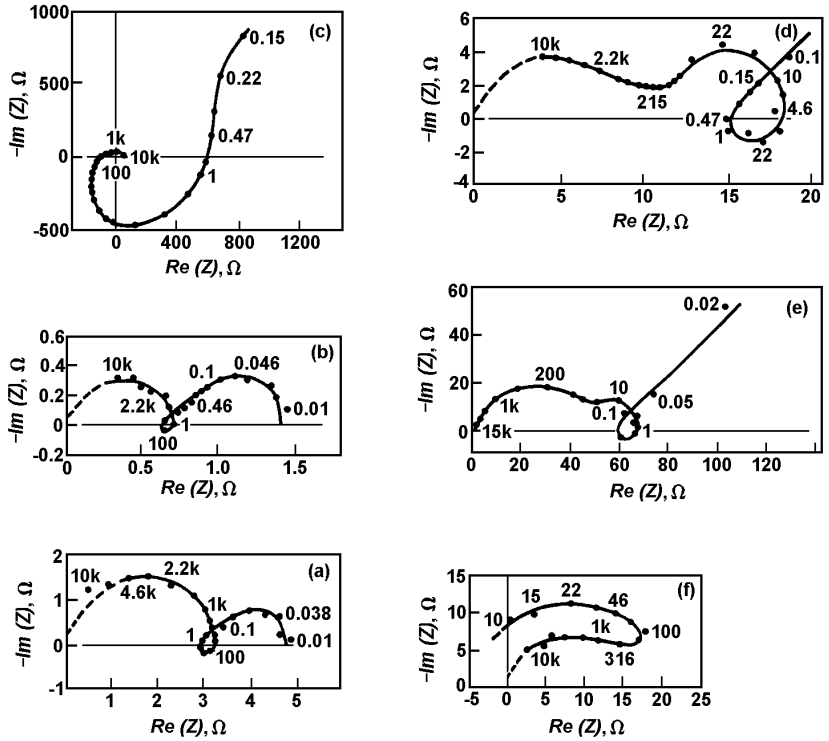

Fig 3.23b Impedance measurements for the electrodes of Fig. 3.23a. Diagrams (a) to (f), correspond to points a to f on the polarisation curves (from [85]).

3.3.3 Stress Corrosion Cracking

From a general point of view, it has been shown that, especially in the case of copper in $CuS0_4$ solution [87], impedance measurements can give similar information about the electrochemical reactions to that obtained by the application of elastic stresses.

Measurement of the impedance of the electrode in the active-passive transition and measurement of stress corrosion at constant strain rate have been performed on the same material. It has been shown that the susceptibility to stress corrosion cracking for low carbon steel is directly related to a time constant.τ deduced from impedance data (see § 1.3.3.2).

Given an impedance diagram such as that depicted in Fig 3.16 (point B) if R_1 and R_2 are the values of the intersection of the semi-circle approximating the low frequency passivating loop with the real axis and ω_o* the characteristic angular frequency of this loop (inverse of the time constant) the value of τ is

$$t = \frac{1}{w_o^*}\frac{R_o + R_1}{R_o} \text{.....where} \frac{1}{R_o} = \frac{1}{R_2} - \frac{1}{R_1} \qquad (26)$$

The time constant τ can be related to the incremental passivation. In Fig 3.24 it can be seen that the maximum of r when it varies with respect to the potential corresponds closely to the maximum susceptibility of the stress corrosion cracking [34, 88]. Hence it has been easy to test the efficiency of stress corrosion inhibitors [33].

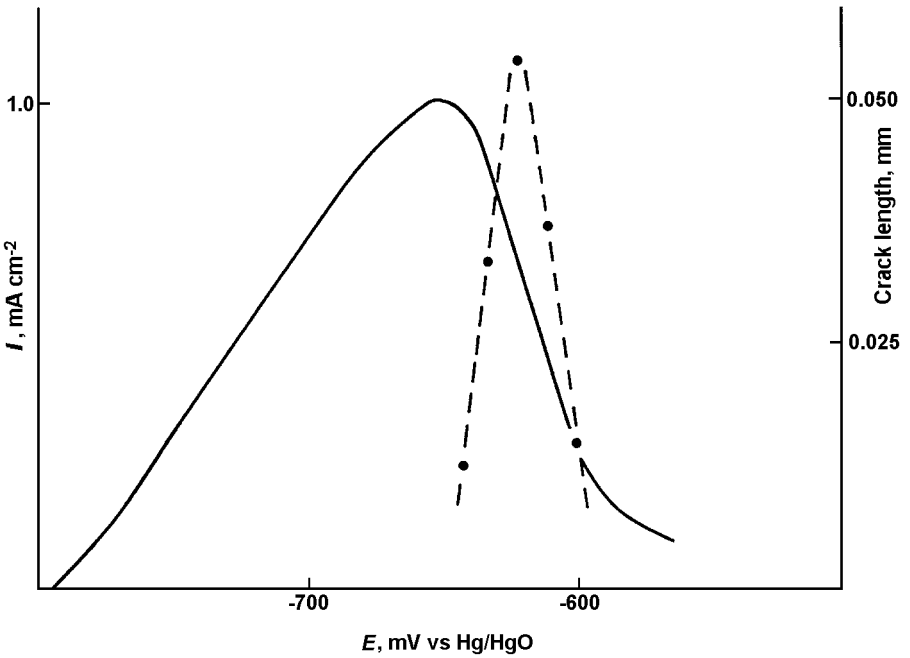

Fig3.24a Stress corrosion cracking study for steel GCS I in solution O.325M $NaHC0_3$ + 0.325M Na_2C0_3 (pH 9.7); disc electrode rotation speed = 270 rpm

Variation in susceptibility to stress corrosion cracking vs electrode potential (-----), and corresponding current-voltage curve (____)

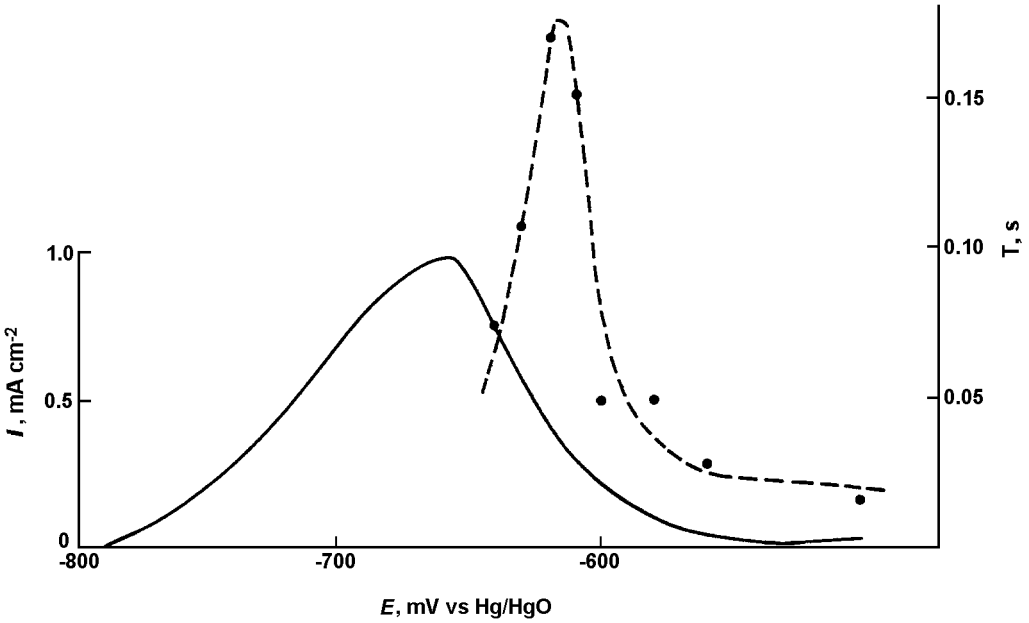

Fig 3.24b Stress corrosion cracking study for steel GCS I in solution 0.325M $NaHCO_3$ + 0.325M Na_2C0_3 (pH 9.7); disc electrode rotating speed = 270 rpm

Variation of τ in the active-passive transition (-----), and the corresponding current-voltage curve (___) (from [34])

3.4 Electrocrystallisation of Metals

The electrocrystallisation of polyvalent metals occurs in several steps, from the transport of the cations M^{z+} from the bulk of the electrolyte up to the incorporation of the metal M in the crystal lattice. Hence many processes can limit the deposition rate and have to be taken into account in devising a model for deposition: diffusion, surface coverage of the adsorbed reaction intermediates and other parameters related to the surface morphology of the deposit.

The adatom model considers that the metal ion is discharged onto the electrode surface and then after diffusion along the electrode surface the resultant adatom is incorporated into the metal at a growth site located at the edge of a nucleus. The crystallisation impedance is therefore a function of diffusion in the solution, charge transfer, surface diffusion and lattice incorporation [89]. Simplified models [90], or more complex models [91, 92], taking into account some or all of these four elementary processes, have been proposed.

The impedance has been calculated for two-dimensional nucleation and growth. The multilayer formation has been considered in two ways. On one hand it has been treated as a cascade process in which the (n + 1)th layer is born out of the nth layer, so that the current can be evaluated by a recurrence relationship. Electrochemical impedance spectra have been calculated by numerical integration using the Fourier transform of the response to positive potential steps of small amplitude [93].

On the other hand, the successive monolayers have been assumed to be generated at a mean nucleation rate and to follow the same ageing law as nuclei formed at random in time and space. The impedance is calculated by means of the usual linearisation method [94].

In some other cases of metal deposition the morphological aspects do not seem to appear in the impedance measurements. Models, similar to those involved in the anodic behaviour of metals (§ 3.2) and based on the relaxation of surface coverage of the reaction intermediates, with or without diffusion in the solution bulk, seem to account quite well for the experimental results.

A few results on the electrocrystallisation of various metals follow.

3.4.1 Nickel

Nickel deposits are extensively used in industrial plating. Hence the experimental deposition baths are very similar, or the same, as those used in industry.

Impedance diagrams relating to nickel electrodeposition in Watts electrolyte (whose pH is close to 4.5) have revealed only one inductive loop (see Fig 3.25a). This low frequency feature has been ascribed to the relaxation of the electrode coverage by an adsorbed intermediate such as (NiOH). Hence, a model of reaction mechanism has been suggested where the elementary steps of the overall reaction of deposit have not yet been distinguished [95]:

$$Ni^{2+} + H_2O \rightarrow (NiOH)^+ + H^+$$
$$(NiOH)^+ + e \rightarrow (NiOH)_{ads} \qquad \text{Mechanism VI}$$
$$(NiOH)_{ads} + (NiOH)^+ + 3e \rightarrow 2Ni + 2OH^-$$

However, by changing the electrolyte composition (especially anion), additional low frequency features have been pointed out which will certainly allow a more detailed mechanism to be established [96]. These features are probably consequent both on the coverage of reaction intermediates particularly linked to hydrogen adsorption and on surface relaxation (see Fig 3.25b and c).

The inhibition of nickel deposit has been equally well studied in a case of diffusion controlled inhibition of electrodeposition [97].

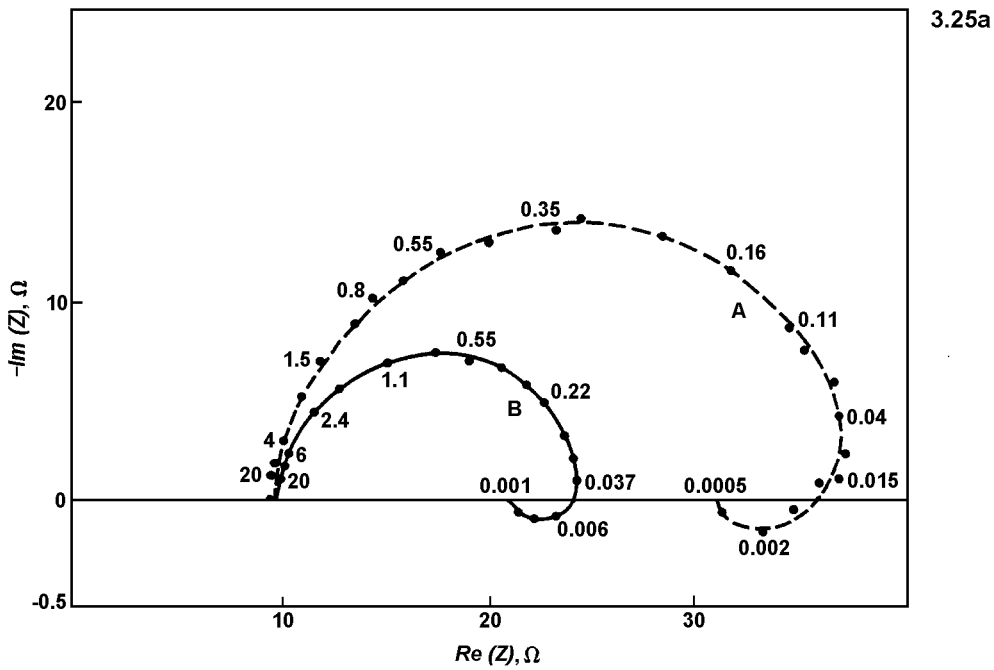

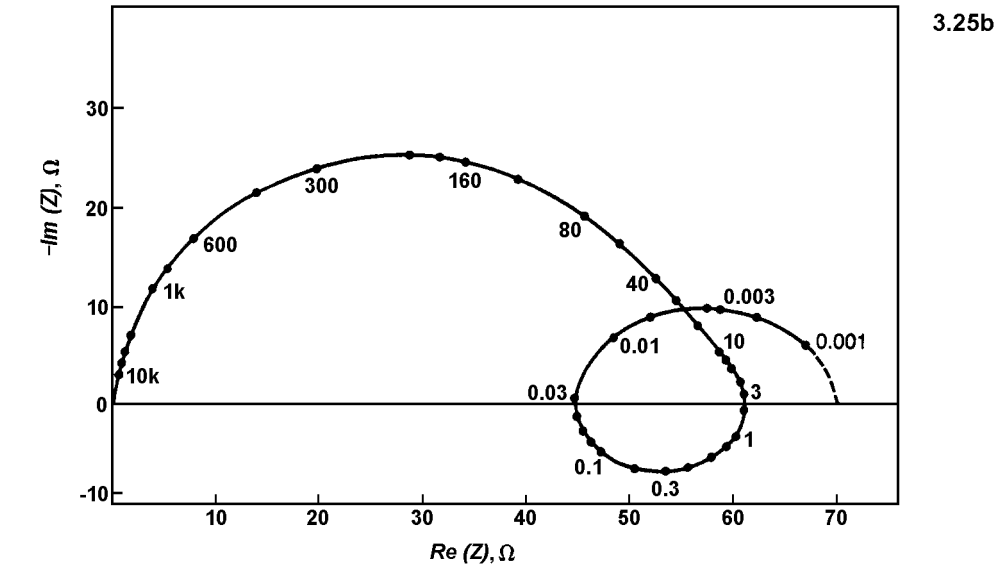

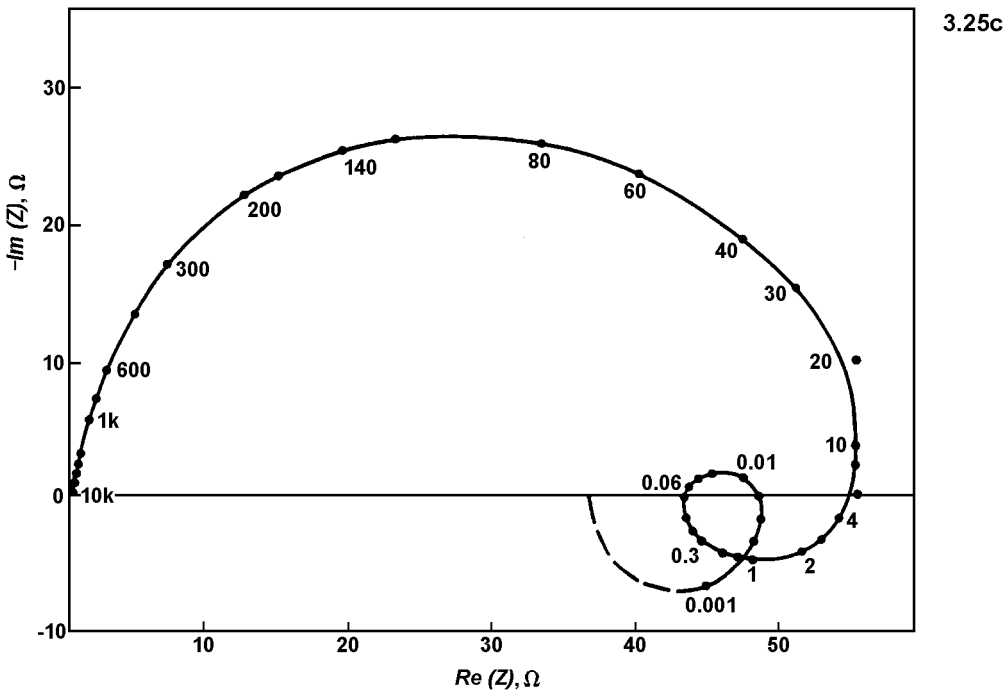

Fig 3.25 Impedance measurement for nickel deposition:

a) Watts solution (300 g/l $NiSO_4.7H_20$ + 35 g/l $NiCl_2.6H_20$ + 40 g/l H_3B0_3); pH=4.5; T=50°C; disc electrode rotation speed = 2000rpm; A=0.2cm^2; curve (A): I=2mA; curve(B): I=4mA (From[95])

b) 1.22M, $NiSO_4$, pH 3, disc electrode rotation speed = 2000 rpm, I = 1mA; T = 50°C (From [96])

c) 1.22M, $NiCI_2$, pH 3, disc electrode rotation speed = 2000 rpm, I = 1mA; T = 50°C (From [96])

3.4.2 Zinc

The study of zinc electrocrystallation is generally considered as being of high interest, mainly because this metal is employed in electrochemical generators. Zinc deposits have been investigated in several acidic and basic media commonly used for industrial purposes (in particular Leclanche media and alkaline electrolytes).

In order to interpret the S-shaped polarisation curve and the measured impedances (Fig 3.26), the authors have suggested that an autocatalytic step (the third step in mechanism VII) is involved in the reaction mechanism [98,99].

$$H^+ + e \rightarrow H_{ads}$$
$$H^+ + H_{ads} + e \rightarrow H_2$$
$$Zn^{2+} + Zn^+_{ads} + e \Leftrightarrow 2Zn^+_{ads}$$
$$Zn^+_{ads} + H_{ads} \rightarrow H^+ + Zn$$
$$Zn^+_{ads} + e \rightarrow Zn$$
$$Zn^{2+} + e \rightarrow +Zn^+_{ads}$$

Mechanism VII

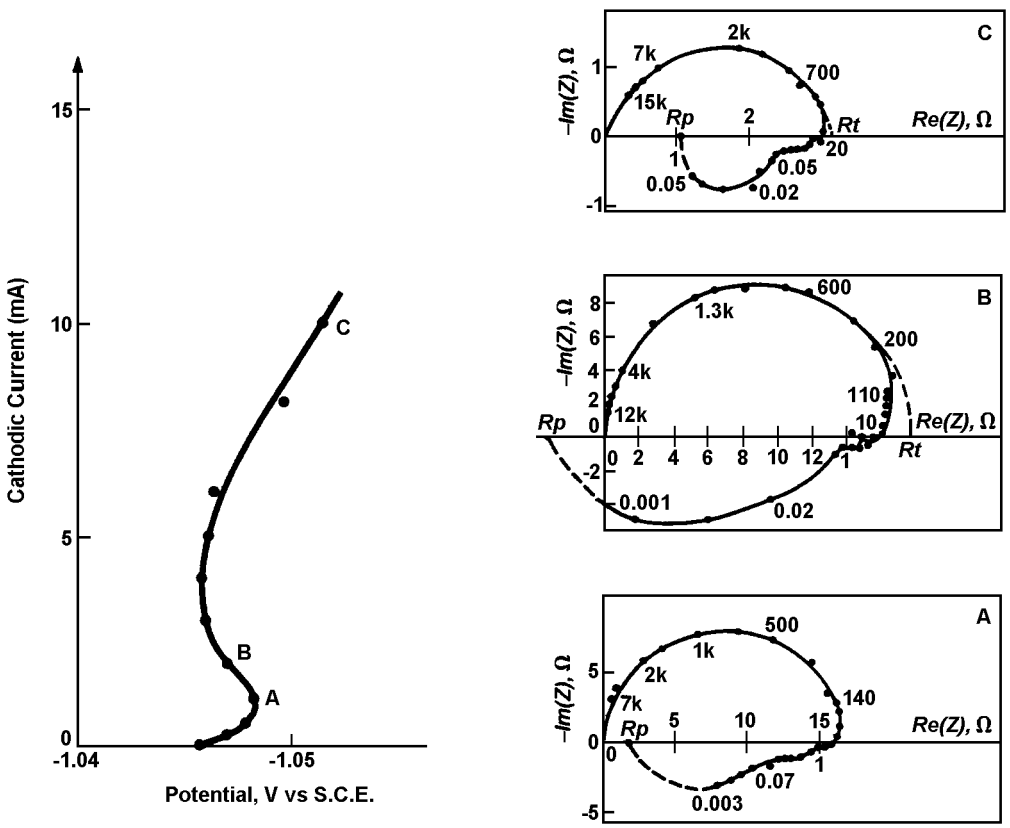

Fig 3.26 Zinc electrocrystallisation in 1M Na_2S0_4 + 1.5M $ZnS0_4$; PH=4.3; disc electrode rotation speed = 3000 rpm; A = 0.28cm^2. (From [98])

a) polarisation curve

b) impedance measurements for points A (2mA), B (3mA), and C(10mA)

However, when the current is increased, spongy, compact and dendritic zinc electro-deposits can be observed successively [100]. An improvement of the model, taking into account the localisation of some of the interfacial reactions on particular sites distinguished with regard to the crystal growth, has allowed this change in the deposit morphology to be explained [99]. The interpretation is based on various couplings, between the interfacial reactions, the surface diffusion of Zn^{+}_{ads} , and the renewal of growth sites. At low current, the electrode kinetics are governed by an equation such as:

$$b\,\frac{dq}{dt} = f(q,E) + bD_S\,\frac{\partial^2 q}{\partial r^2} \qquad (27)$$

where D_s is the surface diffusion coefficient, r the position on the surface, q the surface coverage of Zn^{+}_{ads} and $f(q,E)$ the source term is given by the electrochemical reaction mass balance (See § 1.2.4, eqn (28)).

Inhibition of zinc electrodeposition has been studied in view of the electrode kinetics and the deposit morphology (Fig 3.27). The studied inhibitors specifically modify the rates of interfacial reactions: in particular they give rise to an accelerated nucleation rate, ensuring a faster renewal of active growth sites [101, 102].

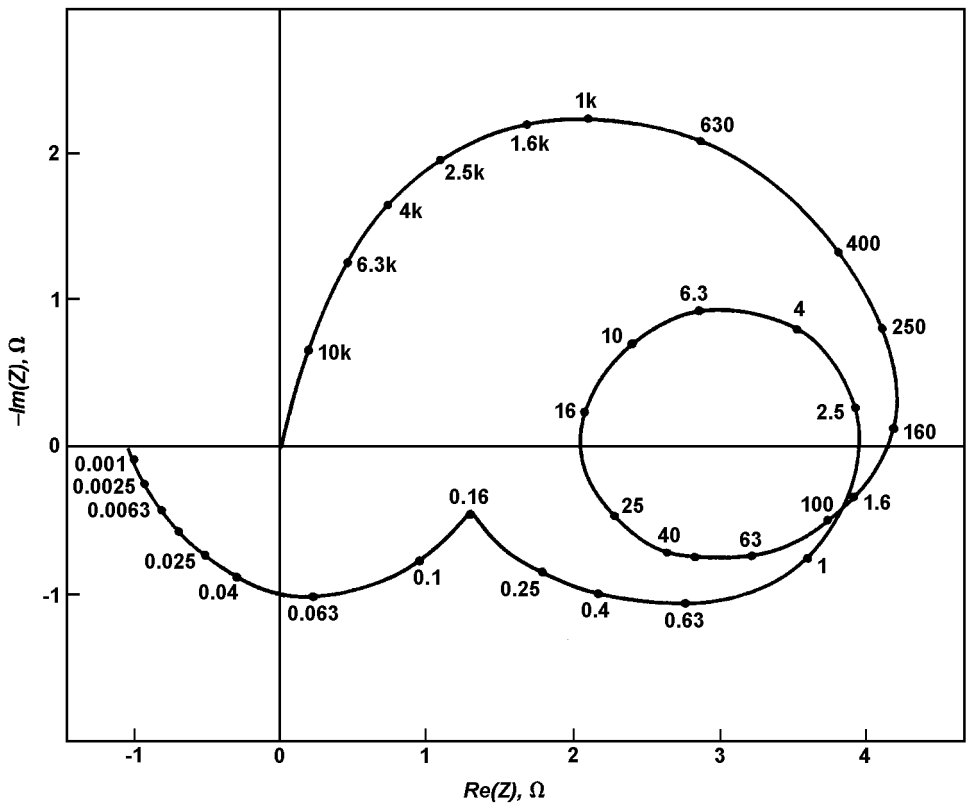

Fig3.27a Inhibition of zinc electrocrystallisation in alkaline zincate electrolyte KOH 7M, ZnO 0.5M; A = 0.28CM^2 5.10^{-5}M, NBu_4Br;

disc electrode rotation speed = 100 rpm (From [101])

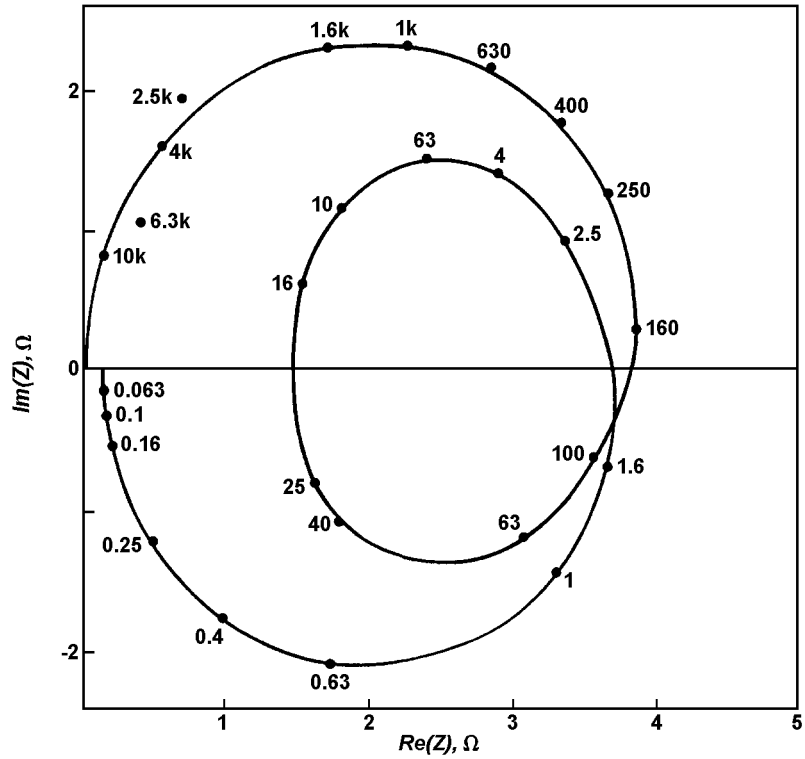

Fig 3.27b Inhibition of zinc electrocrystallisation in alkaline zineate electrolyte KOH 7M, ZnO 0.5M. A = 0.28cm^2 5.10^{-4}M, NBu_4Br; disc electrode rotation speed = 1500 rpm (From [101])

3.4.3 Silver

Silver electrodeposition in acidified 1M $AgNO_3$ was investigated by impedance measurements and compared with morphological studies by scanning electron microscopy. It was shown that the low anodic or cathodic overpotential giving rise to a strong activation of the electrode surface (the surface is blocked at equilibrium) can be explained by a very fast electron transfer. The impedance reveals two time constants which are independent of the value of anodic or cathodic current density, of NO^-_3 concentration and of substrate orientation (Fig 3.28a). These results are perturbed when an additive is added (Fig 3.28b). The authors have shown that the impedance results can be discussed in terms of nucleation and propagation of edges [103, 104] and that the discharge of Ag^+ is not the rate determining step of the reaction [105].

3.4.4 Other Metals

Various metal depositions have been investigated by impedance measurements: copper [106-109], cobalt [95, 107] palladium [110] gold [111] cadmium [112] and tin [113].

Other types of electrodeposition have been similarly studied: chemical (electroless) deposition of nickel from hypophosphite solutions [114], and deposition of silver from a solid phase [115].

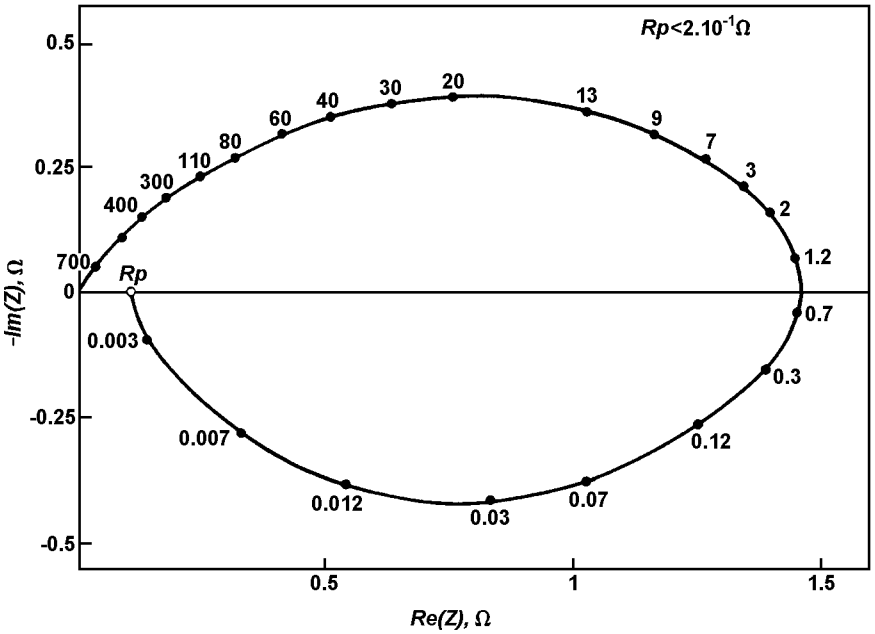

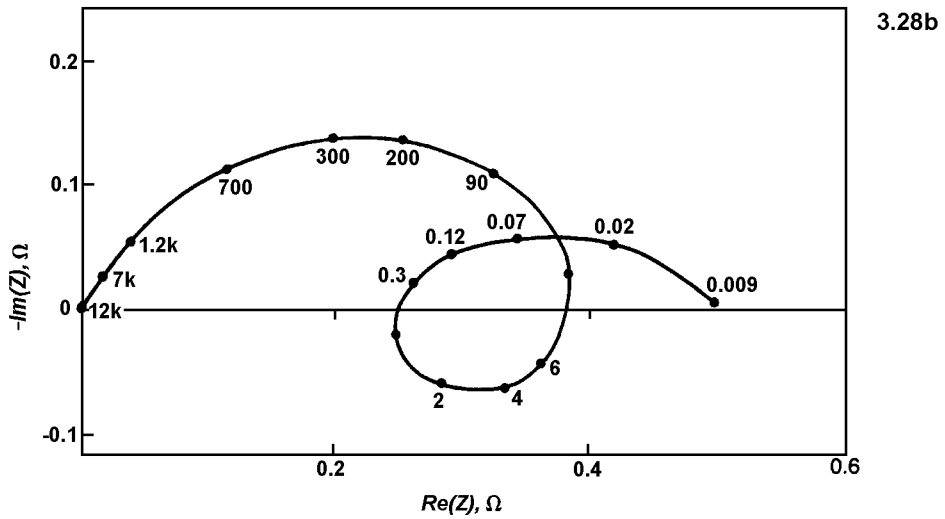

Fig 3.28 Silver electrocrystallisation in $AgNO_3$ 1M + HNO_3 0.5M; disc electrode rotation speed = 2600 rpm (From [1031])

a) I=1mA, disc electrode area = 1.32cm^2

b) + tartaric acid 5.10^{-2}M, I = 20mA, disc electrode area = 1. 77cm^2

3.5 Batteries and Energy Sources

The development of electrochemical energy sources necessitates studies in various fields. The requirement that storage cells possess adequate storage capacity has resulted in the use of electrodes having a high specific surface area. Hence, the capabilities of porous electrodes have to be investigated (see § 3.1.3). The electrolyte is often in the solid state for convenience, and many studies on solid electrolytes have been done. Finally, when the cell is built, a non-destructive, in situ, state-of-charge test is needed.

3.5.1 Solid Electrolytes

Studies in solid electrolytes have concentrated largely on the research of new materials with high electrical conductivity which are used, typically, in galvanic cells with a high density of energy. The ionic conductivity in these materials is due to migration of negative or positive ions with high mobility. The materials are:

i) isotropic anionic conductors with 0^{2-} or F^{-} conduction.

ii) cationic conductors, either isotropic with Ag^{+} or Li^{+} conduction or anisotropic with Na^{+} conduction.

Solid electrolytes have been studied by impedance measurements in order to understand better the various processes involved:

i) transport numbers, concentrations of charge carrying species, electronic and ionic defects and their mobility.

ii) effect on conductivity of oxygen partial pressure, dopant concentration, impurities, grain boundaries and second phase precipitation.

iii) charge transfer and polarisation phenomena at the electrolyte-electrode interface (noble metals are often chosen for electrodes as they are assumed to be chemically inert).

In addition, as solid electrolytes of practical importance are frequently polycrystalline, bulk and grain boundary conductivities have to be taken into account.

Impedance diagrams of solid state electrochemical cells are generally composed of capacitive arcs (semi-circles and diffusion arcs) that can be assigned to the bulk of the ionic conductor and to the electro-chemical reactions taking place at the interface [116, 117]. Hence an ideal diagram with well resolved time constants can be depicted as shown in Fig 3.29 [118]. Depending on the experimental conditions, only a few semi-circles are readily observable. It should be noticed that the frequency range of measurement of the impedance is very wide, e.g. 10^{-3} to 10^{8} Hz in [119].

3.5.1.1 Zirconia and Other Anionic Conductors

At elevated temperatures the conductivity of stabilised zirconia is almost exclusively due to the motion of oxygen vacancies and hence it is used in galvanic cells [120-122]. In particular, these cells are used as monitoring elements when analysing oxygen (in a 10^{-20} to 1atm. range) or when extracting oxygen from a gas mixture by electrolysis.

Impedance measurements have been used to select materials for electrochemical applications [123] and for fundamental investigations. It has been shown that polarisation phenomena at the electrode-electrolyte interface have a significant effect on the cell behaviour [124]. This is demonstrated in Fig 3.30 where Faradaic reaction (right), space charge (middle) and bulk conductivity left can be distinguished.

In the same way the influence of oxygen pressure and temperature on doped thoria conductivity has been investigated [125].

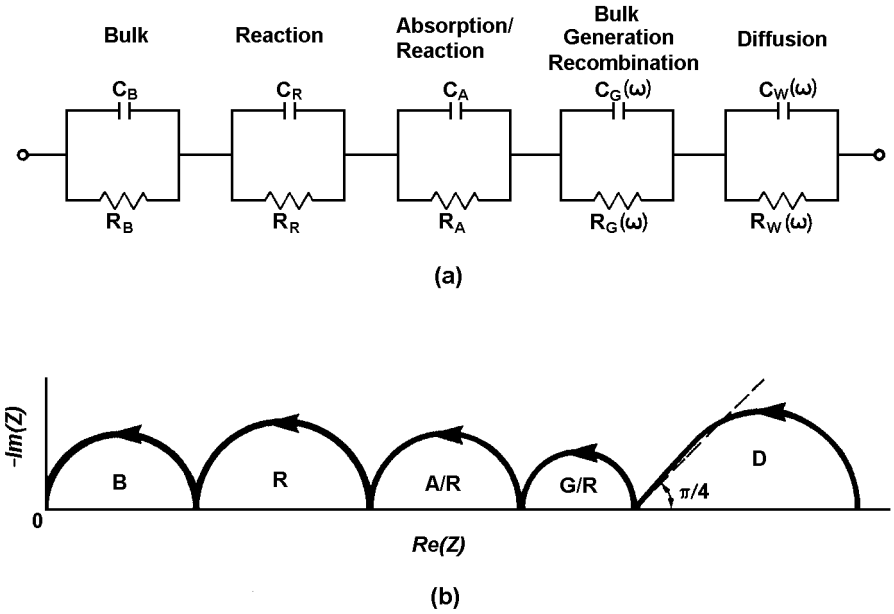

Fig 3.29 Impedance schematic of an ideal solid electrolyte (from [118])

a) equivalent circuit

b) impedance plot

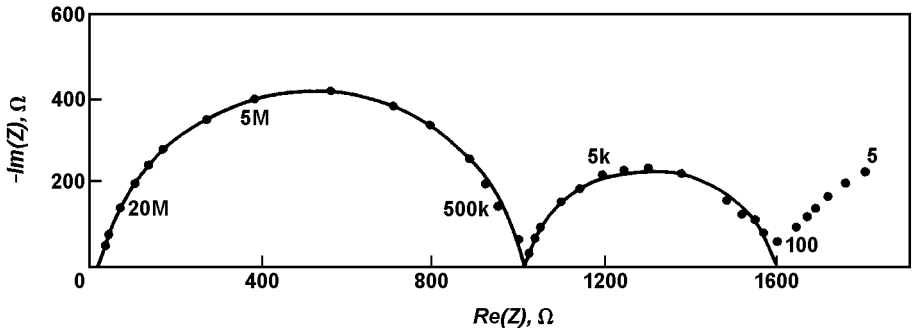

Fig 3.30 Impedance measurement of a Pt/YS Z/Pt cell in 0_2 at 45 7.4°C (from [124])

Other anionic conductors have been considered. Fluorides MF_2 (M = Ca, Sr, Ba, Pb) are electronic insulators, but are also very good ionic conductors. Hence, the ionic conductivities of solid solutions of $Ca_{1-X}Y_XF_{2+x}$ have been studied by impedance measurements which were correlated with structural properties [126, 127].

3.5.1.2 b Alumina

β alumina is a sodium aluminate in which the sodium ions have a very high mobility. It has been used as a separator in sodium-sulphur batteries. Impedances have been measured on sintered discs of doped and undoped β-alumina (Fig 3.31). Hence intergranular and bulk phenomena have been separated in the conductivity [128 - 130]. However, a smooth surface, which results in intimate contact with liquid sodium, gives different impedance values to those obtained with a coarse surface, where the contact is poorer [131].

Other Na^+ conductors have been studied by impedance measurements, e.g. $Na_{1+X}\ Zr_2\ Si_X\ P_{3-X}\ 0_{12}$ ceramics in [132].

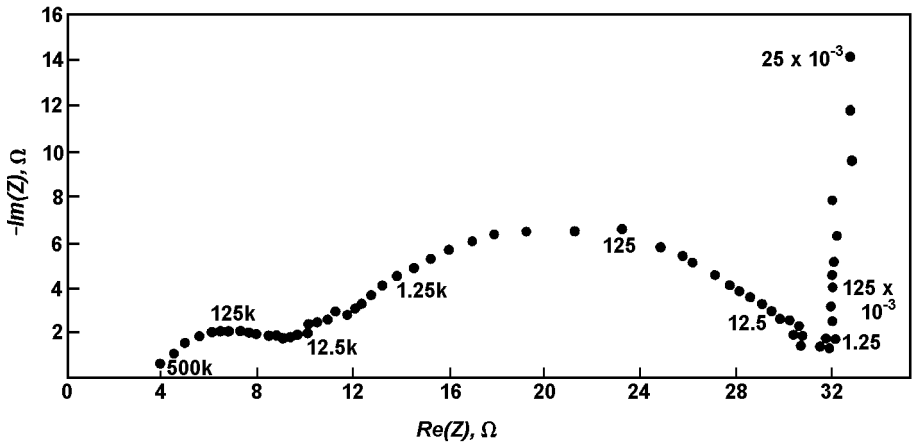

Fig 3.31 Impedance measurement of an Hg / propylene carbonate + NaI/β alumina / propylene carbonate+ NaI / Hg cell at 295K (from [130])

3.5.1.3 g Manganese Dioxide

Manganese dioxide is one of the most commonly employed electrochemically active materials, due to its application as the cathode in Leclanche cells and alkaline dry batteries. Impedance measurements for γ - MnO_2 powder dispersions in electrochemically active materials have been performed (Fig 3.32). Information about the interfacial processes, diffusion in the solid phase, electronic resistivity and the influence of microporosity and macroporosity can be extracted from experimental results. An equivalent circuit in the form of an electrical transmission line has been devised to explain diffusion in the electrolyte which filled channels between the particles [133].

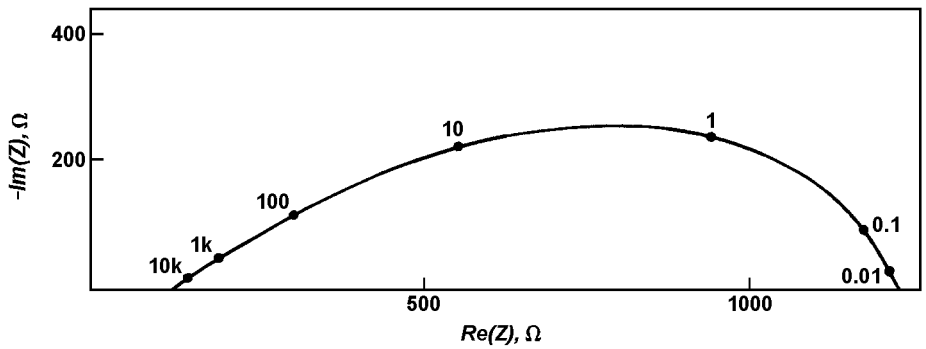

Fig 3.32 Impedance measurement of γ manganese dioxide powder dispersed in an electrolyte of resistivity 379Ω.cm (from [133])

3.5.1.4 $Ag_4 Rb I_5$

This species is decomposed to give iodine, which diffuses in the solid electrolyte. Rate constants for the electrochemical oxidation of I^- to I_2 on Pt have been determined, from impedance measurements. Variation with pressure and particle size (usually 50μm) of the electrolyte have been investigated [134, 135].

Other solid electrolyte studies include silver salt electrochemistry with ionic or electronic contacts [136], lithium nitride [137, 138] and $LiTa_30_8$ β [139]: these are good lithium ion conductors and seem promising for electrochemical cell applications.

3.5.2 Batteries

In order to improve the performance of batteries, fundamental studies are still necessary. In addition greater demands on the reliability of electrochemical power sources have led to batteries being renewed periodically, or renewed whenever there is doubt about their operational usefulness. This results in a high wastage rate of partially discharged but still usable batteries. On the other hand, continuous state-of-charge monitoring is often needed, e.g. in electrically powered cars. The state-of-charge of a battery is the ratio of residual capacity, at a given instant, to the maximum capacity **I** available from the battery. Hence, users need a simple, rapid and reliable, non-destructive check on the energy available in a power source. Tests based on impedance measurements of electrical storage cells have been devised for various cells [140, 141].

3.5.2.1 Nickel-cadmium Cells

Before the cells were tested, their performance was made reproducible by activating the electrode surface with a deep charge-discharge cycle. The various states-of-charge were obtained by discharging at a constant current at a ten hour rate **I**/10 (**I** =4Ah). It was found that the impedance of the nickel-cadmium cell, measured over a rather narrow range of frequencies (5-30Hz), is predominantly controlled by diffusion (Fig 3.33). The internal resistance is dominated by the resistance of the solution and the separator (inserted between the electrodes to increase the cell capacity) and is therefore not useful in characterising the state of-charge. The authors suggest the use of the imaginary part of the impedance, measured at a sufficiently low frequency to predict the latter [142].

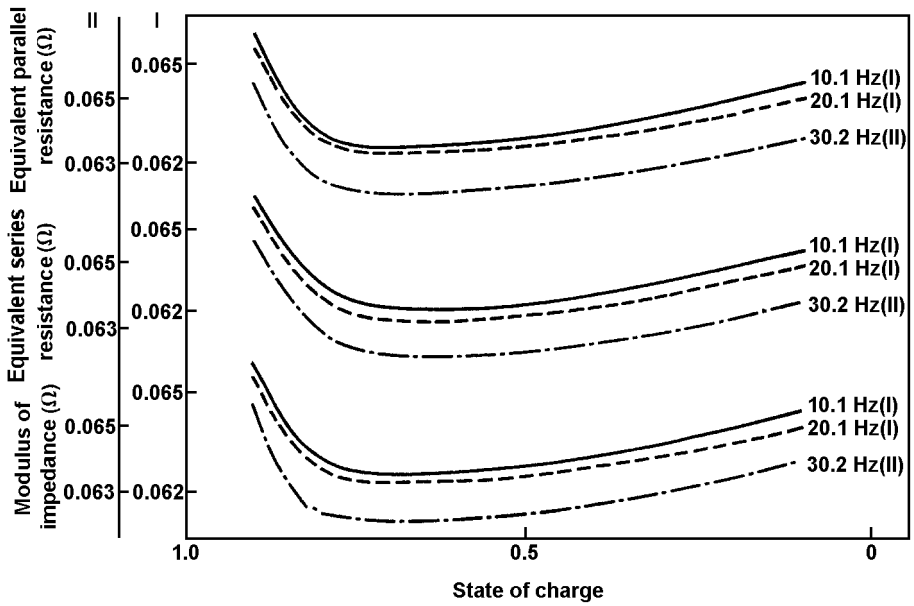

Fig3.33 Impedance measurements of nickel-cadmium cells (from [142]): dependence of equivalent parallel resistance, equivalent series resistance, and moduli of impedance on state-of-charge at different frequencies.

3.5.2.2 Leclanche Cell

The irnpedances of undischarged and discharged cells have been measured at various states-of-charge (Fig 3.34). For an undischarged cell the impedance is similar to that of a system controlled almost completely by the processes of charge transfer at a planar electrode and transport of the charge transfer products in the solution. For a discharged cell the reduction of the slope of the tail (45° in Fig 3.34) is interpreted by the authors as being due to development of pits which behave like semi-infinite pores (whose slope would give $\pi/8$, see § 3.1.3). In addition, the degeneration of the high frequency semi-circle into a straight line could be attributed to the double layer capacity increasing as the cell discharges (pitted zinc electrode would have a larger surface). The authors suggest the use of the impedance modulus |Z| at 31.2Hz to indicate the state-of-charge value [143-145].

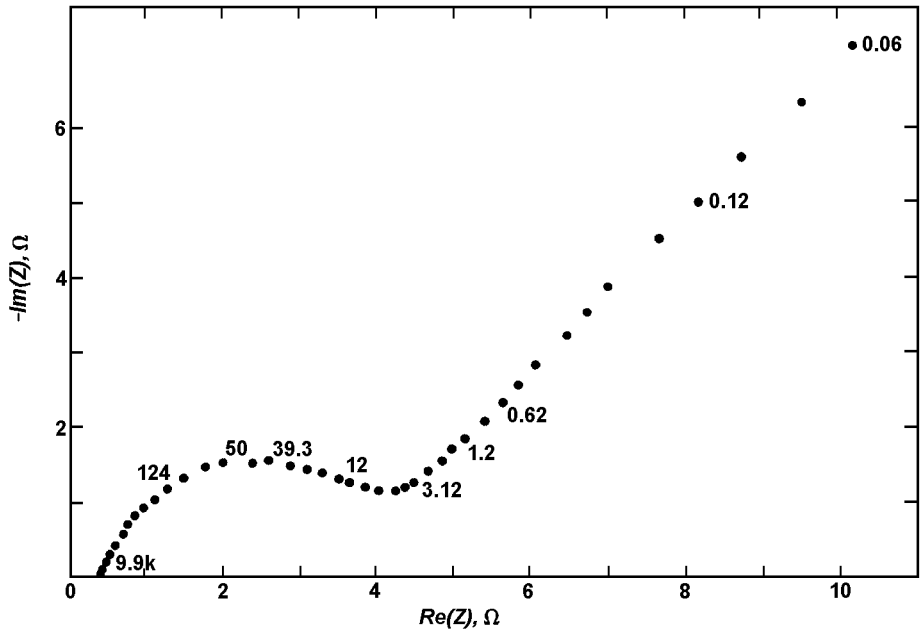

Fig. 3.34 Impedance measurement of an undischarged Leclanche cell (Ever Ready SP11) (from [143])

3.5.2.3 Silver Oxide - Zinc Cells

Impedance measurements at 40Hz have been performed on 50Ah silver oxide-zinc cells. It was shown, on a statistical basis (100 samples), that the impedance of these cells tended to increase with the period of storage and that the magnitude of this rise in impedance depended primarily on temperature and, to a lesser degree, on storage mode. Impedances decrease appreciably and rapidly within the first few milliseconds of discharge. The cause of this impedance variation is attributed to changes that occur at the positive electrode [146].

3.5.2.4 Magnesium - Manganese Dioxide Cells

An impedance analysis of magnesium - manganese dioxide cells (2.5Ah) has shown that the processes are mainly diffusion controlled for undischarged cells but are charge transfer controlled during cell discharge. In spite of the narrow frequency range analysed the authors claim that determination of state-of-charge is not possible by the measurement of impedance parameters [145].

3.5.2.5 Lead - Sulphuric Acid Cell

The electrochemistry of the lead dioxide electrode, especially in sulphuric acid medium, is of considerable interest due to its important industrial use as an oxidation electrode for synthetic organic electrochemistry and its use as an energy storage electrode. Hence, fundamental aspects of the processes which govern this interface have been investigated. Impedance measurements have been made of massive and porous lead dioxide [147], anodic dissolution of lead in oxygenated and deoxygenated sulphuric acid solution [148] and electrochemical oxidation of Pb to form $PbSO_4$ [149].

Due to the fact that ions of the electrolyte solution or molecules of the solvent take part in the electrode reactions of a battery by:

$$Pb + PbO_2 + 2H_2SO_4 \Leftrightarrow 2PbSO_4 + 2H_2O$$

it may be anticipated that the density of the solution may change with the state-of-charge, and hence the series resistance.

In the 15-100Hz range the lead-acid cell (7Ah) is largely controlled by charge transfer and the authors are dubious about the possibility of predicting the state-of-charge from such a narrow frequency range [150]. However, investigations performed over the frequency range 10^{-3} to 10^{3} Hz, on the negative [151] and positive plates, do show differences of impedance between charged and discharged cells [152] (Fig 3.35a). The same investigations also reveal impedance differences between cells of different construction and/or nominal capacity [153]. (Fig 3.35b).

Expander action in the lead-sulphuric acid cell has similarly been investigated by impedance measurements [154-156].

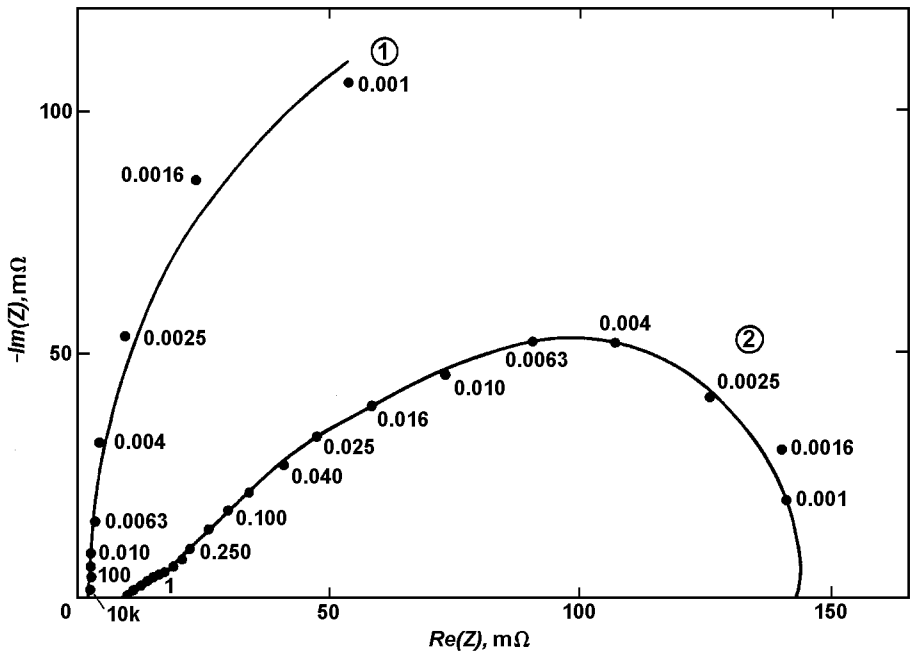

Fig3.35a Impedance measurement for lead-sulphuric acid batteries.

I = 7Ah, fully charged battery, I = 0 (From [152])

curve 1: positive plate

curve 2: negative plate

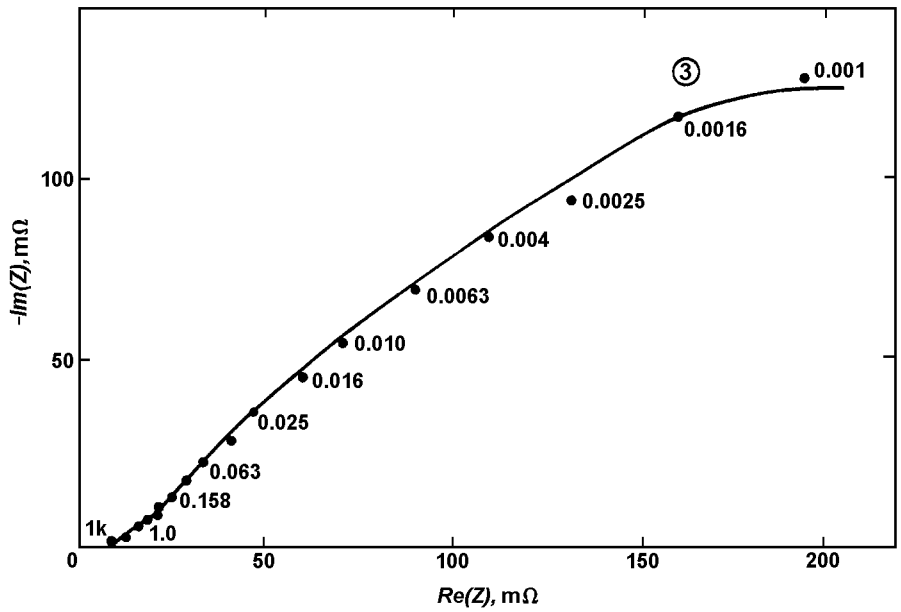

Fig 3.35a (cont)

curve 3: overall battery

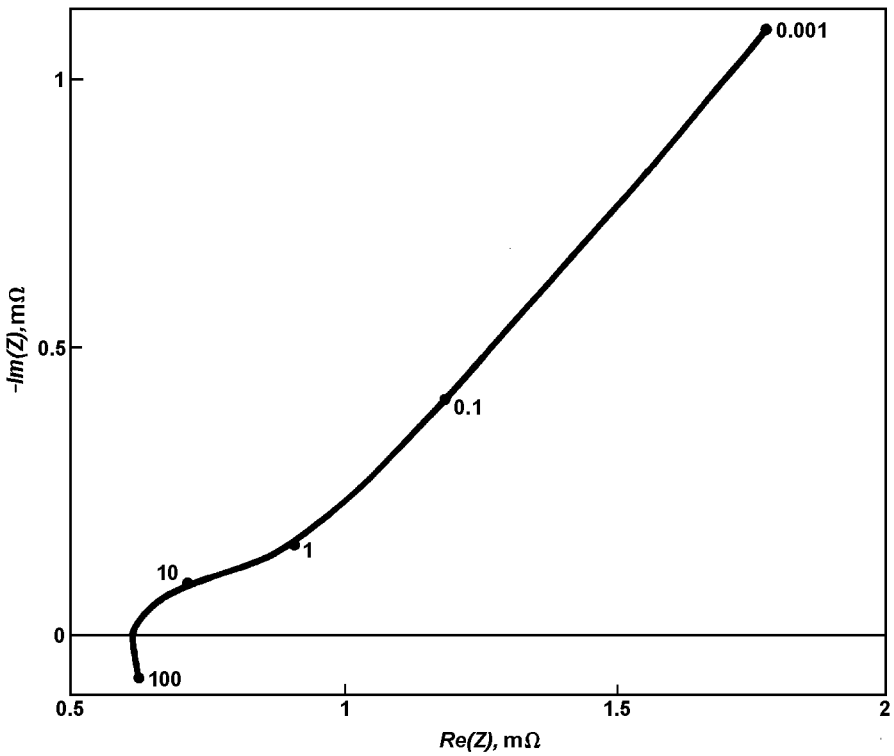

Fig 3.35b Impedance measurement for lead-sulphuric acid batteries.

I = 390Ah. Fully charged Tudor battery after 3 days of rest (From [153])

3.5.2.6 Lithium Cell

The behaviour of secondary lithium and aluminium-lithium electrodes in propylene carbonate has been investigated by impedance measurements [157]. It was shown that an improvement in cycling possibilities is obtained by using an aluminium-lithium electrode instead of a massive lithium one. An analysis of the electrochemical impedance measured on an aluminium-lithium electrode has shown that two processes can be observed during both anodic and cathodic polarisations (Fig 3.36):

a) a fast charge transfer process, corresponding to the high frequency capacitive loop, independent of the current value for $0 \leq I \leq 10mA\ cm^{-2}$.

b) a rnass transfer process through a porous layer, corresponding to the low frequency capacitive loop, depending on the current density.

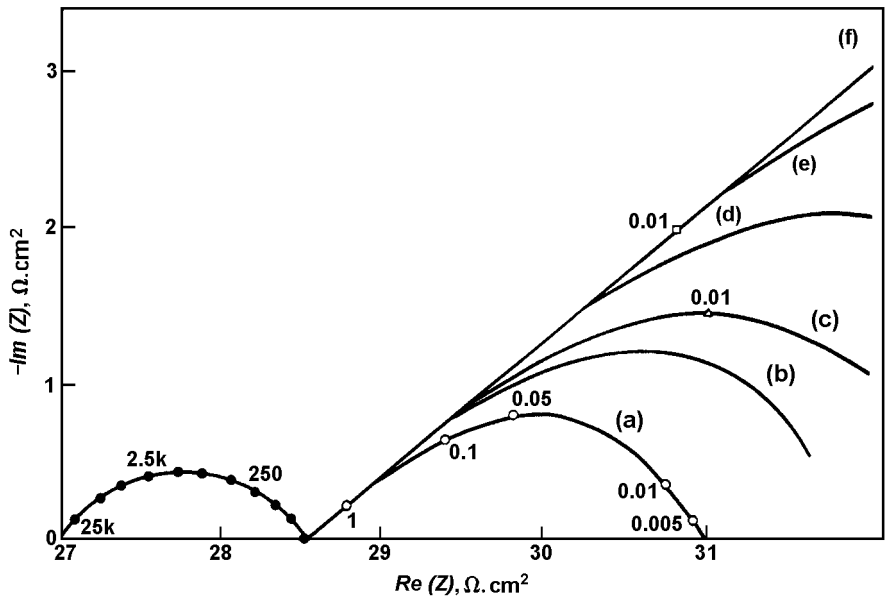

Fig 3.36 Impedance measurement of an aluminium-lithium electrode measured for I = (a) $10mA.cm^{-2}$; (b) $7.5mA.cm^{-2}$; (c) $5mA.cm^{-2}$; (d) $2mA.cm^{-2}$; (e) $1mA.cm^{-2}$; (f) $0mA.cm^{-2}$. (from [157])

3.6 Miscellaneous Applications

Impedance techniques are extremely versatile and can be used in many diverse fields of scientific study. Some examples of these uses are given below.

3.6.1 Photoelectrochemistry

Photoelectrochemistry is the science which investigates the effect of light on an electrochemical interface. By the use of impedance techniques, information has been obtained on the nature and characteristics of surface films, mainly oxides, on metal electrodes. Such studies have been carried out under galvanostatic or potentiostatic conditions and from the variations in photoresponse. Conclusions were drawn on changes in the properties of the surface film with electrode potential. The interpretation is generally based on the treatment of semiconductor electrochemistry.

In the case of copper and copper alloy electrodes it seems that the oxide films could be more easily destroyed under illumination. This may be related to the fact that copper can exhibit stress corrosion cracking in the dark but not in the light [158] (Fig 3.37a). Oxide layers on iron in borate buffer solution exhibit a similar effect under illumination (Fig 3.37b) [159].

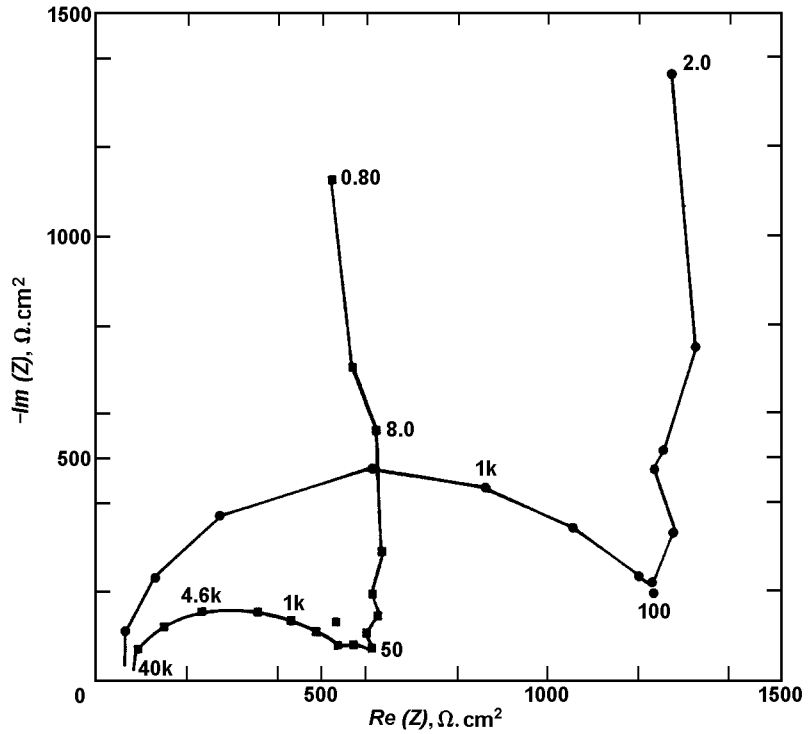

Fig 3.37a Impedance measurement of bulk Cu_2O in 0.05M Cu acetate, under illumination (■) and in the dark (●). Open circuit. (From [158])

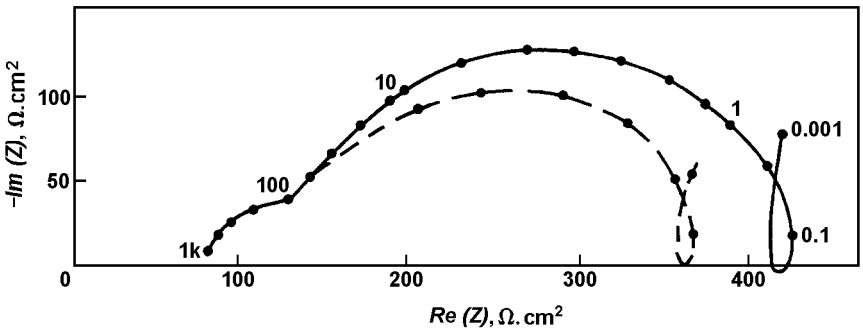

Fig3.37b impedance measurement of thermally oxidized iron in borate buffer solution V = 650mV vs SSE under illumination (broken line) and in the dark (solid line) (From [159])

3.6.2 Molten Salts

Electrode processes in fused salts are much faster than in other solvents due to the higher temperature and to the change in the structure of the co-ordination shell of the ions. Therefore the Faradaic impedance method should be a useful tool in systematic studies of these processes. In spite of this, not many impedance measurements in fused salts have hitherto been performed [160, 161]. Organic [162] and inorganic [163] salts were used as a solvent in order to study various oxido-reduction reactions. As an example, the impedance has been measured during the oxidation of the sulphide ion in molten $PbCl_2$ - KCI at 440°C (Fig 3.38). The first oxidation step has been found to be rapid and diffusion controlled. The processes occuring during the second step are not yet clearly understood.

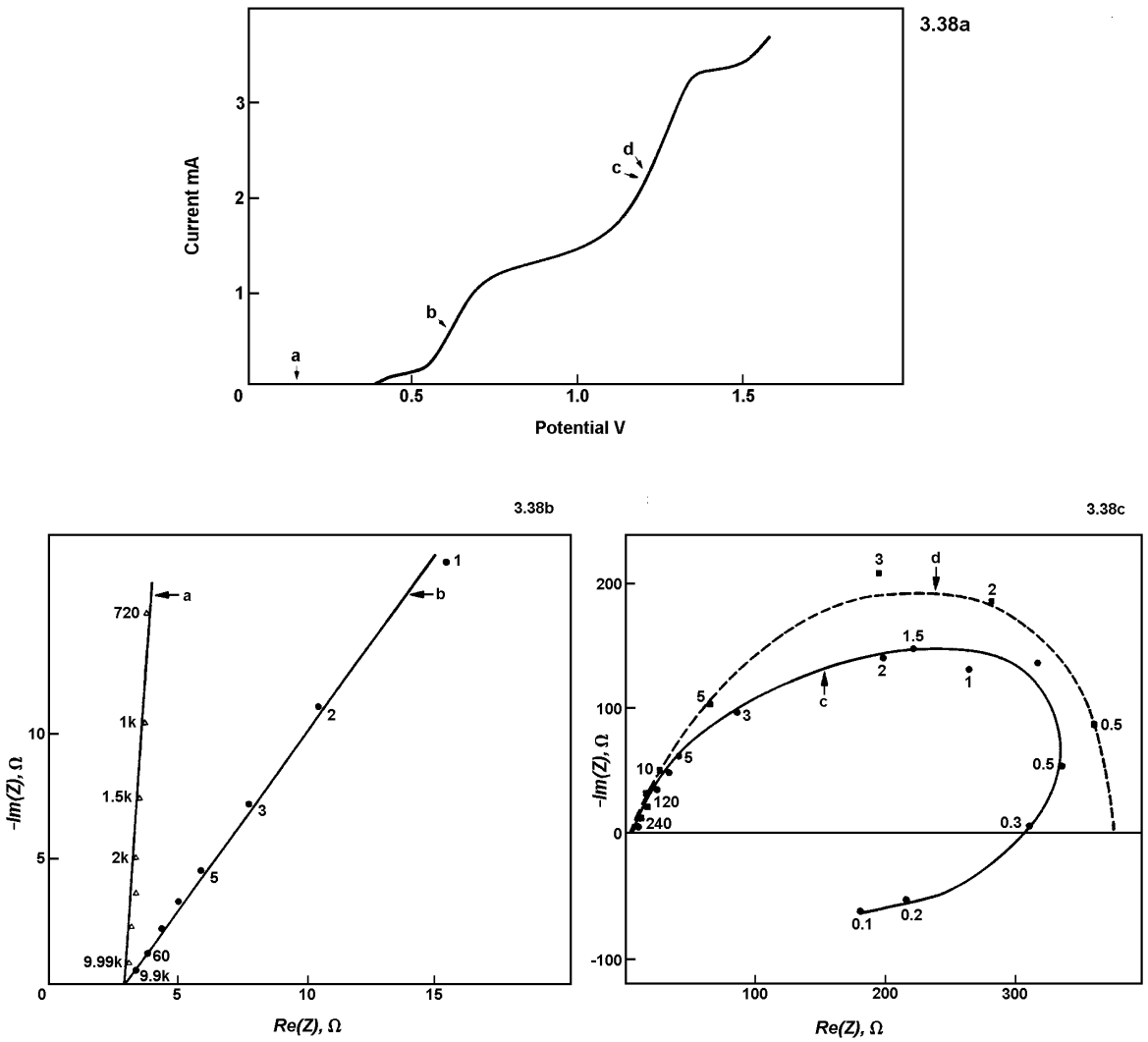

Fig 3.38 Impedance measurement in molten $PbCl_2$ – KCl: oxidation of PbS at a glassy carbon electrode (From [163])

3.6.3 Semiconductor - Electrolyte Interface

The semiconductor-electrolyte interface bears a great similarity to a semiconductor-metal interface. It has been usefully applied in investigations of the properties of the semiconductor side, with precautions being made to minimise the process on the electrolyte side [164-167]. The basic phenomena, which are associated with distribution of charges at the interface (of major importance in photoelectrochemistry), can be represented in terms of generalised equivalent circuits. The components of the latter have been obtained in the case of TiO_2 -aqueous electrolyte interface and it has been shown that they can be interpreted in terms of two space charge layers with two different doping levels [168].

In ion implantation processes the damage done by bombardment of the crystal lattice with energetic ions is a considerable problem. To investigate this problem, impedances have been measured at an interface formed between silicon implanted with energetic ions and an electrolyte. A great sensitivity to the surface damage caused by ion implantation was found. To measure the extent of the damage, thin layers were removed from the surface of the silicon by electrochemical etching and impedance measurements were made after the removal of each layer [169] - see Fig 3.39. In the example illustrated by Fig 3.39 it can be seen that the effect of ion bombardment damage extended to a depth of approximately 2,400A since, with this thickness of the surface removed, the conductivity curve of the interface began to approach that of the undamaged substrate.

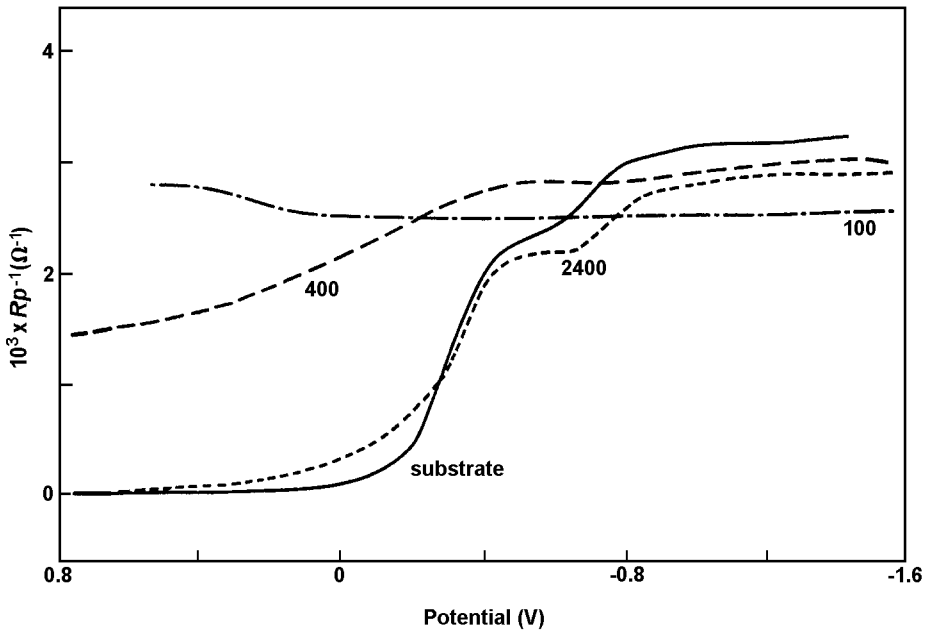

Fig 3.39 Characteristics of an n-Si surface (100Ω.cm) implanted with 10^5 P.cm^{-2} at 30keV: I/R_p versus potential. The number indicates the removed layers (A) (From [169])

3.6.4 Organic Electrochemistry

Following their successful use in the field of inorganic electrochemistry, impedance measurement techniques have begun to be used in the study of organic electrochemistry [170-172]. In this field, impedance measurement has proved to be a convenient diagnostic tool and has been used, for example, to detect and study the adsorption phenomena of electroactive or electroinactive compounds on an electrode and to obtain the electrode capacity, the solution resistance and, most important of all, the characteristics of the electro-chemical reactions.

Various reaction mechanisms have been investigated in aqueous solvents or non-aqueous solvents (aprotic or not) on a mercury electrode - See Fig 3.40.

In the determination of rapid electrode reactions of aromatic compounds in aprotic media [173], strong adsorption of electroactive species has been considered from the point of view of both a Langmuir and a Frumkin isotherm [174].

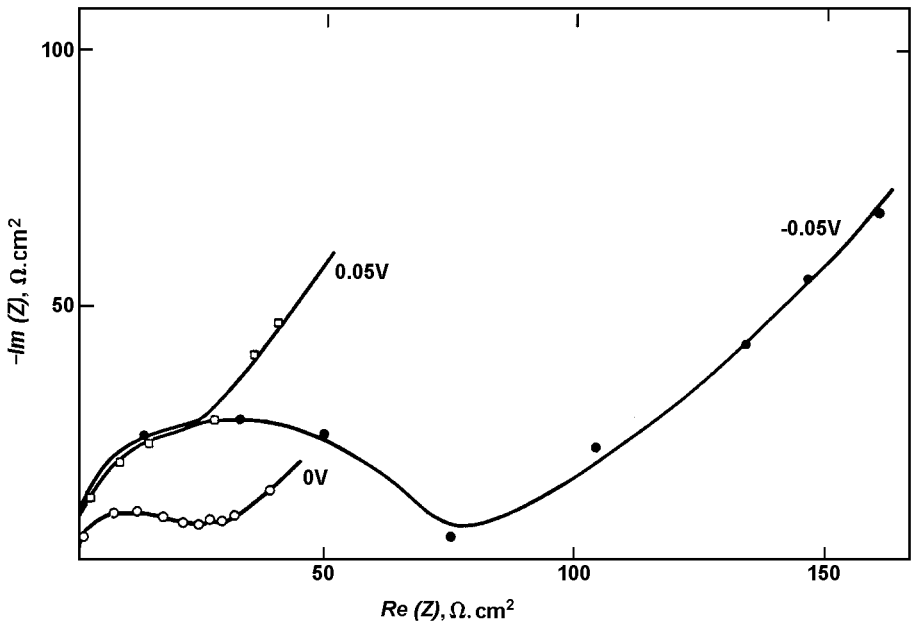

Fig 3.40 Impedance measurement after correction of double layer capacitance for the solution of ImM macrobicyclic (222) ligand in 0.1M tetrahexylammonium perchlorate in propylene carbonate (from [170])

3.6.5 Biology and Bioelectrochemistry

For many years pioneers such as K.S. Cole [175, 176] have been using impedance measurements in the fields of biology and bioelectrochemistry. During that time the investigation of impedance data has provided information on many interfaces of biological interest. Typical examples of the research done include studies of:

0 the tenderness and maturity of meat [177]

m contrast gain control in the retina of a cat's eye [178]

m permeability of the erythrocytic membrane in red blood cells [179, 180] - see Fig 3.41.

Further information on the wide variety of possible biological applications is given in reference [181]

3.6.6 Electrochemical Displays

Considerable interest has recently been aroused by the possibility of fabricating displays based on the electrochemical injection of metal or hydrogen atoms into transition metal oxides, usually $W0_3$. The reaction can be written:

$W0_3$ (colourless) + $yM^+ + ye^- \Leftrightarrow M_y\ W0_3$ (coloured)

The electrochemical impedance has been measured at the Li/LiA_5F_6 (0.75M) interface in a propylene carbonate/Li_yW0_3 cell. It was shown that for short periods ($t < 0.5s$) the interfacial charge transfer reaction is important, but for longer periods, the rate of lithium injection is determined by the diffusion kinetics [182].

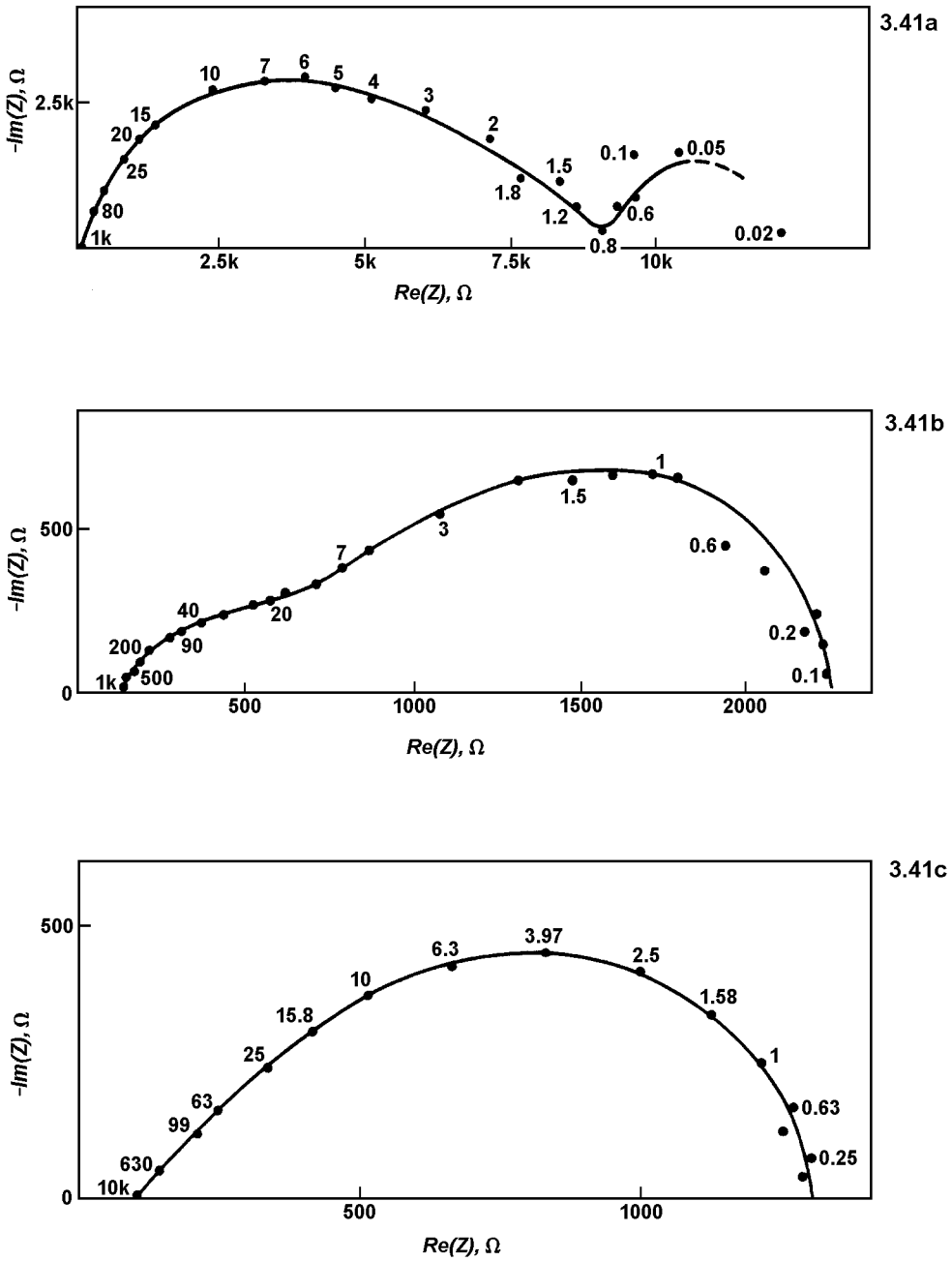

Fig 3.41 Impedance measurements of red blood cell suspension corresponding to a hematocrit of about 40% with ferrocyanide as a tracer at T = 38°C (disc electrode rotation speed = 2000rpm) (from [179])

a) discoidal hardened red blood cell with $[Fe(CN)^{4}_{6}^{-}] = 1.7.10^{-3}M$

b) spherical hardened red blood cell with $[Fe(CN)^{4}_{6}^{-}] = 3.3.10^{-3}M$

c) Normal red blood cell

3.7 Impedance Dispersion: Roughness and Current Distribution

In the various examples of impedances described earlier, depressed semi-circles appear whose centre is below the real axis. This phenomenon is well known in homogeneous media studies where the Cole-Cole dispersion

$$H(w) = \frac{1}{1 + (jwt)^{1-a}} \tag{28}$$

is the rule for dielectric relaxation [183]. The phenomenon is explained by a repartition of the time constants of the processes around a central value. This dispersion has been observed in electrochemistry both in solid and in liquid electrolytes. The repartition of the time constant is generally explained either by the roughness of the electrode surface or by geometrical effects leading to a non-uniform repartition of the current density on the surface.

3.7.1 Surface Roughness

The surface roughness theory for impedance dispersion [12] appears, in some cases, to be contradicted by experimental evidence.

In support of the theory, impedance measurements of the interface between a single crystal (or a sintered disc of β-alumina) and a gold electrode were performed, in the frequency range 1 - 10^4Hz, for various contact roughnesses. As the roughness was increased, a deviation of the impedance characteristics from the vertical and a decrease in double-layer capacitance were observed [184]. Similar effects have been obtained with an AgI/electrolyte solution interface [185] and with copper electro-depositions from a $CuSO_4$ aqueous solution [186].

In detraction of the surface roughness theory, it has been shown that the interface obtained by a pressing of AgBr and graphite powders behaves like a smooth surface [187]. Again, in the case of fused solid electrolytes, no discontinuous changes have been observed in the impedance parameters [188].

Considering both sides of this argument, it would seem that the importance of surface roughness is restricted to particular cases.

3.7.2 Current Distribution

Geometrical effects, e.g. lack of symmetry and the finite dimensions of the electrode, lead to a non-uniform current distribution on the electrode surface, and hence to a non-uniform potential distribution. These effects are well-known on the mercury drop electrode. With this the screening effect due to the capillary and infiltration of the electrolyte into the capillary are responsible for frequency dispersion at high and low frequencies [189 – 192]. Similarly, on the rotating disc electrode, a non-uniform current distribution, due to an edge effect, has been shown [193, 194]. It has also been shown that the current non-uniformity gives rise to frequency dispersion in impedance measurements [195, 196] and these have been tentatively corrected [197, 198].

REFERENCES FOR CHAPTER 3

1 C DESLOUIS, I EPELBOIN, M KEDDAM and J C LESTRADE, JElectroanal Chem 28, pp 57 - 63, 1970

2 J M COUEIGNOUX and D SCHUMANN, JElectroanal Chem 17, pp 245 - 252, 1968

3 0 CONTAMIN, E LEVART and D SCHUHMANN, JElectroanal Chem 84, pp 271 - 294, 1977, and 88, pp 49 - 56, 1978

4 0 DUPRE LA TOUR, These Paris, 1973

5 F SCHELLER, S MULLER, R M LANDSBERG and H SPITZER, JElectroanal Chem 20, pp 375 - 381, 1969

6 E LEVART, D SCHUHMANN, 0 CONTAMIN and M ETMAN, JElectroanal Chem 70, pp 117 - 131, 1976

7 M ETMAN, E LEVART and D SCHUHMANN, JElectroanal Chem 101, pp 141 - 152, 153 - 170, 1979

8 K TOKUDA, T GUESHI and H MATSUDA, JElectroanal Chem 102, pp 41 - 48, 1979

9 C DESLOUIS and B TRIBOLLET, Electrochim Acta 23, pp 935 - 944, 1978

10 C DESLOUIS, I EPELBOIN, B TRIBOLLET and L VIET, Coll Intern du CNRS No 233 "Polymeres et lubrification", pp 283 - 294,1975

11 A WINSEL, Z Elektrochem 66 pp 287 - 304, 1962

12 R de LEVIE, Advances in Electrochemistry and Electrochemical Engineering Vol 6, Inter-science, Wiley, New York, pp 329 - 397, 1967

13 R de LEVIE, Electrochim Acta 9, pp 1231 - 1245, 1964

14 P DROSSBACH and S SCHULZ, Electrochim Acta 9, pp 1391 - 1404, 1964

15 H KAISER, K D BECCU and M A GUTJAHR, Electrochim Acta 21, pp 539 - 543, 1976

16 J P CANDY, P FOUILLOUX, C GABRIELLI, M KEDDAM and H TAKENOUTI, Compt Rend Acad Sciences Paris 292C, pp463-466, 1977

17 R D ARMSTRONG, K EDMONSON and J A LEE, J Electroanal Chem 63, pp 287 - 302, 1975

18 J McHARDY, J M BARIS and P STONEHART, J Applied Electrochem 6, pp 371 - 376, 1976

19 K MUND, Siemens Forsch u Entwicke 4, pp 68 - 74, 1975

20 R S K RANGARAJAN, P F SEELIG and R de LEVIE, J Electroanal Chem 100, pp 33 - 62 1979

21 T R BRUMLEVE and R P BUCK J Electroanal Chem 90, pp 1 - 32, 1978

22 F S STOVER and R P BUCK, J Electroanal Chem 107, pp 165 - 176, 1980

23 R de LEVIE, N G SEIDAH and D LARKIN, J Electroanal Chem 49, pp 153 - 159, 1974

24 R de LEVIE and D VUKADIN, J Electroanal Chem 62, pp 95 - 109, 1975

25 J MARTENS, P VAN DEN WINKEL and J VEREECKEN, J Electroanal Chem 85, pp 277 - 287, 1977

26 R P BUCK, J Electroanal Chem 18, pp 363 - 399, 1968

27 M J D BRAND and G A RECHNITZ Anal Chem 41, pp 11 85 - 1191,1969; 42 pp 478 - 483, 1970

28 J R SANDIFER and R P BUCK, J Electroanal Chem 56, pp 385 - 398, 1974

29 P SETA and C GAVACH, CR Acad Paris 275C, pp 1231 - 1234,1972, and 277C, pp 403 - 406, 1973

30 C GAVACH, P SETA and F HENRY, Bioelectrochem and Bioenerget 1, pp 329 - 342, 1974

31 D SCHUHMANN and P SETA, J of Coll and Interf Sci 69, pp 448 - 459, 1979

32 I EPELBOIN, C GABRIELLI, M KEDDAM and H TAKENOUTI, Comprehensive Treatise on Electrochemistry, Ed J O'M Brockris, B E Conway and E B Yeager, Vol 4 pp 15 1 - 192, 1981 Plenum Press (New York)

33 R D ARMSTRONG, M F BELL and J P HOLMES, Corrosion Science 19, pp 297 - 304, 1979

34 R D ARMSTRONG and A C COATES, J Electroanal Chem 50, pp 303 - 313, 1974

35 R D GILLES, N A HAMPSON, A MARSHALL and R J LATHAM, JElectroanal Chem 47, pp 535 - 538, 1973

36 0 ROSA-MATTOS, These Paris (to be submitted)

37 B BFCHET, I EPELBOIN and M KEDDAM, J Electroanal Chem 76, pp 129 - 134, 1977

38 I EPELBOIN, C GABRIELLI and M KFDDAM, Corrosion Science 1 5, pp 155 - 17 1, 1975

39 I EPELBOIN, C GABRIELLI, M KEDDAM and H TAKENOUTI, Electrochim Acta 20, pp 913 - 916, 1975

40 I EPELBOIN, C GABRIELLI, M KEDDAM and H TAKENOUTI, CR Acad Sc Paris 276C pp 145 - 148, 1973

41 C GABRIELLI, M KEDDAM, E LISAC and H TAKFNOUTI, Electrochim Acta 21, pp 757 - 766, 1976

42 C GABRIELLI, M KEDDAM and H TAKENOUTI, JElectroanal Chem 61, pp 367 - 371, 1975

43 A AVILLERA, M CID and M C PETIT, J Electroanl Chem 105, pp 149 - 160,1979

44 I EPELBOIN and M KEDDAM, Electrochim Acta 17, pp 177 - 186,1972

45 H G FELLER, H J RATZER-SCHEIBE and W WENDT, Electrochim Acta 17, pp 187 - 195, 1972

46 A JOUANNEAU, M KEDDAM and M C PETIT, Electrochim Acta 21, pp 287 - 292,1976

47 A CAPRANI, 1 EPELBOIN and Ph MOREL, J Electroanal Chem 43, App 2 - 9, 1973

48 R D ARMSTRONG and R E FIRMAN, J Electroanal Chem 34, pp 391 - 397, 1972

49 I EPELBOIN, M KEDDAM, 0 ROSA-MATTOS and H TAKFNOUTI, Corrosion Science 19, pp 1105 - 1112, 1979

50 M E WALTON and P A BROOK, Corrosion Science 17, pp 593 - 602, 1977

51 R D ARMSTRONG and M HENDERSON, J Electroanal C7iem 40, pp 121 - 131, 1972

52 I EPELBOIN, M KEDDAM and Ph MOREL, Proc of the 3rd lnt Meeting on Metailic Corrosion, Moscow, 1966, English ed, Svets-Zeitlinger, Amsterdarn, Vol 1, pp 110 - 118, 1963

53 R D ARMSTRONG and K EDMONSON, J Electroanal Chem 53, pp 371 - 387, 1974

54 R D ARMSTRONG and M F BELL, J Electroanal Chem 55, pp 201 - 211, 1974

55 R D ARMSTRONG, M F BELL and A A METCALFE, J Electroanal Chem 84, pp 61 - 72, 1977

56 D SCHUHMANN, These Paris, 1964

57 M BADDI, C GABRIELLI, M KEDDAM and H TAKENOUTI, Passivity of metals, Ed by R P Frankenthal and J Kruger, The Electrochemical Soc Inc, pp 625 - 645, 1978

58 S HARUYAMA and T TSURU, Passivity of metals, Ed by R P Frankenthal and J Kruger The Electrochemical Soc Inc, pp 564 - 584, 1978

59 G BLONDEAU, M FROELICHER, C GABRIELLI, A HUGOT Le GOFF and V JOVANCICEVIC, J de Physique 38, Coll C5, pp 163 - 165, 1977

60 B LOYRECEK and J SEFAJA, Electrochim Acta 17, pp 1151 - 1155, 1972

61 A K VIJH, Oxides and Oxide Film, Vol 2, Ed by J W Diggle, Marcel Dekker Inc, New York pp 1 - 94, 1973

62 F MANSFELD, Advances in Corrosion Science and Technology Vol 6, Plenum Press, New York, pp 163 - 262, 1976

63 I EPELBOIN, C GABRIELLI, M KFDDAM and H TAKENOUTI, Proc of the ASTM Symp 'Progress in Electrochemical Corrosion Testing, May 1979 Ed F Mansfeld and U Bertocci pp 150 - 166, 1981 ASTM Publ.

64 D D MacDONALD and M C H MACKUBRE, Ibid

65 I EPELBOIN, M KEDDAM and H TAKENOUTI, J of Appi Electrochem 2, pp 71 - 79, 1972

66 I EPELBOIN and M KEDDAM, J Electrochem Soc 117, pp 1052 - 1056, 1970

67 I EPELBOIN, P MOREL and H TAKENOUTI, J of Electrochem Soc 118, pp 1282 - 1287. 1971

68 I EPELBOIN, M KEDDAM and H TAKENOUTI, Third European Symp on Corrosion Inhibitors (Ferrara, Italy, 1970), Annal Univ Ferrara, Sezione V, Suppl No 5, pp 237 - 251

69 A CAPRANI, I EPELBOIN, Ph MOREL and H TAKENOUTI, Fourth European Symp on Corrosion Inhibitors (Ferrara, Italy 1975), Annal Unly Ferrara, N S, Sezione V, Supp No 6, pp 5 17 - 540,

70 T MURAKAWA, S NAGAURA and N HACKERMAN, Corrosion Science 7, p 79, 1967

71 B DUS and Z SZKLARSKA-SMIALOWSKA, Corrosion NACE 25, p 69, 1969

72 M W KENDIG and H LEIDMEISER, J.Electrochem Soc 123, pp 982 - 989, 1976

73 L BEAUNIER, I EPELBOIN, J C LESTRADE and H TAKENOUTI, Surf Technol 4, pp 237 - 254, 1976

74 D G JOHN, P C SEARSON and J L DAWSON, Seminar.. "Electrochemistry and corrosion of steel in concrete", Copenhagen, Denmark, 1979

75 F WENGER, J GALLAND and P AZOU, C R Acad Sciences, Paris 149C pp 149 - 152, 1980

76 H J DE WITT, C WIJENBERG and C CREVECOEUR, J Electrochem Soc 126, pp 779 - 785, 1979

77 J A LIBSCH and 0 F DEVEREUX, J Electrochem Soc 122, pp 1654 - 1660,1975 and 123, pp 864 - 871, 1976

78 J J BODU, M BRUNIN, I EPELBOIN, M KEDDAM, G SERTOUR and H TAKENOUTI, Aluminio 46, pp 277 - 280, 1977

79 J J BODU, M BRUNIN, G SERTOUR, I EPELBOIN, M KEDDAM and H TAKENOUTI, Proc of the 88th manifestation of the European Federation of Corrosion: " Corrosion and Corrosion Protection of aluminium", Budapest, 1976

80 C GABRIELLI, M KEDDAM, H TAKENOUTI, VU QUANG KINH and F BOURELIER, Electrochim Acta 24, pp61-65, 1979

81 D D MacDONALD, B C SYRETT and S S WING, Corrosion NACE 34, pp 289 - 295, 1978

82 N HARA, K SUGIMOTO and Y SAWADA, Bull Met Soc Japan 40, pp 1304 - 1310, 1976

83 U BERTOCCI, JElectrochem Soc 127, pp 1931 - 1934,1980

84 H M CARIM, R B BEARD and A S MILLER, J Electrochem Soc 124, pp 680 - 688,1977

85 I EPELBOIN, C GABRIELLI, M KEDDAM and H TAKENOUTI, Z fur Physikalishe Chem N F 98, pp 215 - 232, 1975

86 K SUGIMOTO and Y SAWADA, Corrosion Science 17, pp 425 - 445, 1977

87 G DEMETS and A P VAN PETEGHEM, Corrosion Science 18, pp 1029 - 1040,1978

88 A C COATES and J P HOLMES, Conf on Electrochem Test Methods for Stress Corrosion Cracking, Firminy, France, 1978

89 R D ARMSTRONG and R E FIRMAN, J Electroanal Chem 45, pp 257 - 266, 1973

90 W LORFNZ, Z Naturforsch 9a, p 716, 1954

91 M FLEISCHMANN, S K RANGARAJAN and H R THIRSK, Trans Farad Soc 63, pp 1240 - 1260, 1967

92 S K RANGARAJAN, J Electroanal Chem 17, pp 61 - 68,1968

93 R D ARMSTRONG and A A METCALFE, J Electroanal Chem 71, pp 5 - 19, 1976

94 C CACHET, I EPELBOIN, M KFDDAM and R WIART, J Electroanal Chem 100, pp 745 - 757, 1979

95 I EPELBOIN and R WIART, J Electrochem Soc 118, pp 1577 - 1592, 1971

96 I EPELBOIN, M JOUSSELIN and R WIART, JElectroanal Chem 101, pp 281 - 284,1979

97 J BRESSAN and R WIART, J Applied Electrochem 9, pp 615 - 621, 1979

98 I EPELBOIN, M KSOURI and R WIART, J Electrochem Soc 122, pp 1206 - 1214,1975

99 I EPELBOIN, M KSOURI and R WIART, Farad Disc of the Chem Soc No 12, pp 115-125,1978

100 M KSOURI and R WIART, Oberflache-Surface 18, pp 61 - 67,1977

101 J BRESSAN and R WIART, J Applied Electrochem 9, pp 43 - 53, 1979

102 J BRESSAN and R WIART, J Electroanal Chem 107, pp 233 - 245, 1980

103 C CACHET, M FROMENT and R WIART, Electrochim Acta 24, pp 713 - 722,1979

104 S G CANAGARATNA and S A G R KARUNATHILAKA, J Electroanal Chem 60, pp 65 - 73, 1975

105 J VEREECKEN and R WINAND, Electrochim A cta 22, pp 401 - 409, 1977

106 I R BURROWS, K L DICK and J A HARRISON, Electrochim Acta 21, pp 81 - 84, 1976

107 F LENOIR and R WIART, Metaux, Comsion, Industrie 557, pp 1 - 20, 558, pp 59 - 70, 1972

108 R WIART, E LEJAY and F LENOIR, Proc of Interfinish 1972, Forster-Verlag, Zurich, pp 84 - 88, 1973

109 I EPELBOIN and R WIART, J Chim Phys 70, pp 589 - 593, 1973

110 W DAVISON, J A HARRISON and J THOMPSON, Faraday Disc of the Chem Soc 56 pp 171 - 179, 1974

111 I R BURROWS, J A HARRISON and J THOMPSON, J Electroanal Chem 53, pp 283 - 291, 1974

112 J A HARRISON and D R SANDBACH, JElectroanal Chem 85, pp 125 - 133, 1977

113 Ph AUBRUN, F WENGER and R WIART, J of Applied Electrochem 7, pp 225 - 233,1977

114 C GABRIELLI and F RAULIN, J Applied Electrochem 1, pp 167 - 177, 1971

115 R D ARMSTRONG, T DICKINSON and P M WILLIS, J Electroanal Chem 59, pp 281 - 293, 1975

116 J E BAUERLE, J Phys Chem Solids 30, pp 2657 - 2670, 1969

117 H J DE BRUIN and S P S BADWAL, J of Australian Ceramic Soc 14, pp 20 - 28,1978

118 J R MacDONALD, Intern Conf on Superionic Conductors Schnectady, New York, 1976

119 R D ARMSTRONG and K TAYLOR, J Electroanal Chem 63, pp 9 - 17, 1975

120 E SCHOULER, M KLEITZ and C DEPORTES, J Chim Phys 70, pp 923 - 935, 1973

121 E SCHOULER, G GIROUD and M KLEITZ, J Chim Phys 70, pp 1309 - 1316, 1973

122 E SCHOULER and M KLEITZ, J Electroanal Chem 64, pp 135 - 142, 1975

123 N B BEEKMANS and L HEYNE, Electrochim Acta 21, pp 303 - 310, 1976

124 S P S BADWAL and H J DE BRUIN, Phys Stat Sol (a) 54, pp 261 - 270, 1979

125 E SCHOULER, A HAMMOU and M KLEITZ, Met Res Bull 11, pp 1137 - 1146, 1976

126 J M REAU, C LUCAT, G CAMPET, J PORTIER and A HAMMOU, J of Solid State Chem, 17, pp 123 - 129, 1976

127 I D RAISTRICK, CHUN HO, YAW WEN HU and R A HUGGING, J Electroanal Chem 77, pp 319 - 337,1977

128 J H KFNNEDY, J R AKRIDGE and M KLEITZ, Electrochim Acta 24, pp 781 - 787, 1979

129 I M HODGE, M D INGRAM and A R WEST, J Electroanal Chem 74, pp 125 - 143, 1976

130 R D ARMSTRONG and D P SELLICK, J Applied Electrochem 9, pp 623 - 629, 1979

131 R D ARMSTRONG, T DICKINSON and J TURNER, J Electroanal Chem 44, pp 157 - 167, 1973

132 M L BAYARD and G G BARNA, J Electroanal Chem 9 1, pp 201 - 209, 1978

133 S ATLUNG and T JACOBSEN, Electrochim Acta 21, pp 575 - 584, 1976

134 R D ARMSTRONG, T DICKINSON and P M WILLIS, J Electroanal Chem 48, pp 47 - 53, 1973

135 R. J GRANT, M D INGRAM and A R WEST, J Electroanal Chem 80, pp 239 - 244, 1977

136 R P BUCK, D E MATHIS and R K RHODES, J Electroanal Chem 80, pp 245 - 257, 1977

137 U V ALPEN, M F BELL and T GLADDEN, Electrochim Acta 24, pp 741 - 744, 1979

138 U V ALPEN and M F BELL, JElectroanal Clzem 99, pp 85 - 92, 1979

139 J M REAU, G MAGNIEZ, L RABARDEL, J P CHAMINADE and M POUCHARD, Mat Res Bull 11, pp 867 - 872, 1976

140 N A HAMPSON, S A G R KARUNATHILAKA, and R LEEK, J Applied Electrochem 10, pp 3 - 11,1980

141 J EULER and K DEHMELT, Ber Bunsengeschls 61, pp 1200 - 1209, 1957

142 S SATHYANARAYANA, S VENUGOPALAN and M L GOPIKANTH, J Applied Electrochem 9, pp 125 - 139, 1979

143 S A G R KARUNATHILAKA, N A HAMPSON, R LEEK and T J SINCLAIR, J Applied Electrochem 10, pp 357 - 363, 1980

144 S A G R KARUNATHILAKA, N A HAMPSON, R LEEK and T J SINCLAIR, Applied Electrochem 10, pp 603 - 609, 1980

145 M L GOPIKANTH and S SATHYANARAYANA, J Applied Electrochem 9, pp 581 - 585, 1979

146 H A FRANCK, W L LONG and A A UCHIYAMA, J Electrochem Soc 123, pp 1 - 9,1976

147 P CASSON, N A HAMPSON and M J WILLARS, J Electroanal Chem 97, pp 21 - 32,1979

148 R D ARMSTRONG and K L BLADEN, J Appl Electrochem 7, pp 345 - 353, 1077

149 A N FLEMING and J A HARRISON, Electrochem Acta 2 1, pp 905 - 912, 1976

150 M L GOPIKANTH and S SATHYANARAYANA, J Applied Electrochem 9, pp 369 - 379, 1979

151 A N FLEMING, J A HARRISON and J M PONSFORD, Electrochimica Acta 22, pp 1371 - 1374, 1977

152 M KEDDAM, S STOYNOV and H TAKENOUTI, J Applied Electrochem 7, pp 539 - 544, 1977

153 N YAHCHOUCHI, These Paris 1981

154 M P J BRENNAN and N A HAMPSON, J Electroanal Chem 54, pp 263 - 268, 1974

155 A LE MEHAUTE, J Applied Electrochem 6, pp 543 - 550, 1976

156 V S SHALDAEV and K V RYBALKA, Electrokhimiya 15, pp 381 - 384, 1979

157 I EPELBOIN, M GARREAU, J THEVENIN and D WARIN, Fall meeting of the Electro-chemical Society Abstracts pp 69 - 71,1979, J Electrochem Soc 127, pp 2100 - 2104, 1980

158 U BERTOCCI, J Electrochem Soc 125, pp 1598 - 1602, 1978

159 M FROELICHER, M MAJA and P SPINELLI, 31st meeting of ISE, Venice, Sept 1980 Proc. pp 804 - 806

160 H A LAITINEN, R P TISCHER and D K ROE, I Electrochem Soc 107, pp 546 - 5 55, 1960

161 J E B RANDLES and W WHITE, Z Elektrochem 59, pp 666 - 671, 1955

162 A KISZA and M GRZESZCZUK, J Electroanal Chem 9 1, pp 11 5 - 124, 1978

163 D LELIEVRE, A DE GUIBERT and V PLICHON, Electrochim Acta 24, pp 1243 - 1245, 1979

164 R CASTAGNE and A VAPAILLE, Surface Science 28, pp 157 - 193, 1971

165 E C DUTOIT, R L VAN MEIRHAEGHE, F CARDON, W P GOMES, Ber Bunsen Gesselshaft 79, pp 1206 - 1213, 1975

166 M J MADDU, F CARDON and W P GOMES, J Electrochem Soc 124, pp 1623 - 1627, 1977

167 G HOROWITZ, J Applied Phys 49, pp 3571 - 3573, 1978

168 M TOMKIEWICZ, J Electrochem Soc 126, pp 2220 - 2225, 1979

169 M T PHAM and J HUELLER, J Applied Electrochem 7, pp 531 - 537, 1977

170 L POSPISIL, J KUTA, F PETER and M GROSS, J Electroanal Chem 90, pp 251 - 259, 1978

171 F PETER, L POSPISIL, J KUTA and M GROSS, J Electroanal Chem 90, pp 239 - 249, 1978

172 J F C BOODTS, M SLUYTERS-REHBACH and J H SLUYTERS, J Electronanal Chem 105 pp 189 - 203, 1979

173 H KOJIMA and A J BARD, J Electroanal Chem 63, pp 11 7 - 129, 1975

174 E LAVIRON, J Electroanal Chem 97, pp 135 - 149, 105 pp 25 - 34, and 105 pp 35 - 42, 1979

175 K S COLE and R F BAKER, J General Physiology 24, pp 771 - 788, 1941

176 K S COLE, Membranes, Ions and Impulses, Univ of California Press, Berkeley, 1968

177 N FAURE, Ch FLACHAT, P JENIN, J LENOIR, C ROUILLET and A THOMASSET, Rev Medicale Veterinaire 123, pp 15 17 - 1527, 1972

178 R SHAPLEY and J D VICTOR, Vision Research 19, pp 431 - 434, 1979

179 A CAPRANI, C DESLOUIS and B TRIBOLLET, Proc of: Electrical Phenomena at the Biological Membrane level, Ed E Roux, Elsevier Amsterdam, pp 403 - 416, 1977

180 A CAPRANI, C DESLOUIS, I EPELBOIN and B TRIBOLLET, Bioelectrochem and Bioenerget 2, pp 351 - 357, 1975

181 Proceedings of the meeting: Advances in Bioelectrical impedance measurements held in Lyon (June 1976) Ed CETAC, 18 rue Doyen Lepine 69500 BRON, France

182 C HO, I D RAISTRICK and R A HUGGINS, J Electrochem Soc 127, pp 343 - 350, 1980

183 K TAKAHASHI, Electrochim Acta 13, pp 1609 - 1621, 1968

184 R D ARMSTRONG and R A BURNHAM, J Electroanal Chem 72, pp 257 - 266, 1976

185 D A DE VOOYS and J H A PIEPER, J Electroanal Chem 72, pp 147 - 164, 1976

186 J A HARRISON and P J STRONACH, J Electroanal Chem 72, pp 239 - 242, 1976

187 D O RALEIGH, JElectrochem Soc 121, pp 639 - 645, 1974

188 D O RALEIGH and H R CROW, J Electrochem Soc 118, pp 79 - 86, 1971

189 C CACHET, H CACHET and J C LESTRADE, J Chim Phys 70, pp 557 - 558, 1973

190 D SCHUHMANN, C CACHET, I EPELBOIN and L VIET, J Chim Phys 62, pp 1214 - 1220, 1965

191 G C BARKER, A W GARDNER and M J WILLIAMS, J Electroanal Chem 41, App 1 - 5, 1973

192 R D ARMSTRONG and W P RACE, J Electroanal Chem 33, pp 285 - 290,1971

193 J NEWMAN, J Electrochem Soc 113, pp 501 - 502, 1966

194 V MARATHE, MS thesis Berkeley, Ca (UCRL 18264) 1968

195 K NISANCIOGLU and J NEWMAN, J Electrochem Soc 120, pp 1339 - 1346, 1973

196 J NEWMAN, J Electrochem Soc 117, pp 198 - 203, 1970

197 S H GLARUM, J Electrochem Soc 124, pp 518 - 524, 1977

198 S H GLARUM and S H MARSHALL, J Electrochem Soc 126, pp 424 - 430, 1979

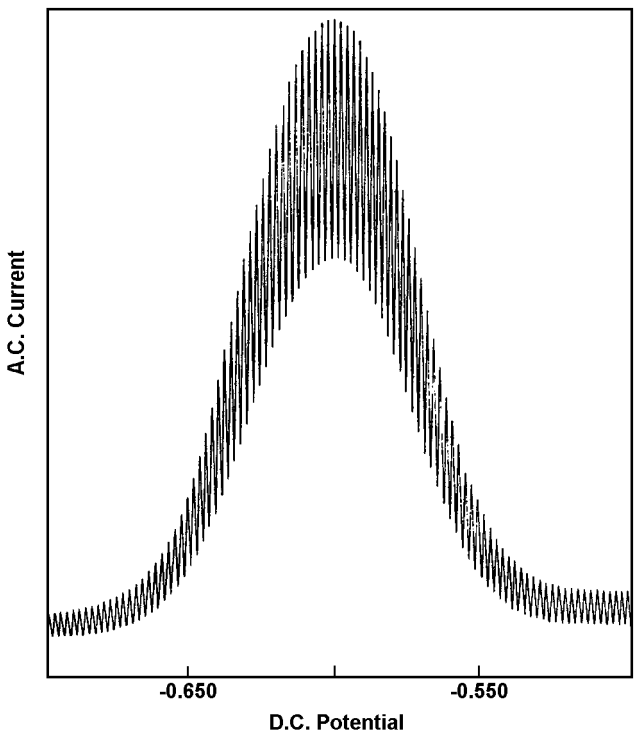

Fig 4.1 Fundamental harmonic ac polarogram (from [4])

System: 3.10^{-3}M Cd(II), 1.0M Na_2S0_4. Applied potential: 10mV peak-to-peak, 320Hz; dc scan rate = 25mV mn - 1

4 Other AC Techniques

All the quantities which can be controlled by the experimenter can be modulated by a sine wave. Hence, pressure [1] surface of a mercury electrode [2] rotation speed of the electrode (§ 4.2) have been modulated in order to obtain information about the kinetics of the processes taking place at the interface. However, the first technique described is ac polarography which is a totally electrical technique very close to the impedance technique described previously.

4.1 AC Polarography

AC POLAROGRAPHY Alternating current polarography became an active area of research in the middle and late 1940's as an improvement of the classical steady-state polarographic method. The ac polarography experiment amounts to determining the impedance of an electrolytic cell under polarographic conditions, while employing small-amplitude (<10mV) alternating potentials. Basically, this technique is very close to the impedance measurement techniques already described. However, instead of measuring the impedance at a given polarisation potential for various frequencies, the impedance is measured at one frequency all along the polarisation curve, by sweeping the potential.

The objective of this technique is the same as that of the previous one: to relate the impedance to the electrode-reaction mechanism, kinetics, and/or concentration of an electroactive material. However, as will be seen later, the way of deriving the analytical expression of the impedance is usually different [3 - 5].

Generally the experiment is very similar to that described in § 2. In order to be compatible with automatic recording methods the small-amplitude alternating potential is normally superimposed on the de potential, which is varied linearly with time. Hence, the frequency range of analysis is limited to the acoustic frequency domain in order to avoid interference with the scan rate.

Fig 4.1 shows a recording of a fundamental polarographic wave (ac polarograrn), which is a function of alternating current amplitude versus de potential. This recording was obtained at a dropping mercury electrode (DME), therefore it includes the drop oscillations. The path followed by the maximum oscillatory values corresponds roughly with the derivative of the I-V characteristic (polarographic wave at dc). A polarographic wave obtained at a stationary electrode has essentially the same shape, without the drop oscillations.

The theoretical analysis of ac polarography is now given and is based on the quasi-reversible ac polaro-graphic wave. The systern is represented by the reaction scheme:

$$Ox + ne \underset{k_b}{\overset{k_f}{\Leftrightarrow}} Red \tag{1}$$

where the current is kinetically controlled by both charge transfer and diffusion (the "quasi-reversible" case) and is governed by eqns (32) to (37) in § 2 for the interfacial process and by eqn (38) for the current.

The application of the Laplace transform to eqns (32) to (35) yields for surface concentration:

$$C_{O_{z=0}} = C_O^* - \int_0^t \frac{I_F(t-u)du}{nFA(D_O pu)^{1/2}} \tag{2}$$

$$C_{R_{z=0}} = C_R^* - \int_0^t \frac{I_F(t-u)du}{nFA(D_O pu)^{1/2}} \tag{3}$$

For simplicity at this stage the reduced form will be assumed to be absent initially from the solution $\left(C_R^* = 0\right)$.

Substituting eqn (2) and (3) in eqn (38 § 2), rearranging, and taking into account that

$$E_{1/2}^r = E^o - \frac{RT}{nF} log\left(\frac{D_o}{D_R}\right)^{1/2} \tag{4}$$

yields the integral expression

$$y\left(t\right) = \frac{k_S}{\sqrt{D}}\left[1 - \int_0^t \frac{y\left(t-u\right)du}{\sqrt{pu}}\right]e^{-aj(t)} - \int_0^t \frac{y\left(t-u\right)du}{\sqrt{pu}} e^{bj(t)} \tag{5}$$

where

$$y\left(t\right) = \frac{I_F\left(t\right)}{nFAC_O^*\sqrt{D_O}} \tag{6}$$

$$j(t) = \frac{nF}{RT}\left[E(t) - E_{1/2}^r\right] \tag{7}$$

and

$$D = D_O^b D_R^a and b = 1 - a \tag{8}$$

If the applied potential is such that

$$E(t) = E_{dc} - \Delta E \sin wt \tag{9}$$

the dc potential term is considered constant. This assumes the rate of scan is slow relative to the rate of change of alternating potential ($w >> \frac{nnF}{RT}$ when ν is the scan rate). However, more complicated calculations, taking into account the scan rate, can be done [6, 7].

Hence the current is the response both to a step in potential of amplitude E_{dc} and to a sine wave $\Delta E \sin wt$, each of which gives a transient and a steady state response.

Substitution of eqn (9) in the exponential term of eqn (5) gives:

$$e^{-j(t)} = e^{-j} \exp\left[\frac{nF\Delta E}{RT}\sin wt\right] \tag{10}$$

where

$$j = \frac{nF}{RT}\left[E_{dc} - E^{r}_{1/2}\right] \tag{11}$$

one then develops the power series

$$exp\left[\frac{nF\Delta E}{RT}\sin wt\right] = \sum_{p=0}^{\infty}\left(\frac{nF\Delta E}{RT}\right)p\frac{(\sin wt)^{p}}{p!} \tag{12}$$

$$y(t) = \sum_{p=0}^{\infty} y_{p}(t)\left(\frac{nF\Delta E}{RT}\right)^{p} \tag{13}$$

Substitution of eqns (12) and (13) into eqn (5) and equating coefficients of equal powers of $\left(\frac{nF\Delta E}{RT}\right)^{p}$ yields a system of integral equations.

$$y_{p}(t) = \frac{k_S}{\sqrt{D}}\left(\frac{a^{p}e^{-aj}(\sin wt)^{p}}{p!} - \sum_{r=0}^{p}\left[\left(a^{r}e^{-aj} + (-1)^{r}\,b^{r}e^{bj}\right)\frac{(\sin wt)^{r}}{r!}.\int_{0}^{t}\frac{y_{p-r}(t-u)du}{\sqrt{pu}}\right]\right) \tag{14}$$

for p varying from 0 to infinity.

The values of p that must be rigorously considered in the derivation of the harmonies are $p = 2q + k$ (q = 0, 1, 2...). However, it can be shown that for sufficiently small amplitudes of the sinusoidal perturbation function ($\Delta E < 0.1V$) only the contribution from the lowest value of p to the kth harmonic need be considered, as the contribution to a given harmonic decreases with increasing p [3].

For p = 0, one obtains:

$$y_{o}(t) = \frac{k_S}{\sqrt{D}}\left[e^{-aj} - \left(e^{-aj} + e^{bj}\right)\int_{0}^{t}\frac{y_{o}(t-u)du}{\sqrt{pu}}\right] \tag{15}$$

which can be solved using Laplace transformation, hence;

$$y_{o}(t) = \frac{k_S e^{-aj}}{\sqrt{D}}exp\; l^{2}terfc\, l\sqrt{t} \tag{16}$$

where

$$l = \frac{k_S}{\sqrt{D}}\left(e^{-aj} + e^{bj}\right) \tag{17}$$

i.e. $I_{F_{1dc}} = nFAk_S e^{-aj} C_O^* \exp l^2 t.\mathrm{erfc}\, l\sqrt{t}$ (18)

which is the response to a single potential step.

For p=1, the fundamental harmonic ac wave is the solution of the integral equation:

$$y_1(t) = \frac{k_S}{\sqrt{D}}\left[G_O(t)\sin wt - \left(e^{-aj} + e^{bj}\right)\int_0^t \frac{y_1(t-u)du}{\sqrt{pu}}\right] \quad (19)$$

where

$$G_o(t) = ae^{-aj} - \left(ae^{-aj} - be^{bj}\right)\int_0^t \frac{y_o(t-u)du}{\sqrt{pu}} \quad (20)$$

The form of eqn (19) is such that $y_1(t)$ can contain only fundamental harmonic terms. Thus it can be written:

$$y_1(t) = A\sin wt + \cos wt \quad (21)$$

Substituting this solution in eqn (19), employing the trigonometric identities

$$\sin w(t-u) = \sin wt\cos wu - \cos wt\sin wu \quad (22)$$

$$\cos w(t-u) = \cos wt\cos wu - \sin wt\sin wu \quad (23)$$

applying the steady-state approximation for the sine-wave response

$$\int_0^t = \int_0^\infty \quad (24)$$

and the relations:

$$\int_0^\infty \frac{\cos wudu}{\sqrt{pu}} = \int_0^\infty \frac{\sin wudu}{\sqrt{pu}} = \frac{1}{\sqrt{2w}} \quad (25)$$

and finally, by using the integral equation for p=0, the fundamental harmonic ac current is

$$I_{F_1}(wt) = \frac{n^2F^2Ac_O^*\sqrt{wD_O}}{4RT\cosh^2\left(j/2\right)}F(t)G\left(w^{1/2}l^{-1}\right)\Delta E\sin\left[wt + \cot^{-1}\left(1 + \frac{\sqrt{2w}}{l}\right)\right] \quad (26)$$

where $F(t) = 1 + \dfrac{\left(ae^{-j} - b\right)\sqrt{D}y_o(t)}{k_S e^{-aj}}$ (27)

and $G\left(w^{1/2} l^{-1}\right) = \sqrt{\dfrac{2}{1 + \left(1 + \dfrac{\sqrt{2w}}{l}\right)^2}}$ (28)

In terms of a complex impedance the fundamental current defines an impedance

$$Z(w) = R_{ct}.F(t).\left(1 + \frac{l}{\sqrt{jw}}\right) \tag{29}$$

where the charge transfer resistance at the steady-state is

$$R_{ct} = \frac{(nF)^2 A k_S c_o^*}{RT}.\frac{e^{-aj}}{1 + e^{-j}}.\left(\frac{D_O}{D_R}\right)^{a/2} \tag{30}$$

Hence, when *t* goes to infinity

$$\lim_{t\to\infty} F(t) = 1 \tag{31}$$

and for the steady-state the classical impedance given by eqn (59) in § 1 is obtained.

One may proceed in a similar manner to obtain higher order current components. Thus solution of the integral equation for p=2 to obtain the small amplitude second harmonic and dc rectification components is readily accomplished. For the dc rectification component, one obtains

$$I_{F_2}(dc) = \frac{n^3 F^3 A C_O^* \sqrt{D_O}\,\Delta E^2\, l J \exp l^2 t.erfc.l\sqrt{t}}{2R^2T^2} \tag{32}$$

and, for the second-harmonic component,

$$I_F(2wt) = \frac{n^3 F^3 A C_O^* (wD_O)^{1/2} \Delta E^2}{R^2T^2}\left[\frac{J^2 + H^2}{1 + \left(1 + (2w)^{1/2}/l\right)^2}\right]^{1/2} sin\left[2wt + \cot^{-1}\frac{J + \left(1 + (2w)^{1/2}/l\right)H}{H - \left(1 + (2w)^{1/2}/l\right)J}\right] \tag{33}$$

where

$$J = \frac{1}{8\cosh^3(j/2)}\left\{\frac{a^2}{2}\left(e^{j/2} + 2e^{-j/2} + e^{-3j/2}\right) - \frac{\left(ae^{j/2} - be^{j/2}\right)\left(2 + (2w)^{1/2}/l\right)}{\left[1 + \left(1 + (2w)^{1/2}/l\right)^2\right]}\left[1 + \frac{\left(ae^{-j} - b\right)D^{1/2}y_O(t)}{k_S e^{-aj}}\right]\right.$$

$$\left. - \frac{\left(a^2e^{-j} + b^2\right)\left(e^{-j/2} + e^{j/2}\right)}{2}\left[1 - \frac{\left(1 + e^j\right)}{l}y_O(t)\right]\right\} \tag{34}$$

$$H = \frac{1}{8\cosh^3(j/2)}\left\{\frac{\left(ae^{-j/2} - be^{j/2}\right)\left((2w)^{1/2}/l\right)}{\left[1 + \left(1 + (2w)^{1/2}/l\right)^2\right]}\left[1 + \frac{\left(ae^{-j} - b\right)D^{1/2}y_O(t)}{k_S e^{-aj}}\right]\right\} \tag{35}$$

An example of an experimental second harmonic ac polarogram is given in Fig 4.2.

Numerous uses have been made of this technique and a large number of models have been devised. Among these are multi-step charge transfer [8], coupled homogeneous Redox reaction [9], amalgam formation [10], pharmaceuticals [11], negative Faradaic admittances [12], dimerisation [13], corrosion [14], and fast non-volmerian electron transfer [15].

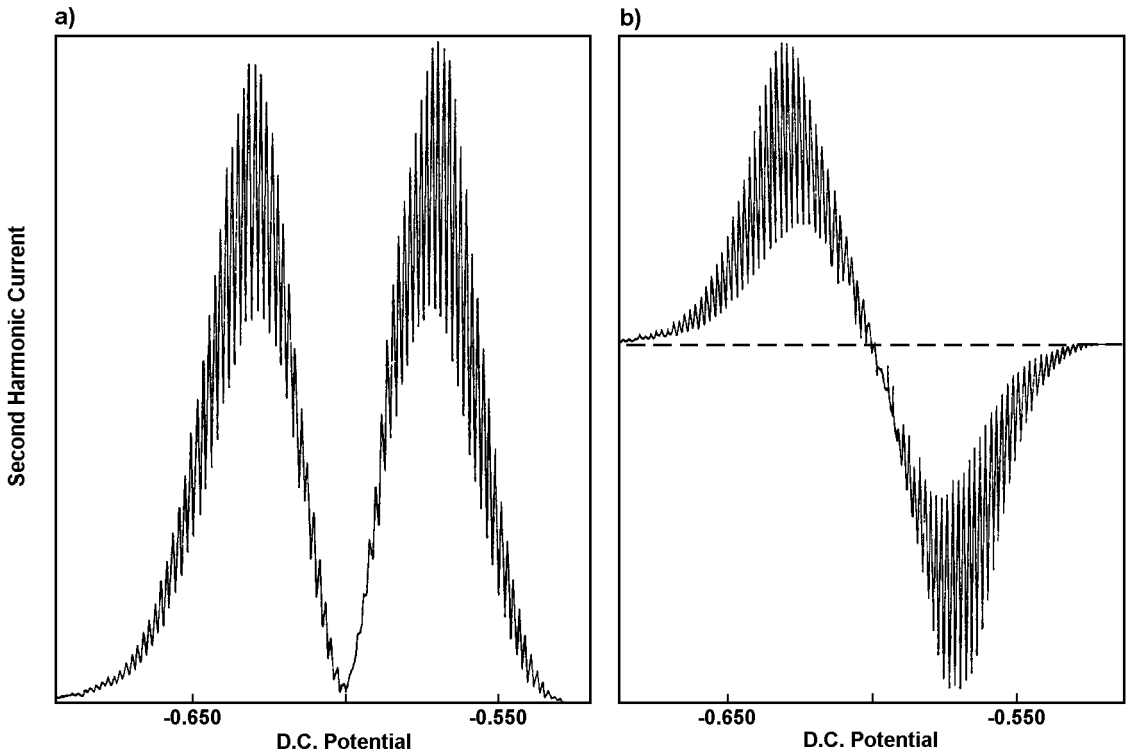

Fig 4.2 Second harmonic ac polarogram (from [41])

System: 3.10^{-3}M Cd(II), 1.0M Na_2S0_4. Applied potential: l0mVpeak-to-peak, 80Hz; dc scan rate = 25mV mn^{-1} (a) conventional second harmonic ac polarogram (b) phase selective second harmonic ac polarogram

4.2 Electrohydrodynamic Impedance

The advantage of the rotating disc electrode is that mass transport can be controlled by the rotation speed Ω. Thus, perturbing the rotation speed amounts to perturbing mass transport. Based on this idea, some authors [16-18] have suggested imposing a sweep, a jump or a sinusoidal modulation on the rotation speed of the disc electrode, and then analysing the current response. In this study the equation of convective diffusion is:

$$\frac{\partial c}{\partial t} = D\nabla^2 c - \vec{n}.\nabla c \qquad (36)$$

c being the concentration of species (either Red or Ox for a Redox couple such as eqn (1))

4.2.1 Sinusoidal Modulation of the Rotation Speed

Two types of modulation have been proposed, i.e.

$$\sqrt{\Omega} = \sqrt{\Omega_O}\,(1 + e\cos wt) \tag{37}$$

$$\Omega = \Omega_O\,(1 + e\cos wt)$$

The current response to the latter is

$$I = \bar{I} + \Delta I_1 \cos(wt - f_1) + \Delta I_2 \cos(2wt - f_2) + ... \tag{38}$$

where $\bar{I}$ is the dc current for a constant rotation speed Ω_O.

However, only the first-order term has been studied. This corresponds to a first-order approximation that is valid when the amplitude of the modulation is small (linear regime).

In the equation of convective diffusion (eq. 25, § 1) only the normal component v_Z of the fluid velocity $\vec{n}$ has an influence. Using the expansion of v_Z as a function of z, Fick's equation has been solved, on one hand numerically [17] and on the other hand by the use of a semi-analytical expression of the form [18]:

$$\frac{\Delta I}{\Delta\Omega} = \frac{\bar{I}}{\Omega_O}\left(A - j\frac{2DB}{w}\right) \tag{39}$$

which defines an electrohydrodynamic impedance

$$\frac{1}{Z_{ehd}} = \frac{\Delta I}{\Delta\Omega} \tag{40}$$

where

$$A = \frac{1}{2}\frac{\sum_{j=1}^{n} a_j\,(w/\Omega_O)^{2j}}{\sum_{j=1}^{m} b_j\,(w/\Omega_O)^{2j}} \qquad \text{and } B = \frac{1}{4D}\frac{(w/\Omega_O)^2\sum_{j=1}^{k} c_j\,(w/\Omega_O)^{2j}}{\sum_{j=1}^{l} d_j\,(w/\Omega_O)^{2j}}$$

a_j, b_j, c_j, and d_j are functions of Schmidt's number $\left(\frac{n}{D}\right)$, where ν is the kinematic viscosity.

For n = k = 2 and m = l = 3 there is good agreement between calculated values and measured values of Z_{ehd} in the case of Schmidt's numbers lower than 2100 and (ω/Ω_o) ranging from 0 to 10. This expression of Z_{ehd} is also in agreement with the numerical integration within the range of (ω/Ω_o) calculated (between 0 and 1). In order to obtain an expression of Z_{ehd} valid for higher Schmidt's numbers, it would be necessary to take account of higher-order terms.

Analytical solutions of this problem have now been proposed. The general solution of eqn (36) is given as a linear function of two fundamental boundary problem solutions. One is imposed by a constant concentration at the electrode surface, the other is imposed by a constant flux of matter at the interface. Hence, an analytical expression has been obtained for the electrohydrodynamic impedance [19, 20].

In addition, it has been shown that a basic relationship can be written between the usual electrochemical impedance $\left(\frac{\partial E}{\partial I}\right)_{\Omega}$ the electrohydrodynamic impedance measured in a potentiostatic control mode $\left(\frac{\partial \Omega}{\partial I}\right)_{E}$, and the electrohydrodynamic impedance measured in a galvanostatic control mode $\left(\frac{\partial \Omega}{\partial E}\right)_{I}$ [21] i.e.

$$\left(\frac{\partial \Omega}{\partial I}\right)_{E} = \left(\frac{\partial \Omega}{\partial E}\right)_{I} \cdot \left(\frac{\partial E}{\partial I}\right)_{\Omega} \tag{42}$$

Fig 4.3 shows the electrohydrodynamic impedance in the complex plane measured, at different rotation speeds, using the experimental set-up given in Fig 4.4. The low frequency limit is equal to:

$$\frac{dI_d}{d\Omega}\left(w / \Omega_O \rightarrow 0\right) = \frac{1}{2}\frac{I_d}{\Omega_O} = \frac{1}{2}\frac{d}{\sqrt{\Omega_O}} \tag{43}$$

since the limiting diffusion current I_d is equal to

$$I_d = d\sqrt{\Omega_O} \tag{44}$$

eqns (43) and (44) allow one to determine d and hence the parameters defining the limiting diffusion current [23, § 1]

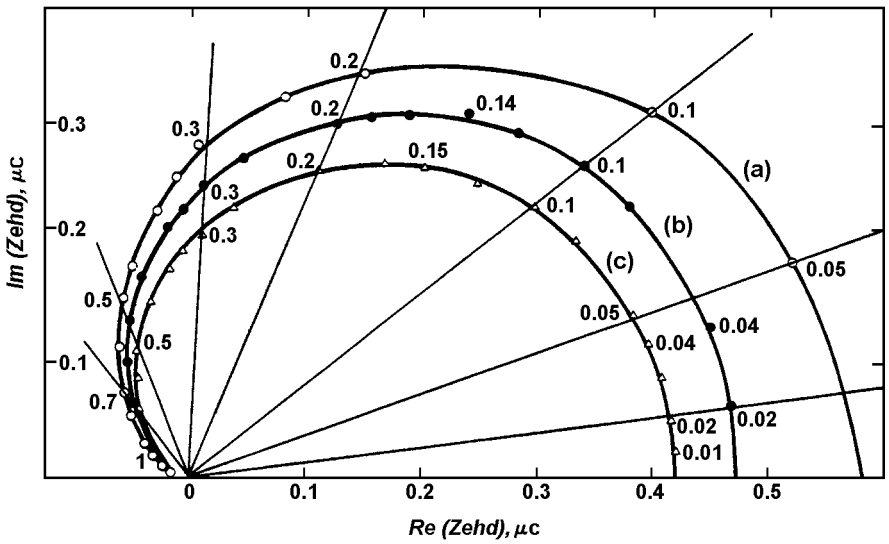

Fig 4.3 Electrohydrodynamic impedance $Z_{ehd}(\omega)$ measured at three rotation speeds of the rotating disc: curve (a) 600 rpm; curve (b) 900 rpm; curve (c) 1200 rpm; obtained in a solution: KCl (M), $K_3Fe(CN)_6$ (10^{-3} M), K_4 $Fe(CN)_6$ (10^{-3} M). The straight lines show that the diagrams are homothetic. The numbers indicate the reduced frequencies in $\frac{w}{\Omega_O}$ (From[18])

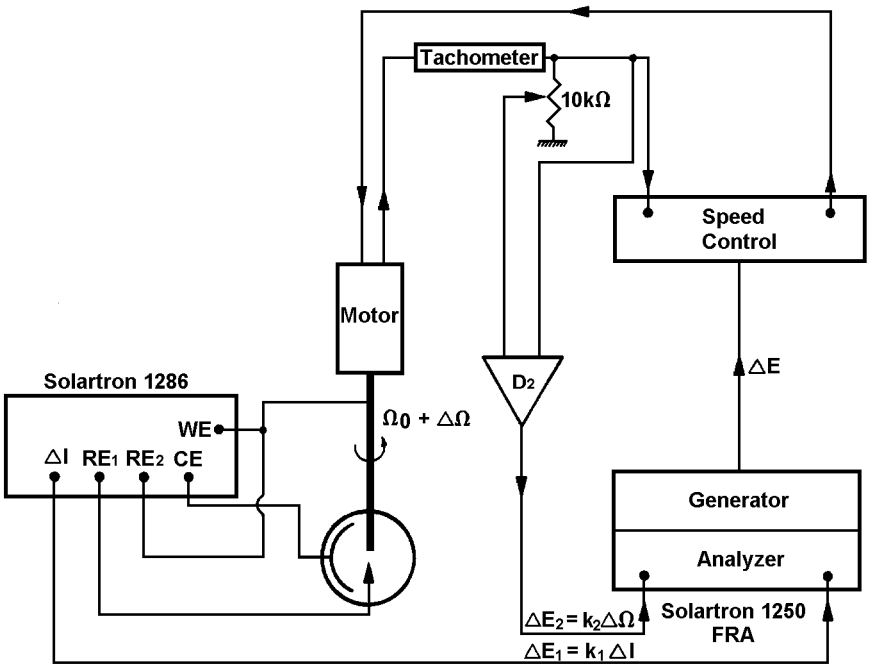

Fig 4.4 Experimental arrangement used for measuring the electrohydro dynamic impedance. FRA: transfer function analyser.

4.2.2 Applications

Analysis of the electrohydrodynamic impedance allows one to extract the diffusion component from an overall current, even if the latter is zero as in a corrosion process, and to determine Schmidt's number [22].

This technique has been applied to the study of partially blocked electrodes [23] and to the analysis of various quantities on the flow of suspensions of red blood cells in the vicinity of a wall [24].

The studies performed hitherto have dealt with the limiting diffusion current. It seems that the application of this technique to processes controlled by both diffusion and charge transfer is very attractive, but presents problems which have still to be solved.

4.3 Electro-Optical Transfer Function

For a decade, electro-optical measurements have been done by modulating the potential of an electro-chemical interface with a sine wave and analysing the response of the reflection factor R in terms of:

$$r = \frac{1}{R}\frac{\Delta R}{\Delta E} \tag{45}$$

which is sometimes called the differential reflectivity. An example of an experimental analysis is given in Fig 4.5 [25]. It was shown that

$$r = \frac{1}{R}\frac{\Delta R}{\Delta q}.\frac{Y(w)}{jw} \tag{46}$$

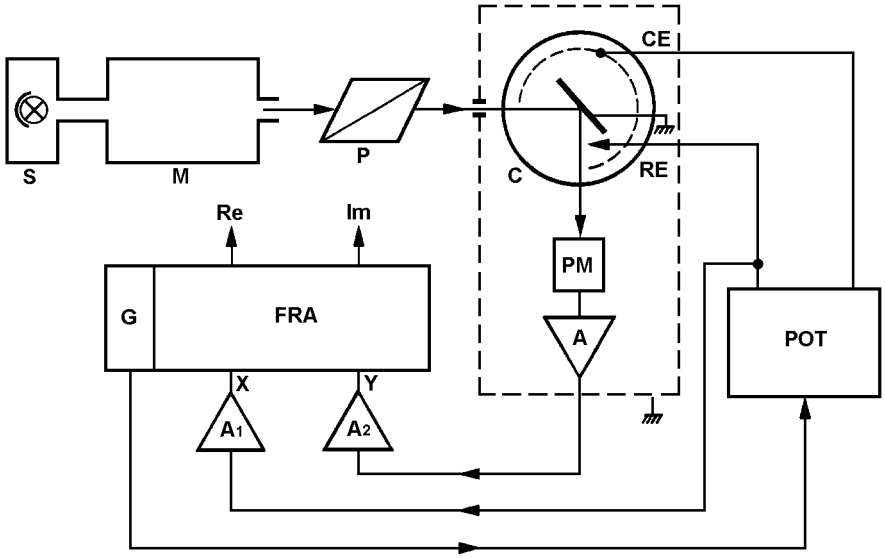

Fig 4.5 Experimental arrangement used for measuring electroreflectance spectra and electro-optical transfer function (from [25]).

S	light source
M	monochromator
P	polariser
C	cell
CE	counter electrode
RE	reference electrode
POT	potentiostat
PM	photomultiplier
A	amplifier
FRA	frequency response analyser
G	generator

where Y(w) is the electrical admittance and $\frac{1}{R}.\frac{\Delta R}{\Delta q}$ the electro-reflection coefficient defined when the electric charge density of the electrode is changed [26]. Differential reflectivity can be analysed in two ways:

i) the frequency of the potential modulation is kept constant and the wavelength of the illumination is changed; this technique is called modulated electro-reflectance.

ii) the wavelength of the illumination is kept constant and the frequency of the potential modulation is changed; this technique leads to an electro-optical transfer function.

To date, the first technique has been widely applied to semi-conductors [27], noble metals [28-31] and more recently to oxide layers [25], adsorption [32-34] and underpotential deposition [35]. Information on surface and volume plasmons and on electronic interband transitions can be obtained. An example of an electro-reflectance diagram is given in Fig 4.6 [36].

The electro-optical transfer function has begun to be applied [37, 38]. However it seems that the interpretation is not yet clear. An example of such a diagram is given in Fig 4.7.

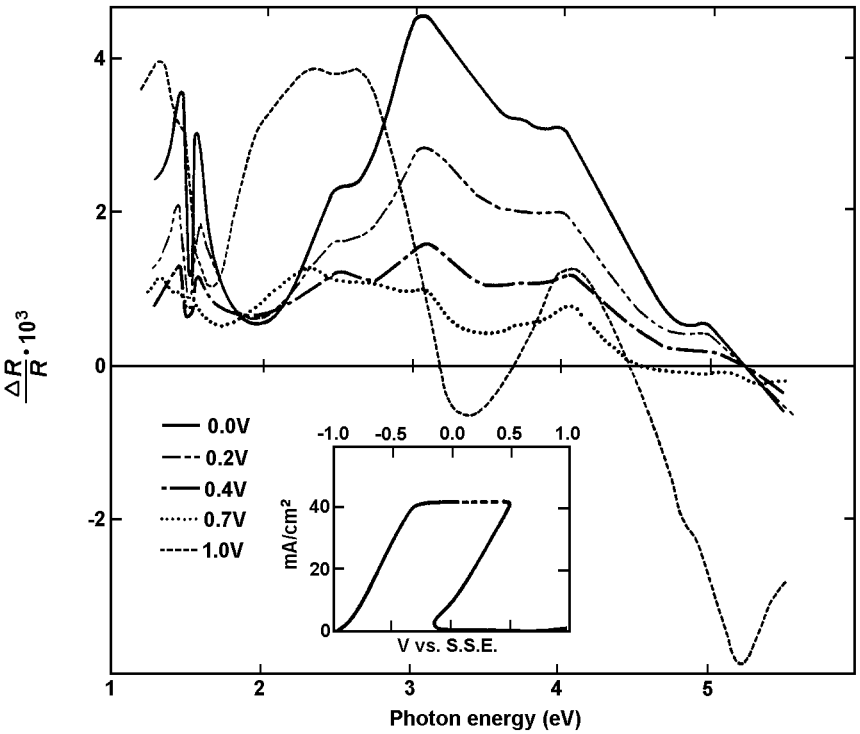

Fig 4.6 Electroreflectance measurement diagram for pure iron (Johnson-Matthey) in 0.1N, H_2S0_4 polarised in the passivity range; incidence angle of light = 45°; modulation ΔE = 50m V, 30Hz. (from [36])

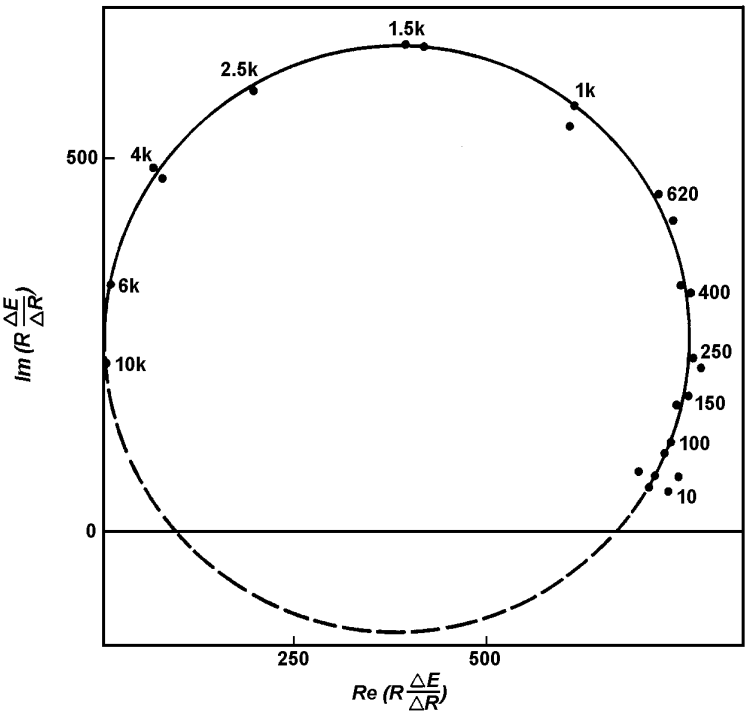

Fig 4.7 Electro-optical transfer function measured for titanium in 1N, H_2S0_4 at -0.6V vs SSE, photon energy 3.9eV, amplitude of the sine wave modulation 50mV. (from [38])

REFERENCES FOR CHAPTER 4

1 P DUMARGUE, Electrochim Acta 17, pp 1377 - 1390, 1972

2 Z FIGASZEWSKI and Z KOCZOROWSKI, J Electroanal Chem 73, pp 1 - 11, 1976

3 D E SMITH, Electroanalytical Chemistry, Vol 1, Ed by A J Bard, Marcel Dekker, New York, pp 1 – I55, 1966

4 D E SMITH, Anal Chem 35, pp 1811 - 1820, 1963

5 D E SMITH, Anal Chem 36, pp 962 - 970, 1964

6 D HENDERSON and J G GORDON, J Electroanal Chem 108, pp 129 - 142, 1980

7 A M BOND, R J O'HALLORAN, I RUZIC and D E SMITH, J Electroanal Chem 90, pp 381 - 388,1978

8 H L HUNG and D E SMITH, J Electroanal Chem 11 pp 237 - 254 and pp 425 - 461, 1966

9 I RUZIC and D E SMITH, J Electroanal Chem 52, pp 157 - 192, 1974, and 58, pp 145 - 175, 1975

10 A M BOND, R J O'HALLORAN, I RUZIC and D E SMITH, Anal Chem 50, pp 216 - 223, 1978

11 A L WOODSON and D E SMITH, Anal Chem 42, pp 242 - 248, 1970

12 D E SMITH and H R SOBEL, Anal Chem 42, pp 1018 - 1022, 1970

13 J W HAYES, I RUZIC, D E SMITH, G L BOOMAN and J R DELMASTRO, J Electroanal Chem 51, pp 269 - 285, 1974

14 G PRABHAKARA RAO and A K MISHRA, J Electroanal Chem 77, pp 121 - 125, 1977

15 D GARREAU, J M SAVEANT and D TESSIER, J Electroanal Chem 103, pp 321 - 333, 1979

16 S BRUCKENSTEIN, M I BELLAVANCE and B MILLER, J Electrochem Soc 120, pp 1351 - 1356, 1973

17 K TOKUDA, S BRUCKENSTEIN and B MILLER, J Electrochem Soc 122, pp 1316 - 1322, 1975

18 C DESLOUIS, I EPELBOIN, C GABRIELLI and B TRIBOLLET, J Electroanal Chem 82, pp 251 - 269, 1977

19 W J ALBERY, A R HILLMAN and S BRUCKENSTEIN, J Electroanal Chem 100, pp 687 - 709, 1979

20 C DESLOUIS, C GABRIELLI, Ph SAINTE-ROSE FANCHINE and B TRIBOLLET. J Electrochem Soc 129, pp 107-118 (1982)

21 C DESLOUIS, I EPELBOIN, C GABRIELLI, Ph SAINTE-ROSE FANCHINE and B TRIBOLLET, J Electroanal Chem 107, pp 193 - 195, 1980

22 A CAPRANI, C DESLOUIS, M KEDDAM, Ph MOREL and B TRIBOLLET, Electrochim Acta 22, pp 1231 - 1235, 1977

23 A CAPRANI, J C CHARBONNIER and Ph MOREL, Metaux, Corr, Ind 54, pp 53 - 62, 1979

24 A CAPRANI, Bioelectrochem and Bioeng 6, pp 413 - 425, 1979

25 G BLONDEAU, M FROELICHER, V JOVANCICEVIC and A HUGOT-LE GOFF, Surface Sci 80, pp 151 – I58, 1979

26 J P DALBERA, C HINNEN and A ROUSSEAU, JPhys Colloque CS, 38, pp 185 - 191, 1977

27 Modulation Spectroscopy, Proc of the first Intern Conf on modulation spectroscopy, Tucson Az, 1972, Ed B 0 SERAPHlN, North Holland, Amsterdam, 1973

28 R KOTZ, H J LEWERFNZ and E KRETSCHRANN, Phys letters 70A, pp 452 - 454, 1979

29 T E FURTAK and D W LYNCH, J Electroanal Chem 79, pp 1 - 17, 1977

30 C NGUYFN VAN RUONG, C HINNEN, J LECOEUR, and R PARSONS, J Electroanal Chem 92, pp 239 - 244, 1978

31 T E FURTAK and D W LYNCH, Phys Rev letters 35, pp 960 - 963, 1975

32 T TAKAMURA, K TAKAMURA and E YEAGER, J Electroanal Chem 29, pp 279 - 291, 1971

33 C HINNEN, C NGUYEN VAN HUONG, A ROUSSEAU and J P DALBERA, J Electroanal Chem 106, pp 175 - 183, 1980

34 D SCHUHMANN, J Electroanal Chem 73, pp 13 - 20, 1976

35 D H KOLB, JPhys (Paris) Colloque CS, pp 167 - 177, 1977

36 V JOVANCICEVIC, Thesis Paris 1980

37 C HINNEN, C NGUYEN VAN HUONG, A ROUSSEAU and J P DALBEPA, J Electroanal Chem 95, pp 131 - 146, 1979

38 V JOYANCICEVIC, Personal communication

A	electrode area	eqn 1.30
b_I	Tafel's slope	eqn 3.14
Cd	Double layer capacity	fig 1.3
c_I	concentration of species i	eqn 1.22
$\overline{c_i}$	steady-state concentration of species I	eqn 1.51
c_I^*	concentration of species I in the bulk of the solution	eqn 1.33
D_I	diffusion coefficient of species I	eqn 1.25
$D = D_O^{(1-a)} D_R^a$		eqn 4.8
E	potential	eqn 1.19
E_{eq}	equilibrium potential	eqn 1.40
E^0	standard (or normal) potential	eqn 1.37
Eref	potential difference between the reference electrode and the working Electrode	eqn 21.24
$E^r_{1/2}$	half wave potential	eqn 4.4
$E^*(w)$	complex conjugate of *E(w)*	eqn 2.28
F	Faraday's constant (96500C)	eqn 1.19
$\mathfrak{I}$	Fourier operator	eqn 1.6
f	frequency	eqn 2.17
$H(w)$	transfer function	eqn 1.4
I	overall current flowing through the interface	eqn 1.27
I_F	Faradaic current	eqn 1.19
I_o	exchange current	eqn 1.40
I_a	anodic current	eqn 3.11
I_{corr}	corrosion current	eqn 3.16
I_c	cathodic current	eqn 3.12
$Im(Z)$	imaginary part of the impedance *Z(w)*	eqn 1.11
j	imaginary operator	eqn 1.11
$j(t) = \frac{nF}{RT}\left[E(t) - E^r_{1/2}\right]$		eqn 4.7
k_f, k_i	rate constant of the forward reaction	eqn 1.31
$k_b, k\text{-}_i$	rate constant of the backward reaction	eqn 1.31
k_S	standard rate constant	eqn 1.38
M	atomic weight	eqn 3.11
$N(w) = \frac{1}{D}\frac{\tanh d_N \sqrt{jw/D}}{\sqrt{jw/D}}$		eqn 1.66
n	number of electrons	eqn 1.19
P	pressure	eqn 1.30
R	molar gas constant	eqn 1.19
R_{ct}	charge transfer resistance	eqn 1.50
Re	Reynolds number	fig 3;3
R_e	electrolyte resistance	eqn 1.24
$Re(Z)$	real part of impedance *Z(w)*	eqn 1.11
R	reflecting factor of light	eqn 4.45

R_p	polarisation resistance	eqn 1.93
T	absolute temperature	eqn 1.19
t	time	eqn 1.1
$\vec{u}$	velocity of the liquid	eqn 1.25
ν_i	reaction rate	eqn 1.83
$Z(w)$	impedance	eqn 1.10
Z_{ehd}	electrohydrodynamic impedance	eqn 4.40
z	normal distance from the electrode surface	eqn 1.32
a	transfer coefficient	eqn 1.19
b_I	maximum surface concentration of species I	eqn 1.29
G_i	surface concentration of species I	eqn 1.83
Δ	small perturbation	eqn 1.20
d_N	thickness of the diffusion layer	eqn 1.63
q_i	surface coverage of species i	eqn 1.29
$l = \frac{k_f}{\sqrt{D_O}} + \frac{k_b}{\sqrt{D_R}}$		eqn 1.59
x_i	chemical source term of species i	eqn 1.22
r	differential reflectivity	eqn 4.45
r_c	electric charge density	eqn 1.21
τ	time constant of the admittance	eqn 1.90
$y(t) = \frac{I_F(t)}{nFAc_o^* \sqrt{D_o}}$		eqn 4.60
Ω	rotation speed of the electrode	eqn 1.30
w	angular frequency (w=2πf)	eqn 1.2